Best Available Copy

AD-787 005

SOVIET MATERIAL ON INTERNAL WAVE
EFFECTS, NO. 2, OCTOBER, 1974

Stuart G. Hibben, et al

Informatics, Incorporated

Prepared for:

Navy Foreign Language Service
Defense Advanced Research Projects Agency

4 October 1974

REPORT DOCUMENTATION PAGE

READ INSTRUCTIONS BEFORE COMPLETING FORM

1. REPORT NUMBER	2. GOVT ACCESSION NO.	3. RECIPIENT'S CATALOG NUMBER
		AD-787005

4. TITLE (and Subtitle)

Soviet Material on Internal Wave Effects
No. 2, October, 1974

5. TYPE OF REPORT & PERIOD COVERED

Scientific . . . Interim

6. PERFORMING ORG. REPORT NUMBER

7. AUTHOR(s)

Stuart G. Hibben, John Kourilo,
B. L. Shresta, M. Ness

8. CONTRACT OR GRANT NUMBER(s)

N00600-75-C-0018

9. PERFORMING ORGANIZATION NAME AND ADDRESS

Informatics Inc.
6090 Executive Boulevard
Rockville, Maryland 20852

10. PROGRAM ELEMENT, PROJECT, TASK AREA & WORK UNIT NUMBERS

DARPA Order No. 2790
Program Code No. L13003

11. CONTROLLING OFFICE NAME AND ADDRESS

Defense Advance Research Projects Agency/TAO
1400 Wilson Boulevard
Arlington, Virginia 22209

12. REPORT DATE

October 4, 1974

13. NUMBER OF PAGES

127

14. MONITORING AGENCY NAME & ADDRESS(if different from Controlling Office)

U. S. Navy Foreign Language Service
4301 Suitland Road, Bldg. 5
Washington, D. C. 20390

15. SECURITY CLASS. (of this report)

Unclassified

15a. DECLASSIFICATION DOWNGRADING SCHEDULE

16. DISTRIBUTION STATEMENT (of this Report)

Approved for public release; distribution unlimited.

17. DISTRIBUTION STATEMENT (of the abstract entered in Block 20, if different from Report)

18. SUPPLEMENTARY NOTES

Scientific . . . Interim

19. KEY WORDS (Continue on reverse side if necessary and identify by block number)

Internal Waves
Capillary Waves
Surface Signature
Turbulent Flow
Ocean Microstructure

20. ABSTRACT (Continue on reverse side if necessary and identify by block number)

This is a second collection of abstracts of recent Soviet articles on generation
and detection of internal waves. It is based on items listed in the second
Bibliography of Soviet Material on Internal Waves, published June 17, 1974
and covering material received in the first quarter of 1974.

The abstracts are divided into internal effects, and surface effects
comprising active and passive measurement of wave states. An
author index is appended.

DD FORM 1 JAN 73 **1473** EDITION OF 1 NOV 65 IS OBSOLETE

SOVIET MATERIAL
ON
INTERNAL WAVE EFFECTS

No. 2, October, 1974

Sponsored by

Defense Advanced
Research Projects Agency

DARPA Order No. 2790

October 4, 1974

informatics inc ▪ Systems and Services Company
6000 Executive Boulevard
Rockville, Maryland 20852
(301) 770-3000 Telex: 89-521

DDC
RECEIVED
OCT 21 1974
B

ia

INTRODUCTION

This is a second collection of abstracts of recent Soviet articles on generation and detection of internal waves. It is based on items listed in the second <u>Bibliography of Soviet Material on Internal Waves,</u> published June 17, 1974 and covering material received in the first quarter of 1974.

The abstracts are divided into internal effects, and surface effects comprising active and passive measurement of wave states. An author index is appended.

TABLE OF CONTENTS

1. Internal Effects

Ozmidov, R. V. <u>Experimental studies of small-
scale ocean turbulence by the Institute of Oceanology
im. P. P. Shirshov of the USSR Academy of Sciences.</u>
IN: Issledovaniye okeanicheskoy turbulentnosti
(Study of ocean turbulence). Moskva, Izd-vo Nauka,
1973, 3-19.

Studies of small-scale ocean turbulence began in 1967.
The first in situ measurements were conducted during a special cruise of
the R/V Dmitriy Mendeleyev * in 1969. These studies were continued during
the 9th cruise of the R/V Akademik Kurchatov and the 5th and 7th cruises of
the R/V Dmitriy Mendeleyev in 1970-1972 (see tracks in Figs la - ld).

Fig. la. Track of 2nd Cruise of R/V Dmitriy
Mendeleyev*

---

* Arabic numerals denote hydrological stations and Roman numerals indicate
special test areas.

Fig. 1b. Track of 9th Cruise of R/V Akademik Kurchatov.*

Fig. 1c. Track of 5th Cruise of R/V Dmitriy Mendeleyev.*

*Arabic numerals denote hydrological stations and Roman numerals indicate special test areas.

-2-
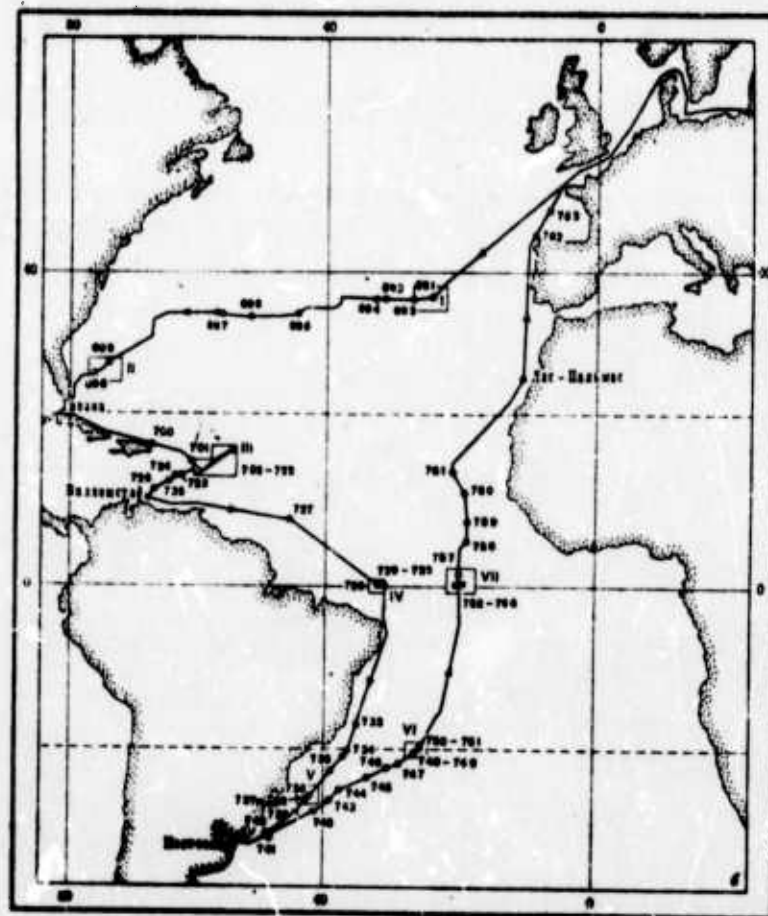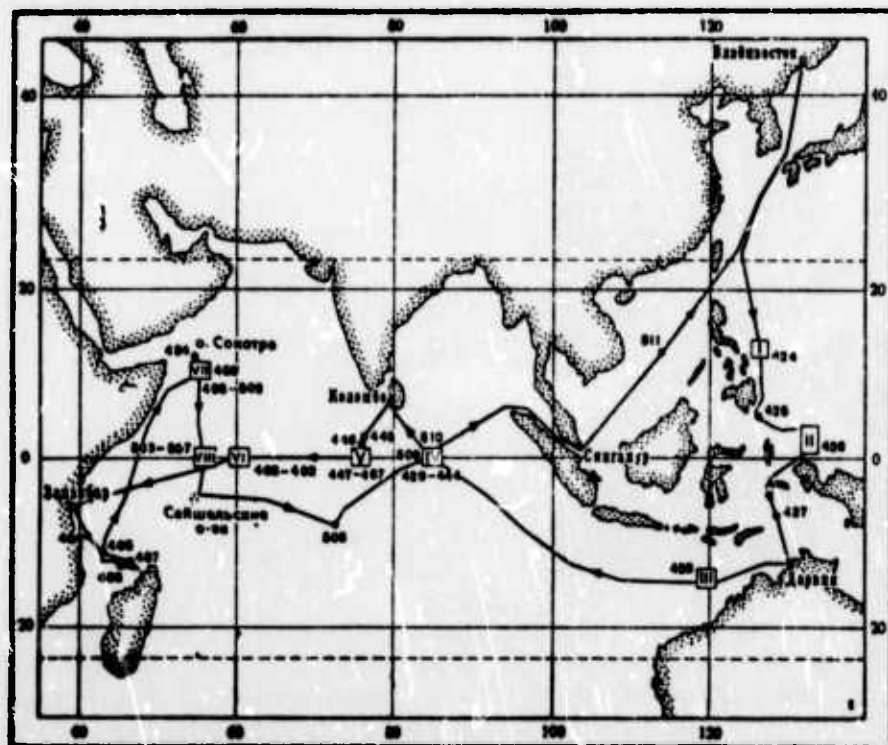
Fig. 1d. Track of 7th Cruise of R/V Dmitriy
Mendeleyev.

The instruments for measuring ocean turbulence were mainly of the hot-
probe type, used in the towing arrangement illustrated in Figure 2.
The instruments were mounted on twin pods (see Fig. 3) and the towing line
consisted of specially designed removable fairings. Measurements of small-
scale ocean turbulence were accompanied by observations of background
hydrological conditions, using both standard and new instruments and techniques.
A typical towed system is illustrated in Figures 4 and 5. Examples of measure-
ment procedures are shown in Figure 6.
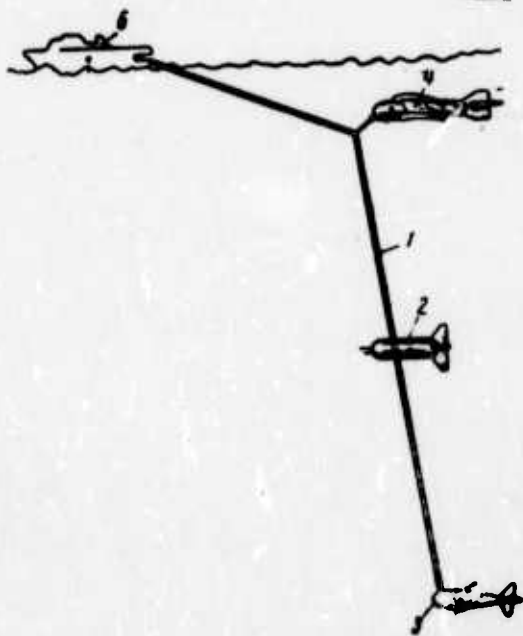
Fig. 2. Arrangement of Towed System.
1- towing line with fairings; 2- twin-pod
instrument package; 3- depressor;
4- intermediate stabilizing fish; 5- ship.

Fig. 3. View of Twin
Instrument Pods, Mounted
on Towing Line.
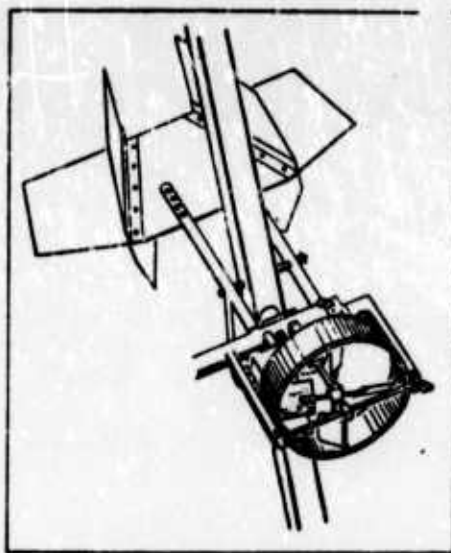
Fig. 4. Flow Meter Mounted on Towing Line.

-4-
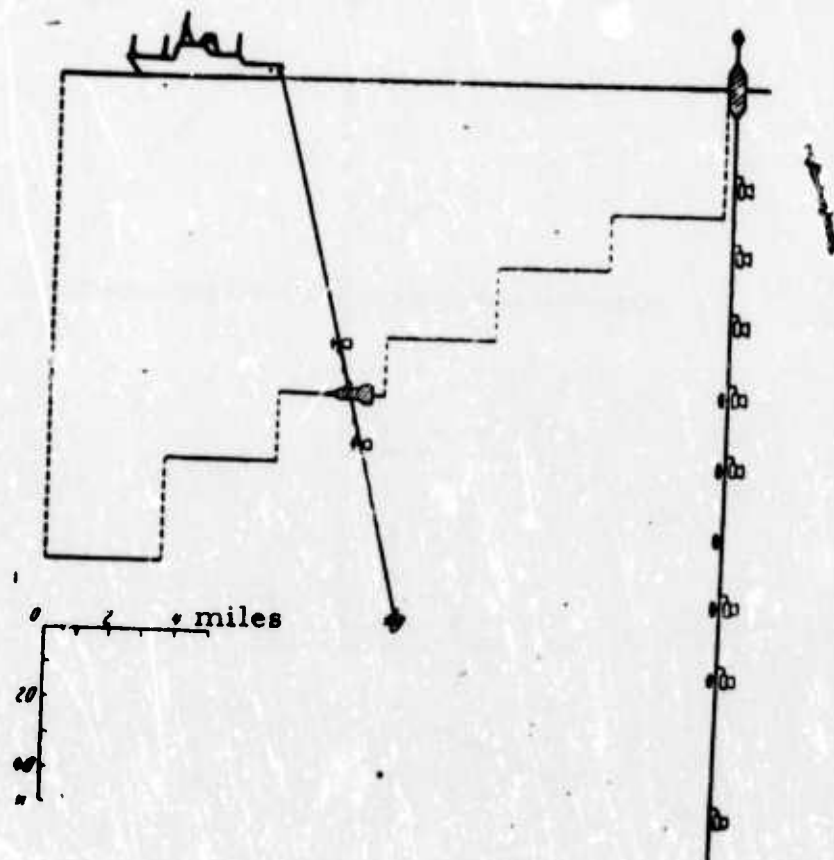
Fig. 5. Measurements of turbulence and background
conditions using moorings with current meters and
photothermographs (right) and towing line with
instrument pods, two current meters, and five
thermistor temperature sensors (9th cruise of
R/V Akademik Kurchatov).
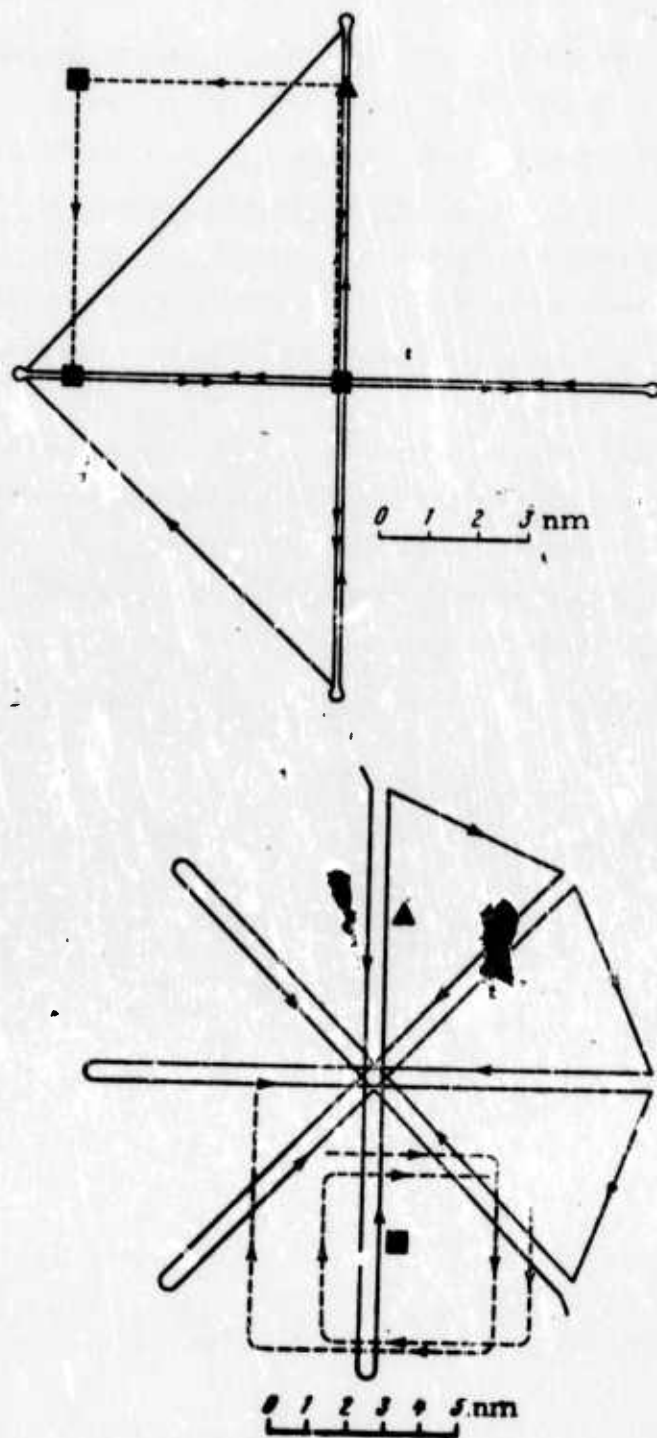
Fig. 6. Examples of Measurement Procedures
Used in Special Test Areas.

Solid lines - tacks with thermistor chain;
dash lines - tacks with turbulimeters; squares - buoys
with current meters and photothermographs;
triangles - radio buoys.

Belyayev, V. S., A. N. Gezentsvey, M. M. Lyubimtsev, R. V. Ozmidov, V. T. Paka, and V. D. Pozdynin. <u>Some results of an experimental study of fluctuations of hydrophysical fields in the upper ocean layer.</u> IN: Issledovaniye okeanicheskoy turbulentnosti (Study of ocean turbulence). Moskva, Izd-vo Nauka, 1973, 20-31.

The results of the measurements of small-scale ocean turbulence were analyzed for three sections run during the 9th cruise of the R/V Akademik Kurchatov. The measuring techniques using towing lines with low-drag fairings provided a relatively low level of vibration noise as illustrated in Figure 1. A block diagram of the measuring-processing channel used in the
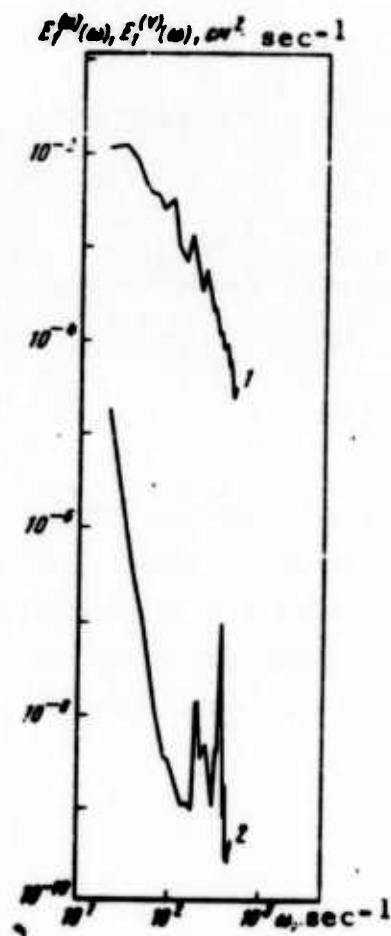
experiments is shown in Figure 2. The measurements of small-scale turbulence were accompanied by observations of background hydrological conditions.
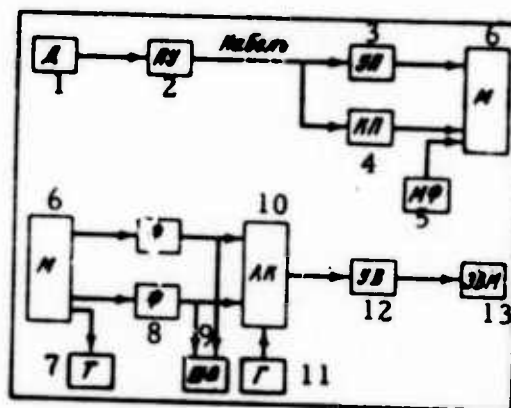
Fig. 2. Block Diagram of Measuring-Processing Channel.

1- sensor; 2- pre-amplifier; 3- fluctuation amplifier; 4- compensator for stationary component; 5- microphone; 6- tape recorder; 7- telephone; 8- low-frequency filters; 9- loop oscillograph; 10- analog-to-code converter; 11- master oscillator; 12- input unit; 13- computer.

The results of the experiments are shown in Figure 3.

Although all measurements were conducted in similar sea states, the intensity of small-scale turbulence was found to vary greatly with an increase in depth as illustrated in Figure 3. High variability of turbulence characteristics in the ocean is manifested in spectral densities of fluctuation of different hydrophysical fields as well (see Fig. 4).
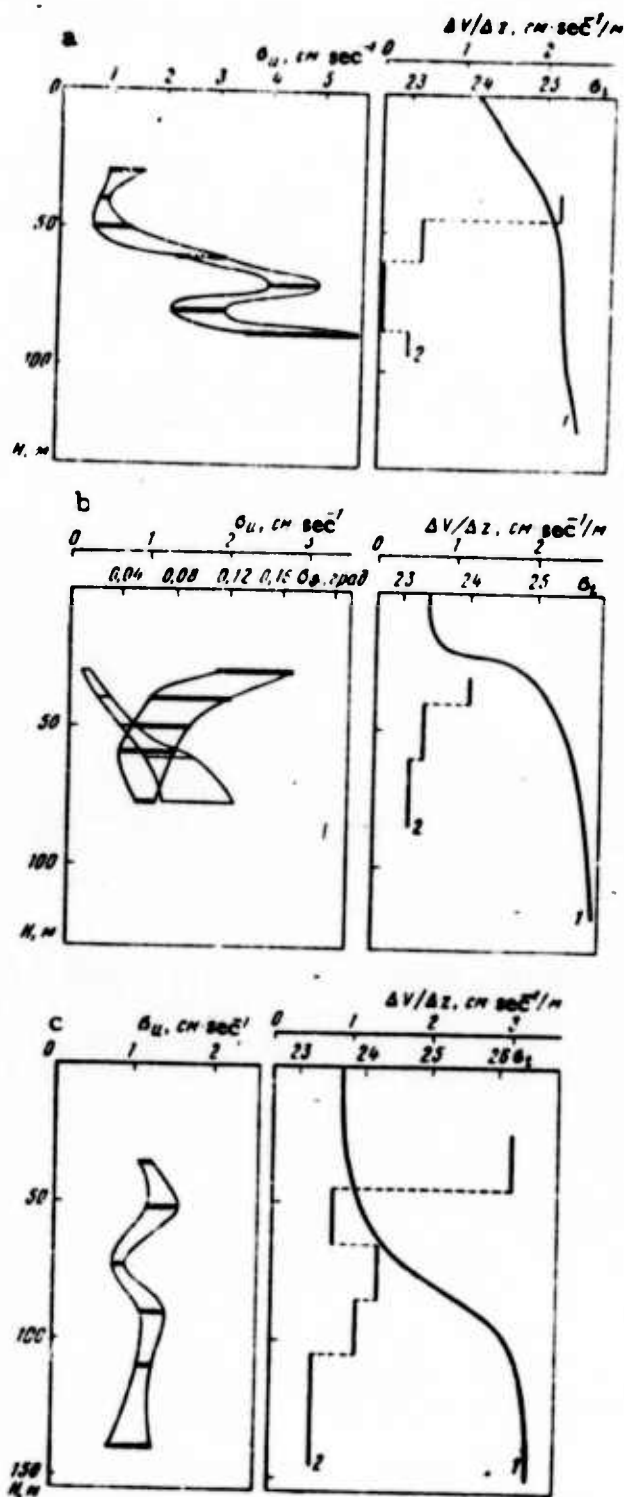
Fig. 3. Vertical distributions of: rms amplitudes of fluctuations of flow velocity σ_u (thick lines); rms amplitudes of temperature fluctuations σ (thin lines); conditional water density σ_t (1); and gradients of the average flow velocity $\Delta V / \Delta Z$ (2).

-9-
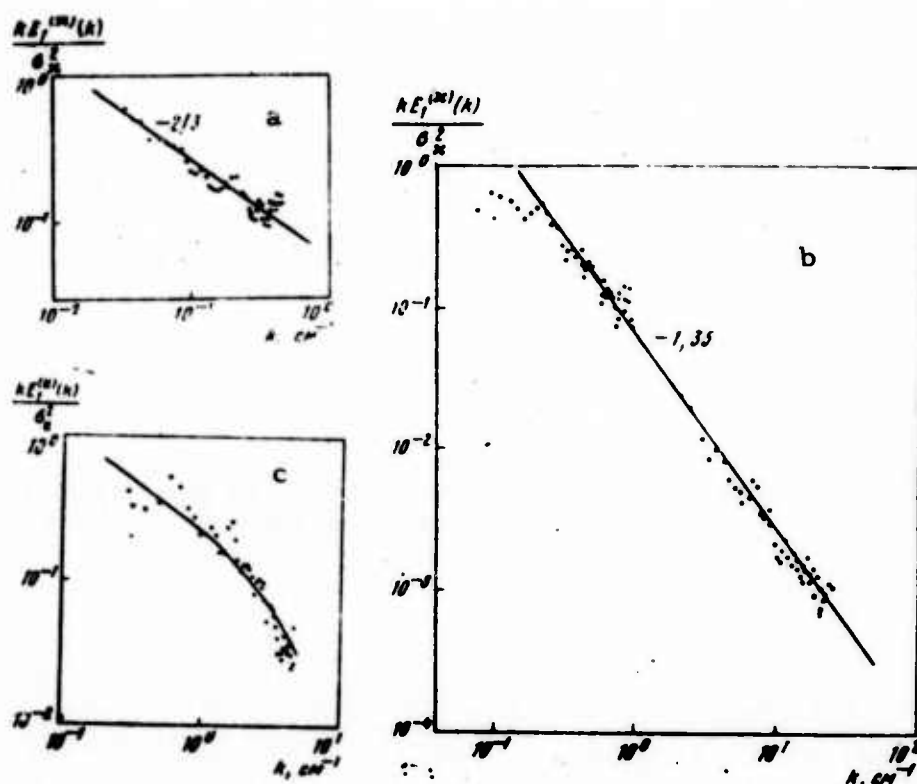
Fig. 4. Examples of one-dimensional normalized spectral function of fluctuations of electrical conductivity (a, b) and flow velocity (c) obtained during the 2-nd cruise of R/V Dmitriy Mendeleyev and the 9-th cruise of R/V Akademik Kurchatov.

Data on the dissipation rate of turbulence energy, estimated graphically and numerically, are shown in Table 1.

Table 1

Горизонт, м	$\bar{\epsilon}$	σ	$\bar{\epsilon}$	σ	A	E	μ
36	14,8	1,8	9,5	0,8	3,9	32,9	0,43
52	35,4	12,3	16,3	2,9	5,6	63,0	0,62
73	11,2	4,6	7,7	1,2	2,4	8,6	0,71
90	39,2	10,2	18,0	4,0	2,6	11,9	0,63
110	24,3	4,8	18,2	2,4	2,1	6,2	0,51
140	3,8	—	3,7	0,8	16,2	38,0	0,46

Note: $\bar{\epsilon}$ is given in 10^{-2} cm^2 sec^{-3}; A and E are coefficients of skewness and excess respectively; μ is correction to the exponent in the universal power law.

Spectral densities of the fluctuations of hydrological fields within a wide range are shown in Figure 5. It was found that in some cases turbulence within an entire range of wave numbers is fed by the same energy source existing in the large-scale portion of the spectrum. However, in some cases there exists an energy influx in the medium-scale portion of the spectrum.
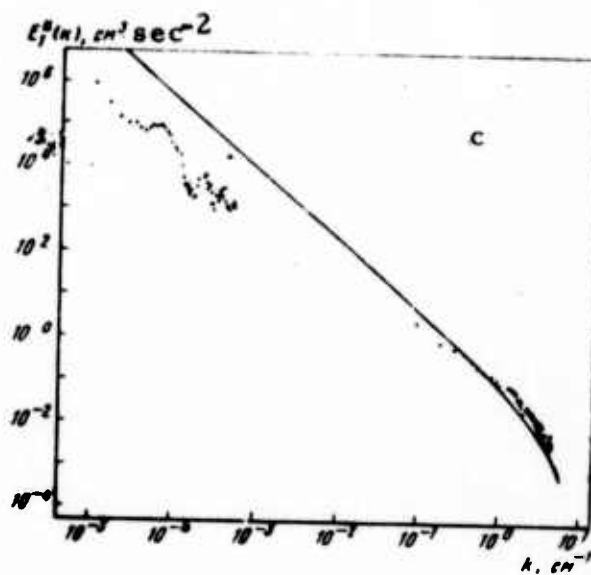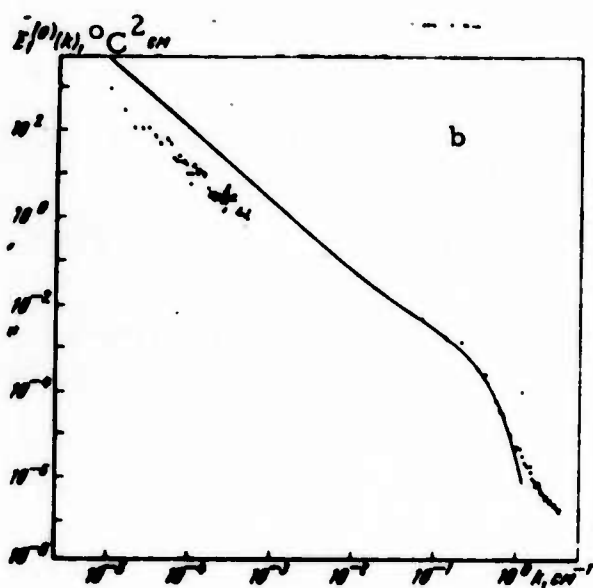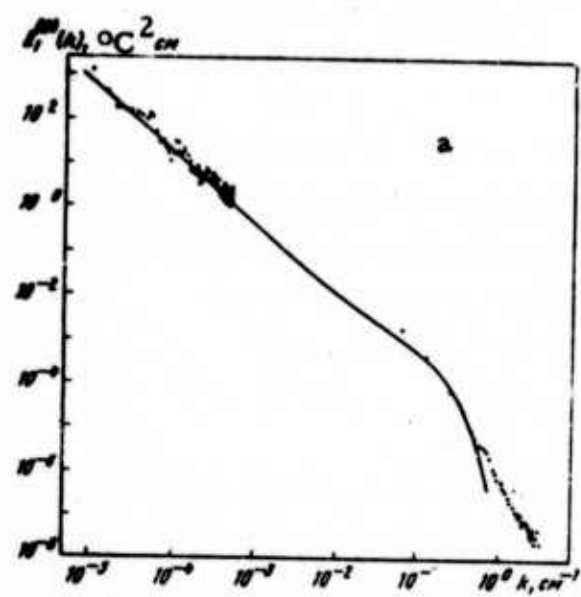
Fig. 5. Spectral densities of fluctuations of temperature (a, b) and flow velocity (c) (from the 9th cruise of the R/V Akademik Kurchatov).

Belyayev, V. S., A. N. Cezentsvey, R. V. Ozmidov, V. T. Paka, and V. D. Pozdynin. Spectral characteristics of small-scale velocity fluctuations in the ocean. IN: Issledovaniye okeanicheskoy turbulentnosti (Study of ocean turbulence). Moskva, Izd-vo Nauka, 1973, 32-43.

The results of the analysis of spectral characteristics of velocity fluctuations in the ocean are summarized based on data obtained during the 9-th cruise of the R/V Akademik Kurchatov (Atlantic Ocean in 1971) and the 7-th cruise of the R/V Dmitriy Mendeleyev (Indian Ocean in 1972).

The results are shown in Figures 1-6.

The measurement of velocity fluctuations during the 9-th cruise of the R/V Akademik Kurchatov reveal that for high turbulence intensity, a fully developed vortex motion can occur and, consequently, some portions of the E(k) curves satisfy the universal power law (see Fig. 1). However, in the majority of cases, the universal power law is either weakly or not at all displayed in E(k) curves.

Measurements made during the 7-th cruise of the R/V Dmitriy Mendeleyev were accompanied by observations of background hydrological conditions, which are shown in Figures 7 and 8.

No relationship was found between characteristics of small-scale turbulence in the ocean and hydrological background conditions (as observed by standard methods).
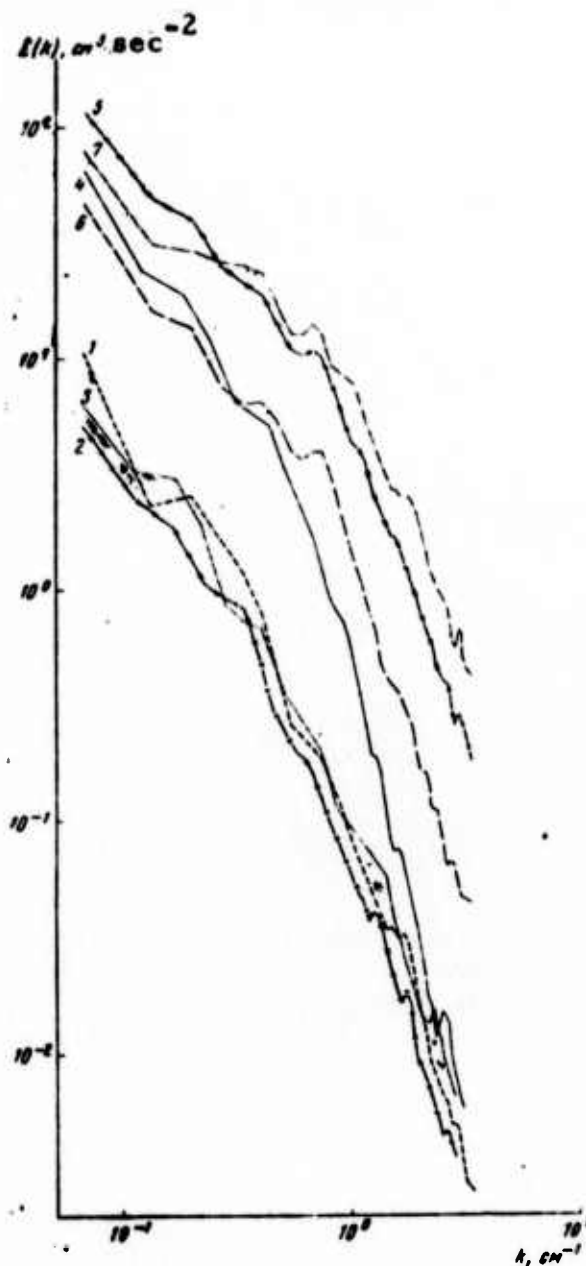
Fig. 1. Spectral densities of velocity fluctuations
based on measurements during the 9-th cruise of
R/V Akademik Kurchatov (test area V).

Curves 1-7 - measurements depths 30, 40, 50,
60, 70, 80, and 87 m, respectively.
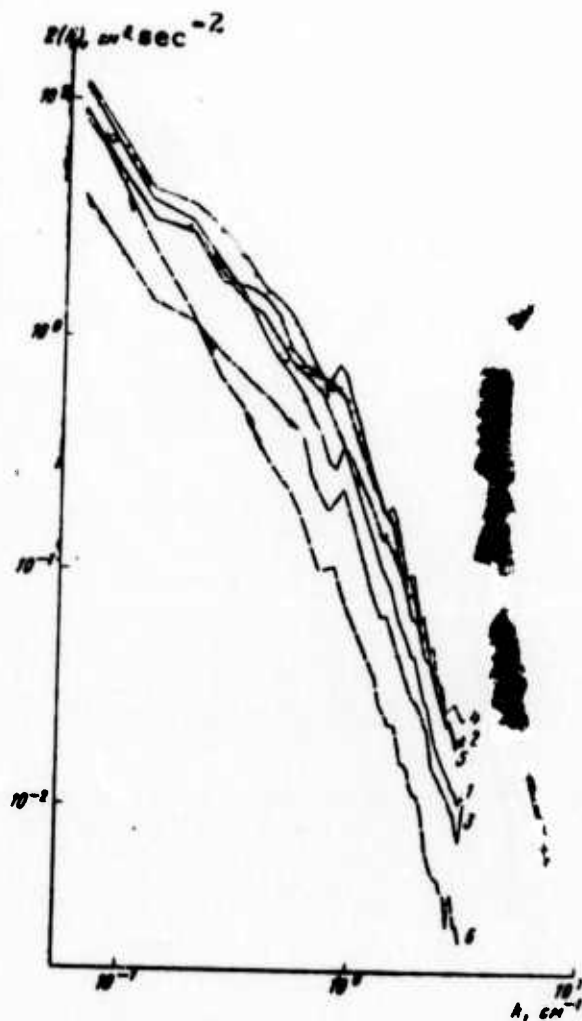
Fig. 3. Spectral densities of velocity fluctuations based on measurements during the 9-th cruise of R/V Akademik Kurchatov (test area VII).

Curves 1-6 - measurement depths 36, 52, 73, 90, 110, and 140 m, respectively.
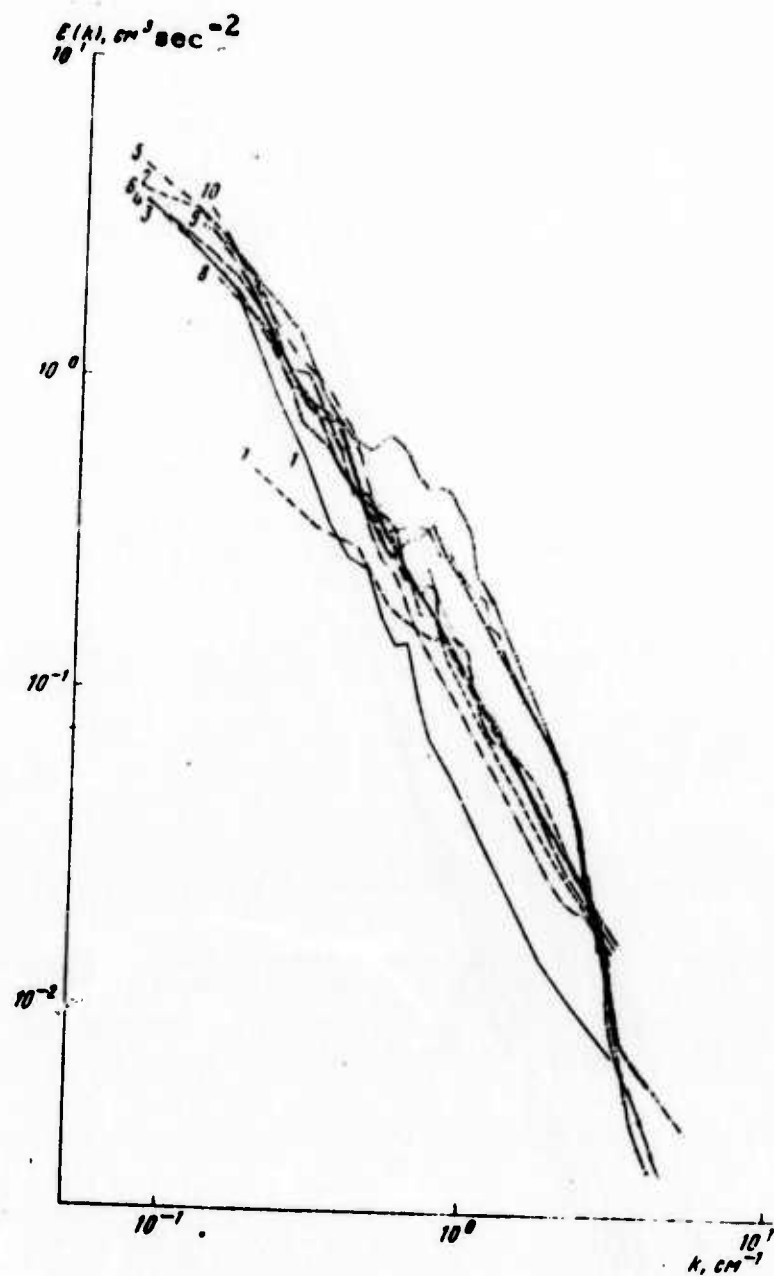
Fig. 4. Spectral densities of velocity fluctuations based on measurements during the 7-th cruise of R/V Dmitriy Mendeleyev (test area V).

Curve 1- depth 105 m; 2-6 - 115 m; 7- 187 m; 8-10 - 100 m.
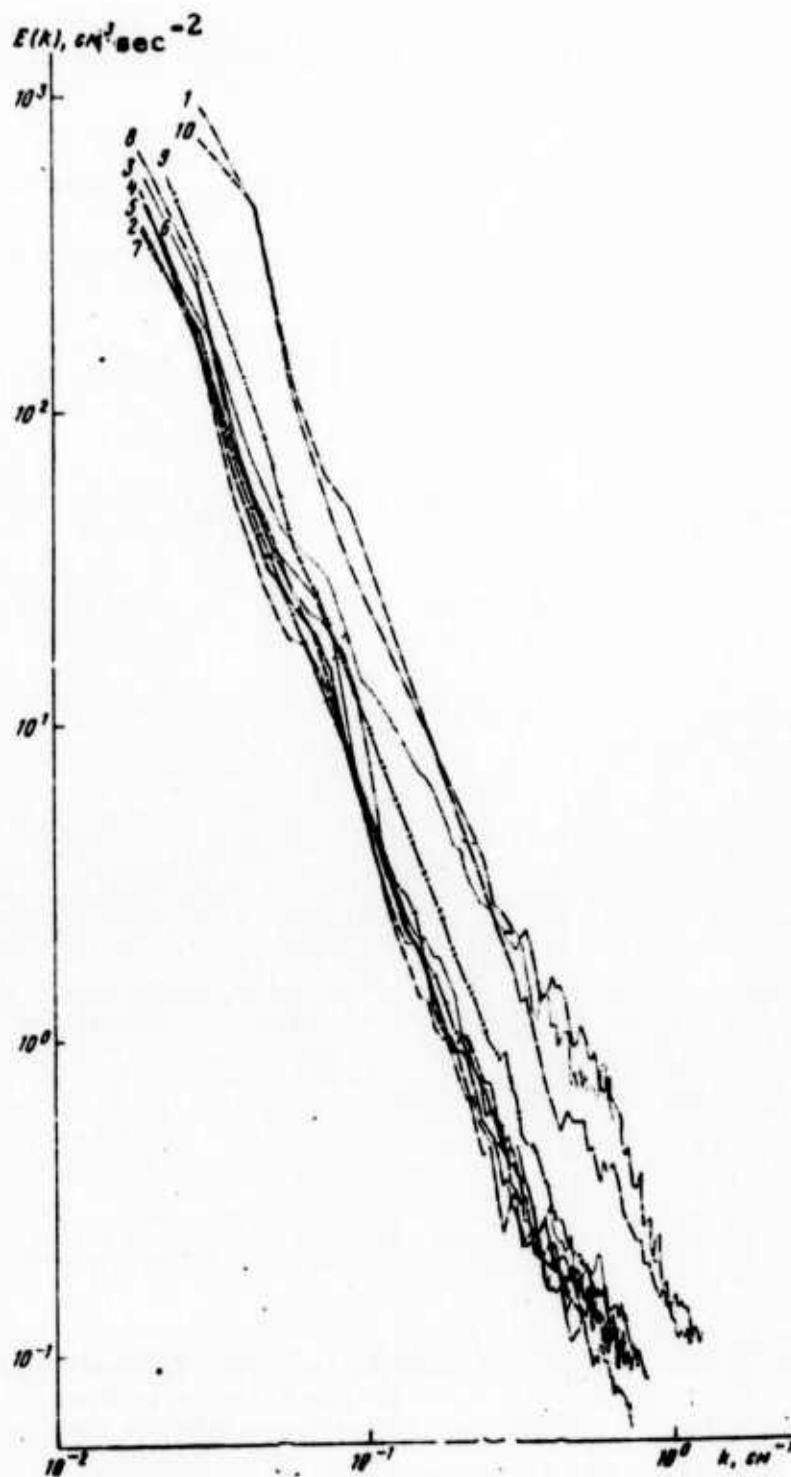
Fig. 5. Spectral densities of velocity fluctuations based
on measurements during the 7-th cruise of R/V Dmitriy
Mendeleyev (test area VI).

Curves 1-10 - depths 90, 136, 142, 150, 163, 176, 142,
128, 104, and 80 m, respectively.
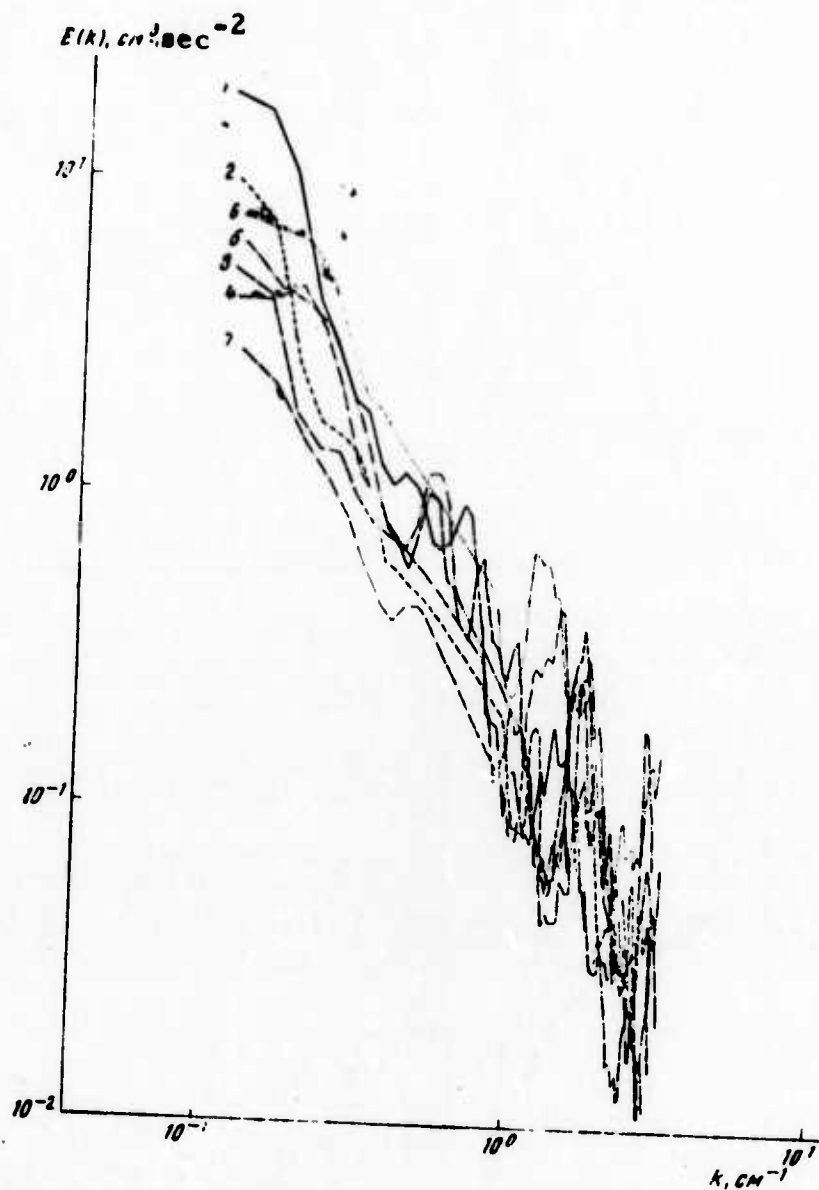
Fig. 6. Spectral densities of velocity fluctuations based on measurements during the 7-th cruise of R/V Dmitriy Mendeleyev (test area VIII).

Curves 1-7 - depths 55, 95, 110, 141, 161, 170 [sic], and 170 m, respectively.
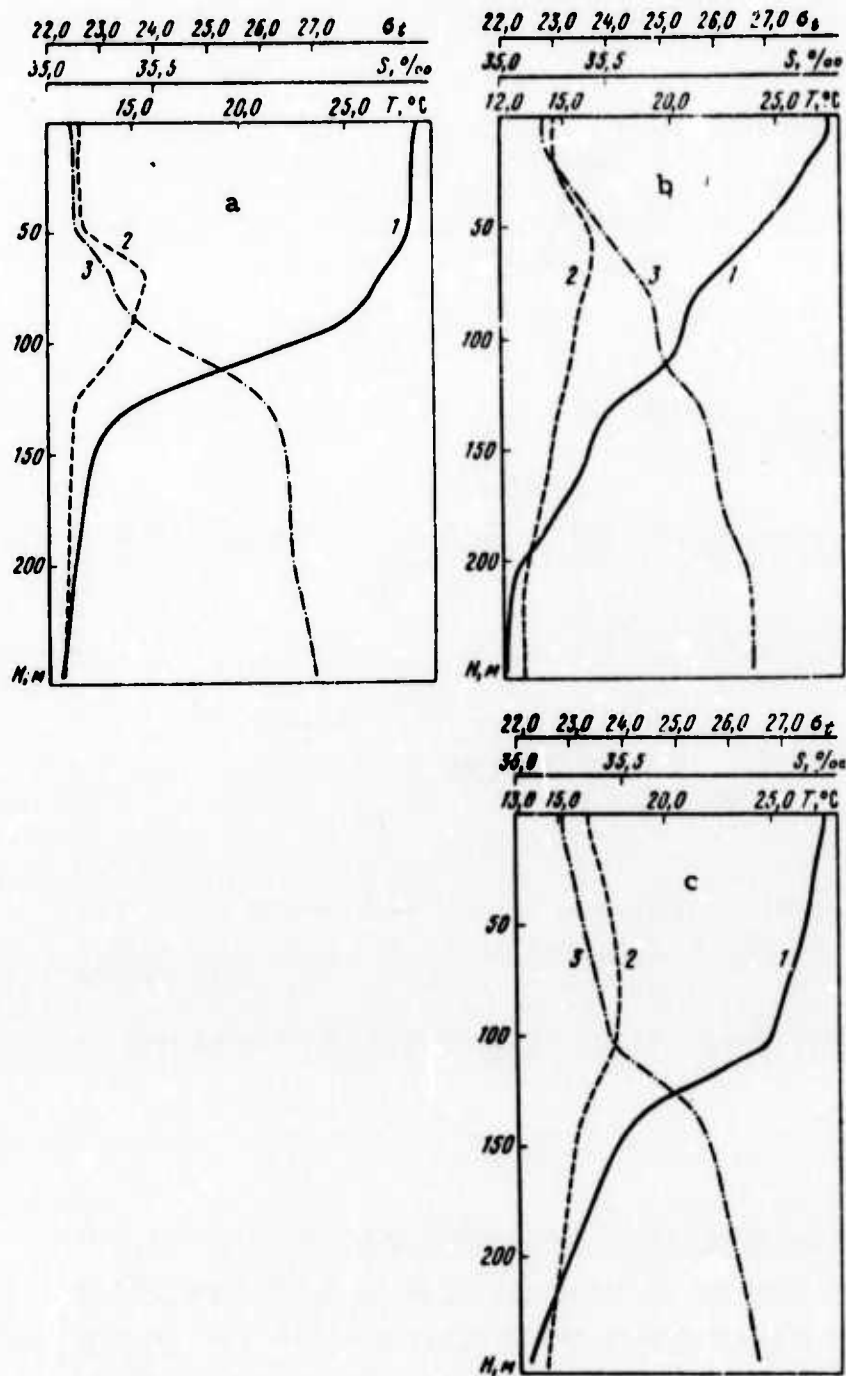
Fig. 7. Vertical profiles of water temperature (1),
salinity (2) and density (3), measured during the 7-th
cruise of R/V Dmitriy Mendeleyev

a- test area V; b- test area VI; c- test area VIII.
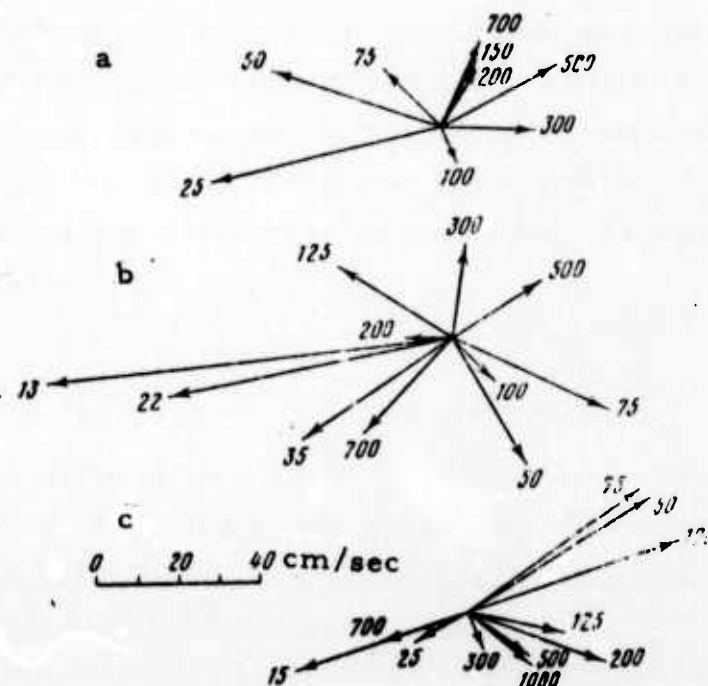
Fig. 8. Vertical distribution of current vectors measured during the 7-th cruise of R/V Dmitriy Mendeleyev.

a- test area V; b- test area VI; c- test area VIII.

Belyayev, V. S. <u>Recording and processing techniques in the measurement of small-scale turbulence in the ocean.</u> IN: Issledovaniye okeanicheskoy turbulentnosti (Study of ocean turbulence). Moskva, Izd-vo Nauka, 1973, 44-48.

Some problems of recording and processing of data on small-scale turbulence in the ocean, based on experience of the Institute of Oceanology of the USSR Academy of Sciences from 1969 to 1972, are

discussed. Examples are given for function check and calibration of the computer input channel, as well as for the conversion from machine to physical units. It is demonstrated that reliable signal quantization can be accomplished if its frequency range does not exceed 1-1.5 decade. The importance, during an experiment, of the determination of the variation of sensor sensitivity at any given towing speed, the amplification factor of the measuring circuit, and the transmission coefficient of the analog tape recorder, is stressed.

Ozmidov, R. V., A. N. Gezentsvey, Le-Kuang-
Toay, S. S. Murav'yev, and J. M. Tatarayev.
Experimental study of diffusion of indicators
artificially introduced into the sea. IN: Issledovaniye
okeanicheskoy turbulentnosti (Study of ocean turbulence).
Moskva, Izd-vo Nauka, 1973, 64-78.

The results of studies of the diffusion of fluorescent dyes, conducted in the Black and Baltic Seas in 1968-1969, are described. The analysis of the data on the averaged fields of the dye concentration was performed within the framework of the semi-empirical theory of diffusion.

The experimental procedure is shown in Figure 1.
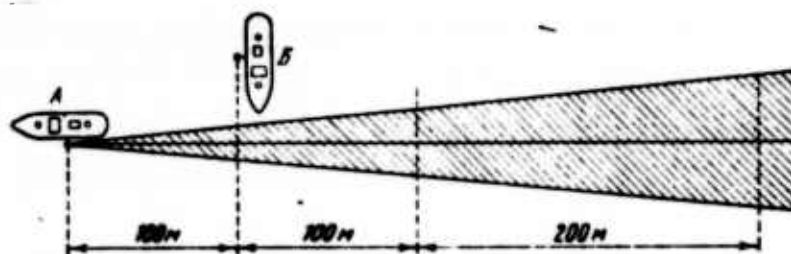
Fig. 1. Procedure for experiment with a continuous point source of the dye.

Some examples of the average dye concentration along profiles perpendicular to the wake are shown in Fig. 2.
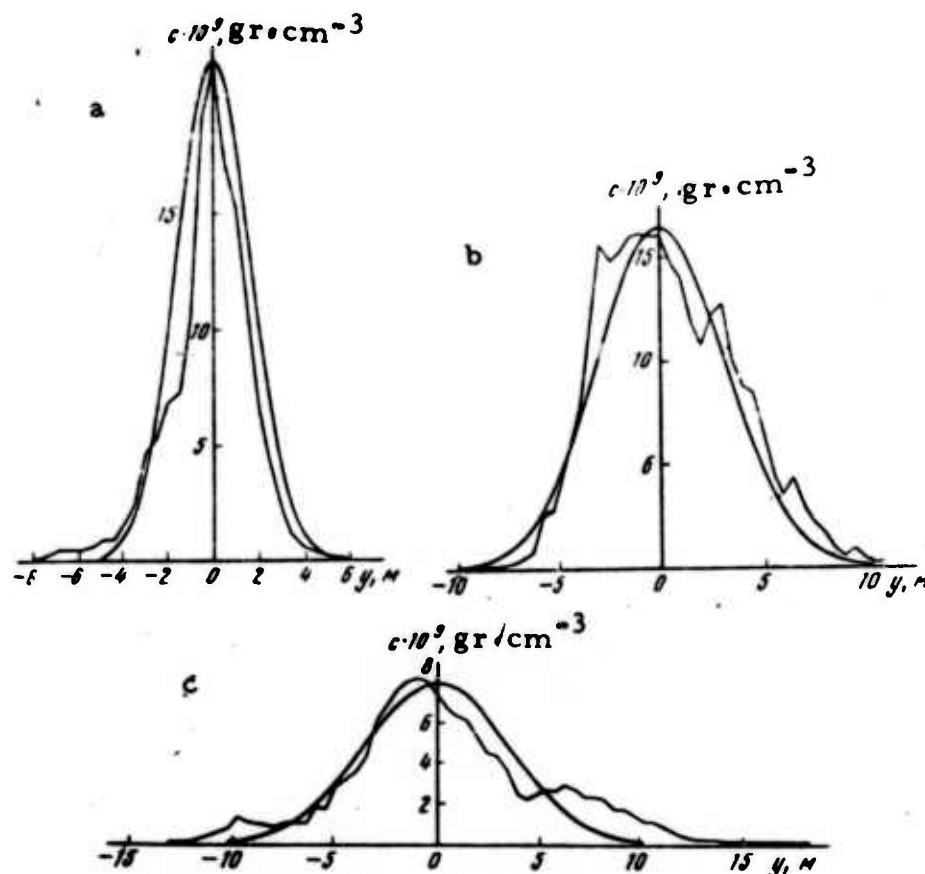
Fig. 2. Averaged profiles of dye concentration (broken lines) and theoretical curves at 100 m (a), 250 m (b) and 300 m (c) from source.

The coefficients of turbulent diffusion K_y and K_z determined from experimental data were found to be of the same order of magnitude and to range from several to several hundreds of CGS units. It was also found that the dye concentration decreases along the longitudinal axis of the wake according to a power law, the power being - 3/2.

The horizontal anisotropy of diffusion in the sea was studied using the experiment as shown in Figure 3. The results of the experiment are shown in Figure 4.
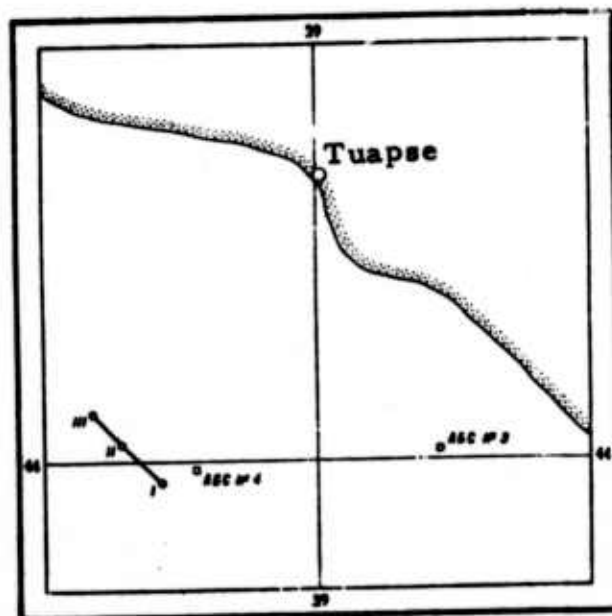
Fig. 3. Location of two self-recording buoy
systems (squares) and motion of a dye-spot
center during an experiment in the Black Sea in
1968 (I, II, III - recordings).

The vertical current velocity gradient determined from
experimental data was found to be $58.5 \times 10^{-4} \ sec^{-1}$.

Spectral densities of the fluctuations of dye concentration
calculated from the data of experiments with dye spots are given in
Figures 5 and 6.
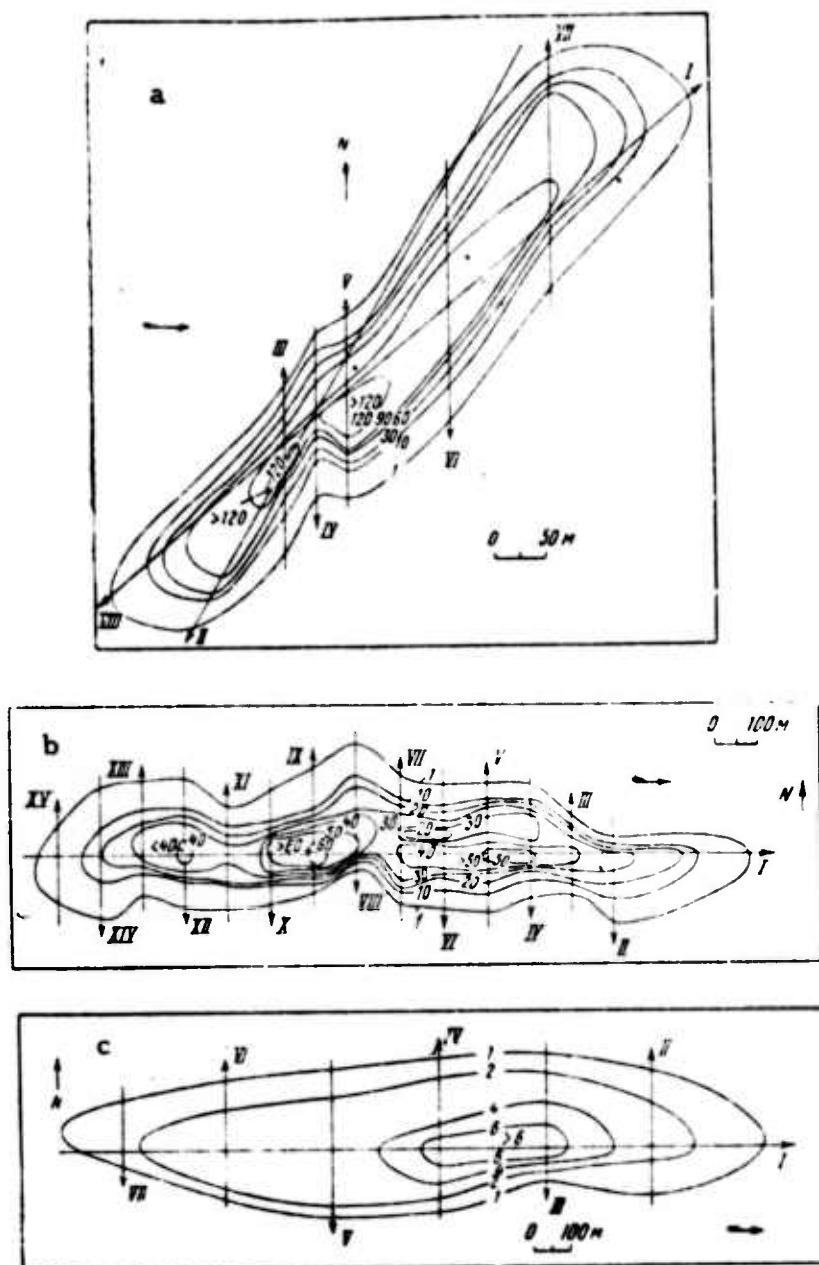
Fig. 4. Distribution of the dye concentration in the spot (in 10^{-9} gr/cm^3).

a - Recording I - 1137 - 1205 hours;
b - recording II - 1328 - 1430 hours;
c - recording III - 1657 - 1747 hours.
Short arrows - wind direction; long arrows - vessel tracks.
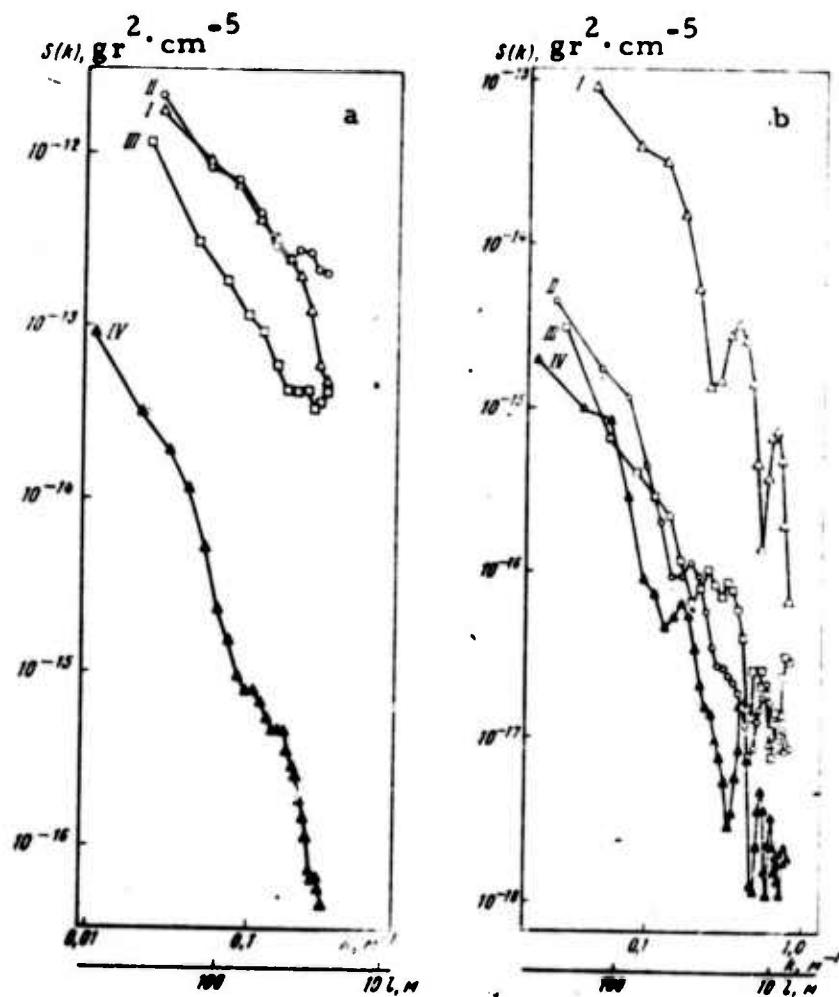
Fig. 5. Spectral densities of the fluctuations of the dye concentration.

a- Black Sea at a depth of 0.5 m; b- Baltic Sea at a depth of 1 m.
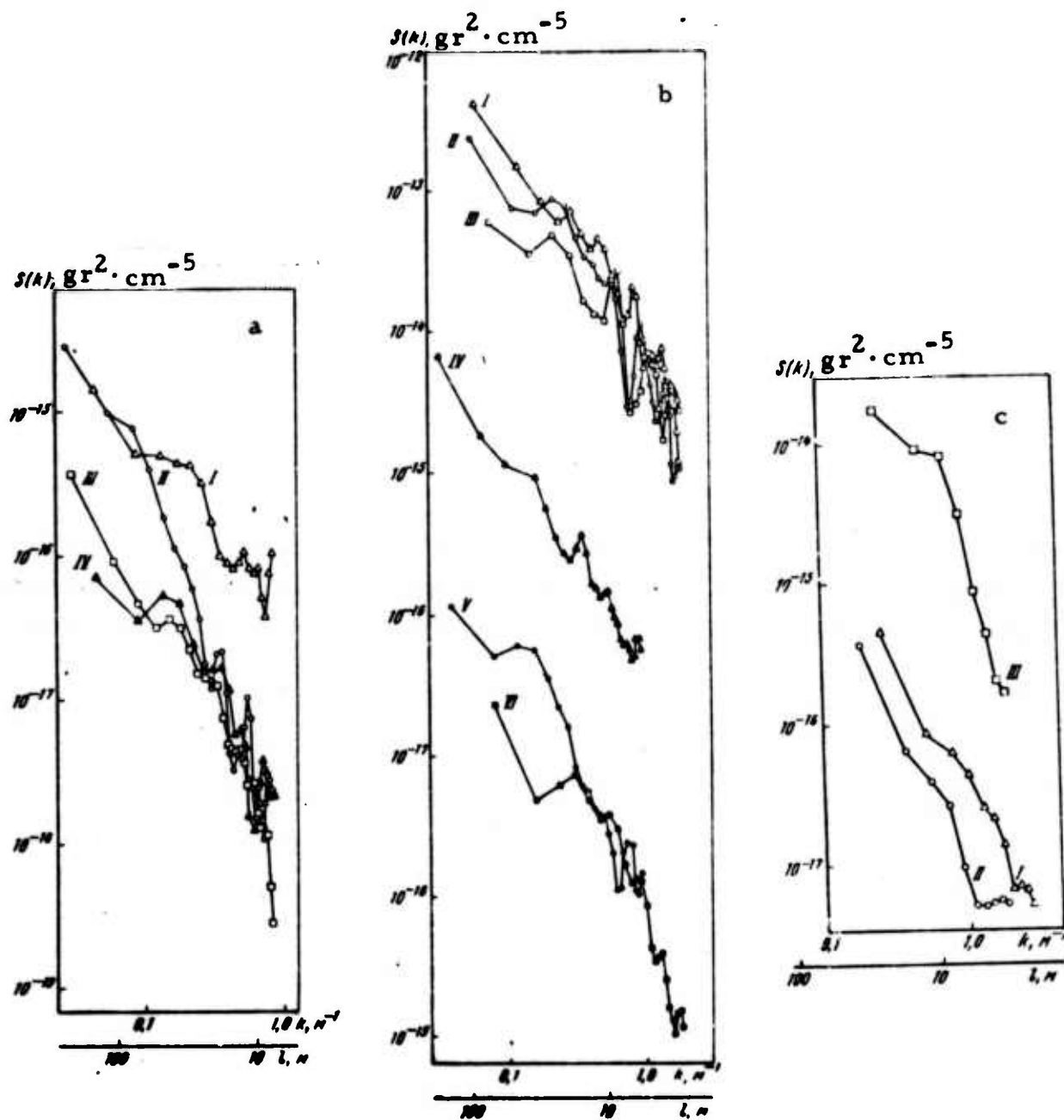
Fig. 6.   Spectral densities of the fluctuation of the dye concentration.

a- Baltic Sea at depths of 1 m (curves II and III) and 7.5 m (curves I and IV);
b- Baltic Sea at a depth of 0.5 m.; c- Baltic Sea at a depth of 0.5 m.

Pozdynin, V. D. Determination of vertical current-speed gradients in the ocean using BPV-2 current meters. IN: Issledovaniye okeanicheskoy turbulentnosti. (Study of ocean turbulence). Moskva, Izd-vo Nauka, 1973, 79-85.

A method is proposed for the calculation of vertical gradients of current speed, based on methods for testing statistical hypotheses on the random fluctuation of data within a sample, an equalities of dispersions and mean values at the upper and lower boundaries of a layer. An example is given of the calculations of vertical gradients in the meridional and latitudinal directions, using data from a 3-day buoy station in the equatorial part of the Atlantic Ocean (2nd cruise of the R/V Dmitriy Mendeleyev).

It is concluded that measurements of the current speed at buoy stations using BPV current meters vertically spaced 25 m apart make it possible to estimate vertical gradients reliably if they exceed 1 cm/sec/m.

Pozdynin, V. D. On some advantages and disadvantages of experimental studies of small-scale turbulence in the ocean. IN: Issledovaniye okeanicheskoy turbulentnosti (Study of ocean turbulence). Moskva, Izd-vo Nauka, 1973, 94-103.

An analysis is made of the advantages and disadvantages of various platforms used to carry measuring equipment: large research ships, drones, conventional and special research submarines, bathyscaphs, and buoys. Emphasis is put on the timeliness and efficiency of conducting measurements from a conventional submarine under the most severe storm conditions and under Arctic ice. Accelerated development of the metrological support to studies of turbulence and new instrumentation for measuring background hydrological conditions are recommended.

Vorob'yev, V. P., Ye. T. Kuznetsov, and V. I.
Fedonov. Hot-probe current-speed pulsation meter.
IN: Issledovaniye okeanicheskoy turbulentnosti (Study
of ocean turbulence). Moskva, Izd-vo Nauka, 1973,
149-153.

A description is given of a current-speed fluctuation meter, based
on the hot-probe principle, developed in the Institute of Oceanology of the
USSR Academy of Sciences in 1968-69.

The instrument sensor (shown in Fig. 1) consists of a thin
platinum film applied to a substrate of optical quartz glass. The thin film
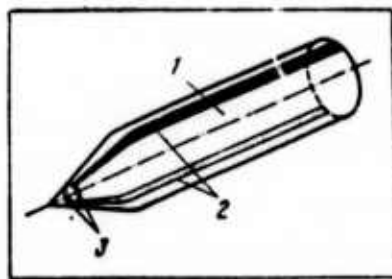
Fig. 1. Schematic of the speed fluctuation meter
sensor (scaled up).

1- substrate; 2- leads; 3- sensor element.

forms a ring 2 mm from the tip. The resistance of the film is 4-6 ohm, its
temperature coefficient of resistance is $2.1\text{-}3.0 \times 10^{-3}\ ^{\circ}C^{-1}$, the dimensions
of the ring are 4 x 0.2 x 0.0001 mm. A block diagram of the instrument is shown
in Figure 2, and its measuring bridge is shown in Figure 3. The specifications of
the instrument are: Operating frequency range ....1.5-150 Hz; Level (rms)
of the instrument noise... 0.12 mm/sec; $1^{\circ}C$ temperature change is equivalent
to a velocity change of 20 cm/sec. (at heatup to $20^{\circ}C$).
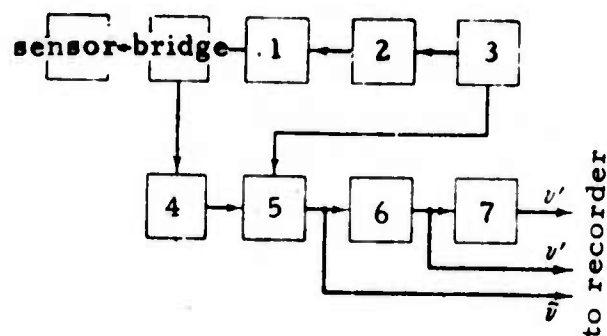
Fig. 2. Block diagram of the current speed fluctuation
meter.

1- power amplifier; 2- heating control; 3- driving
oscillator; 4- imbalance amplifier; 5- DC receiver;
6- fluctuation amplifier; 7- recording amplifier.
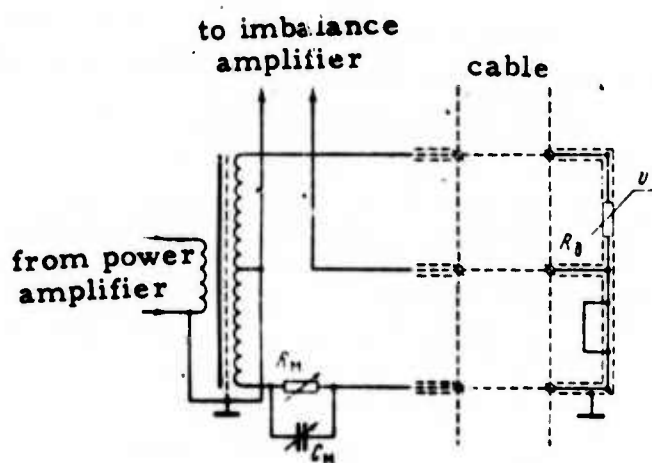
Fig. 3. Measuring bridge of the current-speed
fluctuation meter.

Korchashkin, N. N., and R. V. Ozmidov.
Problems in using lowered instruments to
study the fine structure of hydrophysical fields
in the ocean. IN: Issledovaniye okeanicheskoy
turbulentnosti (Study of ocean turbulence).
Moskva, Izd-vo Nauka, 1973, 154-160.

An analysis is made of distortions introduced into vertical
temperature profiles measured by the AIST STD meter, caused by instrument
inertia and erratic descent rate due to ship roll.

Distortions due to instrument inertia are manifested in a
smoothing of step-like vertical temperature profiles. Thus, instead of horizontal
"steps" with infinite vertical gradients, the instrument records a gradual
decrease of temperature. The dependence of measured gradients on the
temperature jump $\Delta \theta$ calculated for various descent rates V, using a
derived formula, is given in the Table below.

Table 1

$\Delta\theta$, °C	v, cm/sec			
	30	50	70	100
0,10	0,0067	0,0040	0,0029	0,0020
0,13	0,0087	0,0052	0,0037	0,0026
0,16	0,0107	0,0064	0,0046	0,0032
0,19	0,0127	0,0076	0,0054	0,0038
0,22	0,0147	0,0088	0,0063	0,0044
0,25	0,0167	0,0100	0,0071	0,0050
0,28	0,0187	0,0112	0,0080	0,0056
0,31	0,0207	0,0124	0,0089	0,0062
0,34	0,0227	0,0136	0,0097	0,0068
0,37	0,0247	0,0148	0,0106	0,0074
0,40	0,0267	0,0160	0,0114	0,0080
0,43	0,0287	0,0172	0,0123	0,0086
0,46	0,0307	0,0184	0,0132	0,0092
0,49	0,0327	0,0196	0,0140	0,0090
0,52	0,0347	0,0208	0,0149	0,0104

The effect of ship motion on the measured temperature gradients is illustrated in Figure 1.
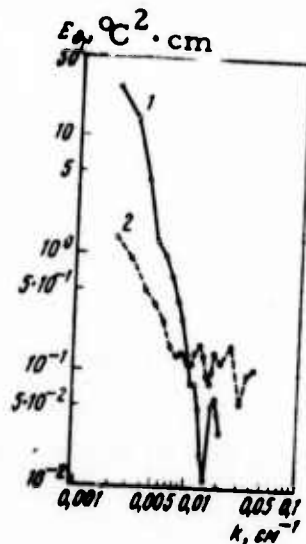
Fig. 1. Spectral densities of temperature fluctuations (period and amplitude of ship roll 10 sec and 2 m, respectively).

1- descent rate 70 cm/sec; 2- descent rate 30 cm/sec.

Pozdynin, V. D. Evaluation of modern
oceanological instruments on the basis of
information theory of measuring devices.
IN: Issledovaniye okeanicheskoy turbulentnosti.
Moskva, Izd-vo Nauka, 1973, 86-93.

An analysis is given of characteristics of instruments for
measurement of small-scale ocean turbulence and background vertical
distribution of flow velocity, based on information theory. An example is
given for evaluating the feasibility of turbulence meters, using as a criterion
the index $pC = lgC/lgW_n$ where C is energy threshold and W_n is thermal noise.
In addition, an example is given for the evaluation of the information capability
of a chain of sensors for measuring the rate and direction of flow velocity.
The author notes that thresholds of existing sensors are in the range of
10^{-12}--10^{-16} joule.

The calculations show that a turbulence meter with characteristic
as shown in Fig. 1 is feasible, since its pC index (0.31) falls within the range
of existing instruments (0.11-0.89).
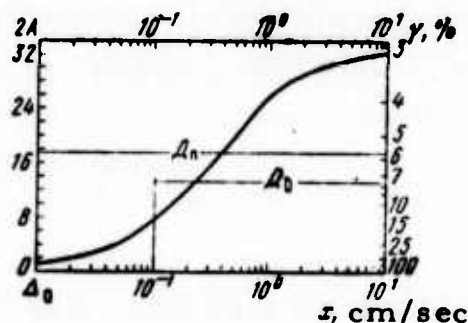
Fig. 1. Graph of instantaneous accuracy of
measures of flow velocity pulsations in the ocean.

A = accuracy; γ = relative (entropy) error;
Δ_O = 0.01 cm/sec = absolute (entropic) zero
error; D_o = optimal response range of
instrument.

The author also shows that each measuring channel of a sensor chain with a vertical spacing of two meters, required to measure flow velocity changes from 1-30 cm/sec approximately, with $\gamma = 0.05$ can reliably detect velocity differences of 0.4 cm/sec (see Fig. 2).
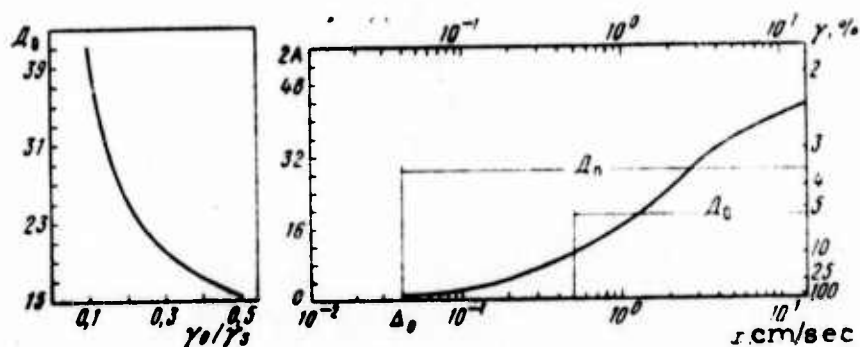
Fig. 2. Optimal response range D_o vs. ratio of relative null error γ_0 and sensitivity γ_s.

Benilov, A. Yu. Evaluation of statistical characteristics of random hydrodynamic fields in the upper ocean layer: IN: Issledovaniye okeanicheskoy turbulentnosti, Moskva, Izd-vo Nauka, 1973, 49-63.

Statistical characteristics of temperature $T(t)$ and wave $\xi(t)$ fields in the upper ocean layer were analyzed, using data acquired in the Mediterranean Sea in 1968. The segregation of turbulent $T_T(t)$ and wave $T_\omega(t)$ components from the overall turbulence expression $T(t)$ was made, using a linear approximation. A possibility was demonstrated for the recovery of the $T_T(t)$ component using the non-linear transformation $T_\omega(t) = g[\xi(s)]$.

Some results of the spectral analysis are shown in
Figs. 1-6.
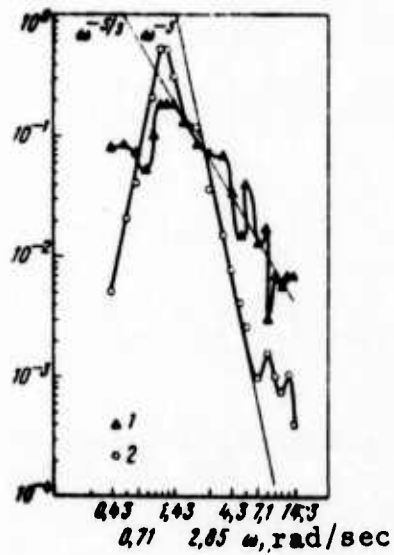
Fig. 1. Normalized spectral densities of
T(t) (1) and ξ(t) (2).
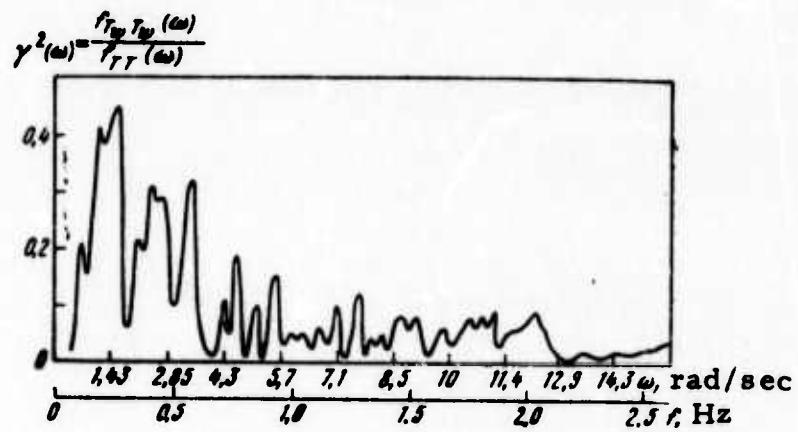
Fig. 2. Fraction of wave noise in the
spectral density T(t).
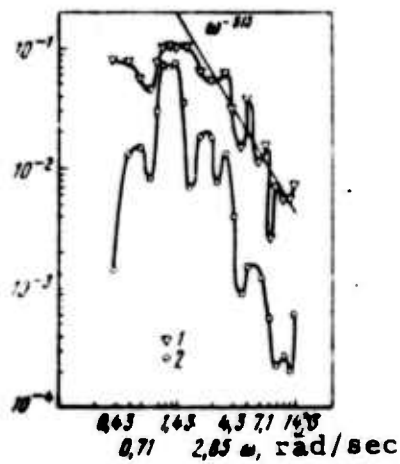
Fig. 3. Normalized spectral densities of $T_T(t)$ (1) and $T_\omega(t)$ (2).
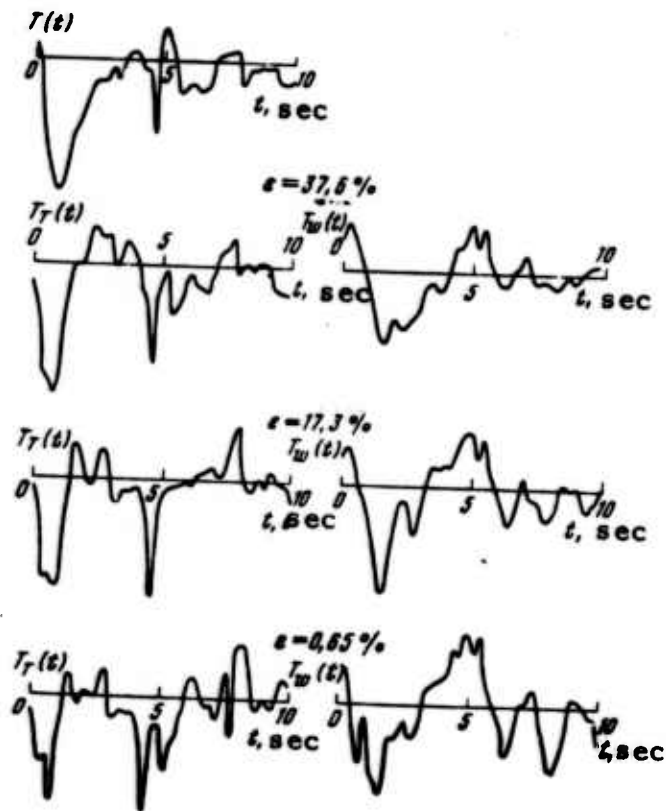
Fig. 4. Forms of $T_T(t)$ and $T_\omega(t)$ at different filtration errors ε_m.
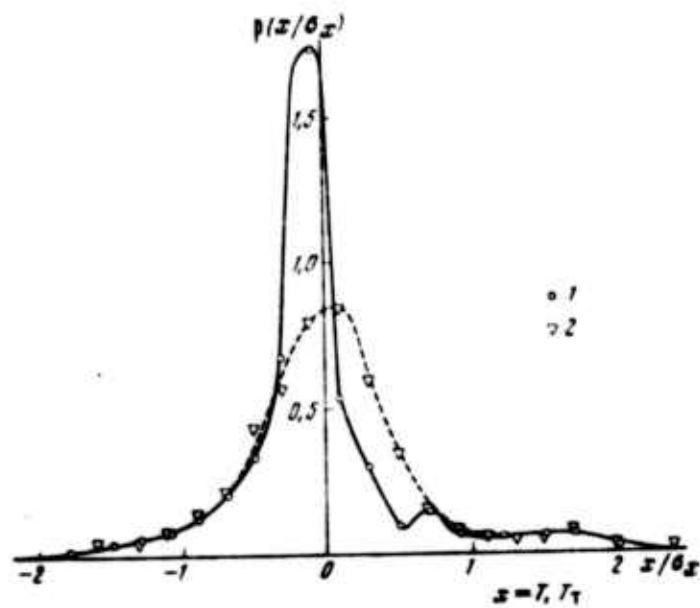
Fig. 5. Probability distribution densities
of T(t) (1) and T_T(t) (2).
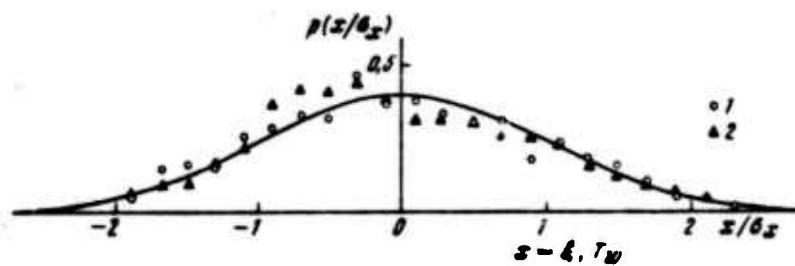
Fig. 6. Probability distribution densities
of ξ(t) (1) and T_w (t) (2).

Palevich, L. G., G. N. Panin, V. D. Pozdynin, and V. I. Fedonov. Test and calibration of turbulimeters for experimental studies in the ocean. IN: Issledovaniye okeanicheskoy turbulentnosti (Study of ocean turbulence). Moskva, Izd-vo Nauka, 1973, 161-168.

A description is given of the calibration and maintenance of turbulimeters developed by the Institute of Oceanology of the USSR Academy of Sciences. Data are presented on the stability and reproducibility of the turbulent regime of a test stand with fully immersed flow, used for the calibration of turbulimeters.

The first part of the calibration procedure includes determination of the following instrument characteristics: the dependence of the output voltage on the average flow speed; sensitivity to velocity fluctuation at a medium flow speed; amplitude-frequency response; and instrument noise level.

The second part of the procedure is conducted in accordance with the information theory of instruments. It includes the determination of:

a). graph of instantaneous measurement accuracy (see Fig. 1) using formula $A = V/2(\gamma_0 + \gamma_s V)$, where γ_0 is error of determination of the instrument zero level, γ_s - error of determination of instrument sensitivity, V - instantaneous value of velocity fluctuation;

b). resolution, using formula $R = \frac{1.15}{\gamma_s} \lg \frac{\gamma_0/\gamma_s + 1}{\gamma_0/\gamma_s + v_{min}/v_{max}}$.
where v_{max} and v_{min} are the limits of the instrument range;

c). optimum range, using formula $R_{opt} = \frac{2 + 6.6\gamma_0/\gamma_s + 3(\gamma_0/\gamma_s)^2}{\gamma_0/\gamma_s}$.

An example of the instantaneous accuracy of a turbulimeter is shown in Figure 1.
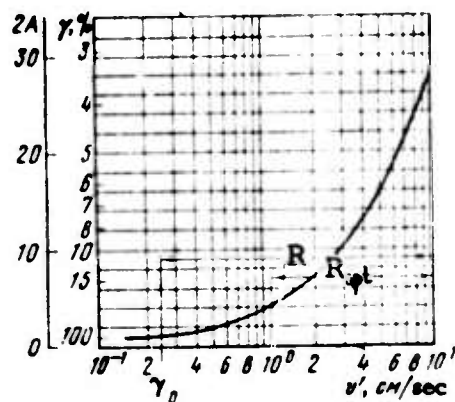
Fig. 1. Graph of instantaneous accuracy of the hot-probe current meter of the Institute of Oceanology, USSR Academy of Sciences.

A comparison of the characteristics of a DISA production model hot probe (55D01) which was used as a standard, and the hot probe of the Institute of Oceanology, is given in the table below.

Table 1

| Instrument | Range | | Sensitivity, V/cm/sec | Error, rms | | Resolution | |
	dynamic	frequency, Hz		instrument sensitivity, V/cm/sec	instrument zero, cm/sec	measurement gradations	gradation value
DISA model 55D01 hot probe	50	0-500	0.63	0.004	0.10	18	0.57
Hot probe of the Institute of Oceanology	60	1.5-150	0.65	0.005	0.12	16	0.60

Pivovarov, A. A., and Vo Van Lan'.
Nature of the change in coefficient of turbulent
heat exchange in a stratified ocean. VMU,
no. 1, 1974, 3-7.

This article deals with calculation of the turbulent heat
exchange coefficient, k, using experimental data on annual temperature t
and salinity S variations in a stratified ocean. The t and S data were obtained
from measurements of t, S and density vertical profiles at two geographical
points: 21° N latitude and 158° W longitude (I) and 50° N latitude and 145° W
longitude (II) in the Northern Pacific. The measurements were made over
a period of one year in 1958 and 1960.

The formula

$$k = \frac{n\omega}{\rho^2 A_n^2 \frac{d\varphi_n}{dz}} \int_h^z \rho^2 A_n^2(z)\, dz, \tag{1}$$

where A_n and φ_n are the amplitude and phase of the nth harmonic of a
t wave over a given period T; h is the depth at which t fluctuations become
insignificant; and z is the instantaneous vertical coordinate,is used to
calculate k for a given ρ profile. It is shown that the first harmonic
(n = 1) sufficiently approximates annual t variations, hence A_1 and φ_1
were used in k calculations. The tabulated k data (Table 1) decrease rapidly
from the surface to a certain z, then increase continuously with further
increase in z. The pattern of k variations is closely related to the dt/dz
(Fig. 1) and stability of the body of water profiles at the two points.

Comparison of the k data in Table 1 with the dt/dz data in
Fig. 1 and the dS/dz data [not shown] indicates that the k minimum is
observed at the same level as the dt/dz maximum or maximum stability, if
the dt/dz and dρ/dz maxima coincide. This conclusion led to an approximation

21°N lat.	158° W long.	50° N lat.	145° W long.
depth, M	k, (cm^2/sec)	depth, M	k, (cm^2/sec)
30	31	15	10.3
70	21	25	3.6
110	17	35	1.3
150	17	45	0.77
190	11	55	0.70
230	6.5	65	0.98
270	5.2	75	1.4
310	21	85	1.4
350	27	95	2.1
-	-	105	5.4
-	-	115	6.3
-	-	125	6.6

Table 1.   Vertical profile of k in points I and II.
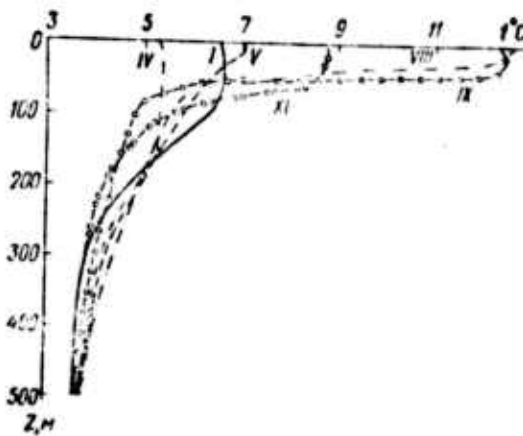
Fig. 1.   Vertical water t profile at different times (Roman numerals indicate months of the year).

of k variations by the expressions

$$k = k_0\left(1 + a\frac{dt}{dz}\right)^\alpha.$$ (2)

$$k = k_0(1 - AE_0)^\beta,$$ (3),

where k_0 is the k value at $dt/dz = 0$ or $E_0 = 0$, respectively. Analysis
showed that Eq. (2) at $\alpha = 1$ and Eq. (3) at $\beta = 1$ closely approximate
the k values calculated from (1) with the use of experimental data to
120-150 m and 90-110 m depths, respectively. Hence, the mean annual
variation of k vs. depth in a stratified ocean can be described by linear
equations of the (2) and (3) types, depending on the initial data characteristics.
Eqs. (2) and (3) can also be used as a base of calculations of $dk/d\gamma$ variations
(γ = time) over the period of one year.

Zykov, I. D., A. P. Nagurnyy, V. G.
Savchenko, and M. A. Chepurina.
<u>Distribution law of current velocity</u>
<u>components and water temperature.</u>   IN:
Trudy Arktich. i antarktich. n. -i. in-ta,
Leningrad, vol. 312, 1974, 27-31.

Statistical characteristics of current velocity components
and water temperature are calculated from selected data obtained in a
hydrophysical test area in the Atlantic during the 11th cruise of the R/V
Professor Vize. The coordinates of the buoy station 20 were $53°47.8'$ N
latitude and $17°37.8'$ W longitude. The mean value, the i-th moment
($i = 2, 3, 4$) around the distribution center, the asymmetry factor A, and
the coefficient $\mathcal{E}$ of excess are calculated for the meridional(u) and zonal(v)
current velocity components (Fig. 1) and water temperature t (Table 1).
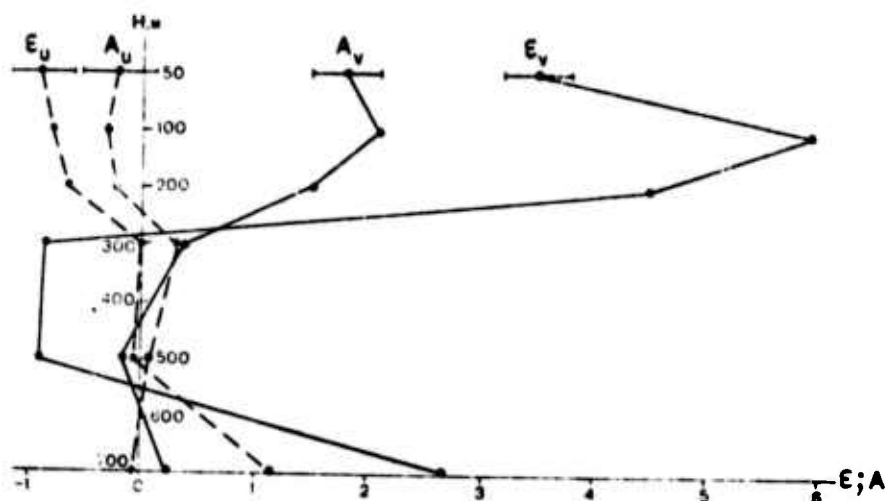
Fig. 1. Variations in depth of A and $\mathcal{E}$ for components u and v. Horizontal lines are confidence intervals with 0.80 confidence coefficient.

Depth level	T, °C	σ_t, °C	A	ε
50	11,20	0,27	0,14	—0,66
200	10,24	0,28	0,05	—0,16
500	8,87	0,66	0,00	—1,58

Table 1. Statistical distribution of water temperature. T = arithmetic mean, σ_t - rms deviation.

Fig. 1 shows a sharp difference between the A and $\mathcal{E}$ values for u and those for v. The A and $\mathcal{E}$ distributions in depth determined the goodness-of-fit test λ value of empirical distribution F_e versus theoretical normal distribution F_T. The difference $(F_e - F_T)$ is considered insignificant, if the calculated probability $P(\lambda) > 0.05$. The calculated $P(\lambda)$ (Table 2) shows that v distribution, except at 300 m depth, does not satisfy a normal distribution law. The empirical distribution of u component is in satisfactory

Medium parameter	Depth level					
	50	100	200	300	500	750
u	0.07	0.15	0.18	0.88	0.67	0.00
v	0.00	0.00	0.00	0.10	0.03	0.00
t	0.06	—	0.07	—	0.00	—

Table 2. P(λ) values for velocity components and water temperature (Station 20).

agreement with the theoretical distribution at all depth levels except 750 m.   Also, t at the 50 and 200 m levels approximately follows a normal distribution.   The horizontal anisotropy (component v) of current velocity is attributed to a relatively stable orientation of the average current along a parallel.

The tabulated P(λ) values for u and v components, from observation data of the buoy stations located 5 and 10 miles from Station 20, generally confirmed the spatial stability of distribution characteristics of u and v.   Anisotropy of the u component is weak, although the number of levels at which $F_e - F_T = 0$ decreased.

In summary, the distributions of u and v components and water t under complex hydrological conditions in the testing area satisfied the normal distribution law at certain depth levels only.   Distribution of the u component agrees with the normal distribution law more often than distribution of the v component.

Borisenkov, Ye. P., O. A. Vladimirov, A. P. Nagurnyy, and V. G. Savchenko. Structural functions of current speed components and water temperature for a hydrophysical test area in the Northeast Atlantic. IN: Trudy Arktich i antarktich n. -i. in-ta, v. 312. Issledovaniya po programme POLEKS, Leningrad, 1974, 12-19.

Structural functions are calculated from data obtained in 1971 by three buoy stations in the test area of Rockall Bank. The functions are

$$D(\tau) = \overline{[T(t+\tau) - T(t)]^2}, \tag{1}$$

where $T(t)$ is the value of the studied variable at an initial time or initial point, $T(t + \tau)$ is the value of the same variable at an interval τ from the first, and τ is expressed in units of time or space. The functions $D(\tau)$ thus calculated are analyzed to determine the limits of applicability of the 2/3 exponential law to the observed current velocity components u and v and water temperature data.

Typical $D(i)$ plots, where $i = 3\tau$, are shown for the zonal velocity component v (Fig. 1) and temperature (Fig. 2) data from one station. At all depth levels below 100 m, the portions of the $D(i)$ curves in Fig. 1 within 6 to 16 hour periods satisfy the 2/3 exponential law. The closest agreement with the cited law is noted for particular levels at the three stations. The law is satisfied within 2 to 4 hour periods. The cited data indicate that $D(i)$ of the current velocity components may vary significantly within a relatively short horizontal distance (10-15 mi). The $D(i)$ functions of temperature at most depth levels obey the 2/3 exponential law (Fig. 2).
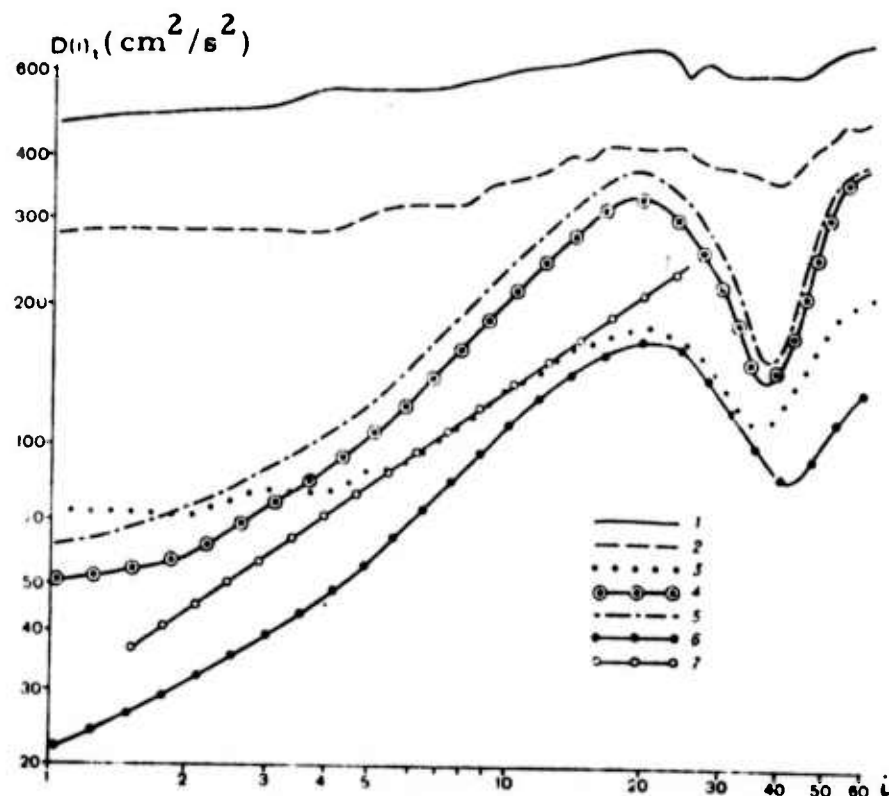
Fig. 1. Structural functions of v component at the 50, 100, 200, 300, 500, and 750 m levels (1, 2, 3, 4, 5, and 6, respectively) for buoy station 20; 7 is the theoretical plot according to the 2/3 exponential law.
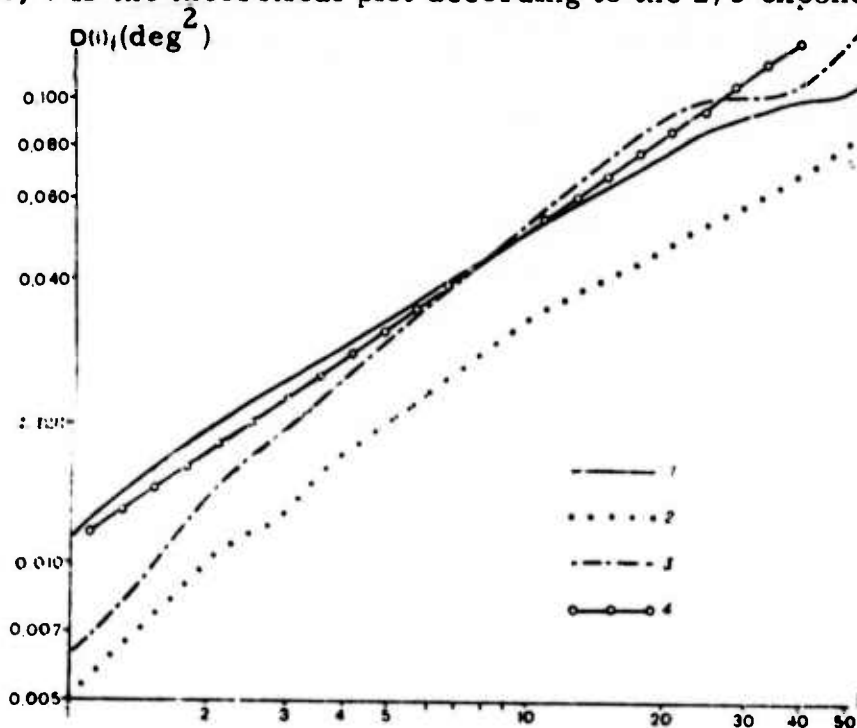
Fig. 2. Structural functions of sea water temperature at the 50, 200, and 300 m levels (1, 2, and 3, respectively) for buoy station 20; (4) is the theoretical plot according to the 2/3 law.

Comparison between D(i) of current velocity and D(i) of temperature shows significant differences. First, the 2/3 law is satisfied within a wider time interval for temperature fluctuations than for fluctuations of current velocity components. Secondly, the observed water temperature data are quite well approximated by the cited law not only at the deep levels but also at the upper levels. The noted differences are attributed to the different nature of horizontal and vertical distributions of the temperature and velocity fields in a thermally homogeneous water. Eddies do not cause significant temperature fluctuations hence D(i) of temperature does not deviate from the 2/3 law in a locally, horizontally homogeneous water in the test area.

Random errors of the velocity vector components and temperature measurements are evaluated by analyzing D(i). The total random error ξ is evaluated as the sum $(\alpha + \beta)$ of the random errors of the instrument and the measurement method; the α^2 value of the instruments is known. The error β depends on positioning of the instrument (type BPV or FTG) at the recording buoy station. According to the normal distribution law, the mean standard deviation of β is calculated as

$$\sigma = (\pi/2 \cdot \eta)^{1/2} \tag{2},$$

where η is the mean absolute error of the measurement method. The tabulated σ and η values of the u and v components measurement are especially high (15-19.3 and 12-15.4 cm/sec, respectively) for the 50 and 100 m levels, but, as a rule, decrease at greater depth. The σ and η values of water temperature measurement practically approach zero at all levels. The authors conclude that the current velocity and direction data recorded by BPV instruments must be considered very suspect, at least for the active oceanic layer.

-47-

Sachkov, K. N., and R. I. Mukhtarov. The use of lasers to measure current velocities. IN: Trudy Gos. okeanograf. inst., no. 117, 1973, 78-90.

A basically new method is introduced for measurement of dispersed flow velocity with the use of lasers. It is shown that all existing laser-based velocity transducers, including the differential Doppler velocimeter, are not practical for measurement of sea current velocity because of their complicated optical systems. The new velocity measuring device uses a single-beam optical system, is refraction-insensitive, and independent of light propagation velocity within the medium.

The device is based on space-time analysis of interference patterns produced by laser beam scattering from dispersed particles in a flow. The interference patterns thus produced have been studied experimentally in a monodispersive suspension of lycopodium, illuminated with a single-mode He-Ne laser beam at 40 mW output power. A microscopic study of interference spots showed that their motion becomes oriented when the particle flow is oriented, and their shift velocity is also proportional to the flow velocity. In the case of an ordered motion of particles, mathematical treatment of laser radiation scattering in a flow indicates that the observed spotty structure is the result of superposition of regular oscillations of scattering field intensity I at the observation point (X, Y). The expression

$$\omega_{ij} \leq \frac{2\pi d v}{\lambda R}.$$ (1)

where R is the distance from a scattering particle to the point (X, Y), and ω_{ij} is the maximum characteristic frequency of intensity oscillations I (X, Y) can be used for a rough estimate of particle velocity v.

Further analysis of the $I(X,Y,t)$ expression led to the conclusion that the system of interference spots shifts along the observation plane at velocity $= v$, hence the dispersed flow velocity can be determined from the spot shift velocity data. The latter can be measured by placing an amplitude scanning grating in front of a photosensor. It is shown that the variable component of photo signal from a single spot motion contains harmonics with a frequency

$$\omega_m = 2\pi m v / T \tag{2}$$

where T is the grating period and m is the harmonic number. Thus the problem of determining v reduces to that of determining ω_m. The frequency of a photo signal from a system of interference spots fluctuates around a central frequency ω_f. The latter, and hence v, can be determined by analyzing the frequency spectrum of the photo signal. The mean frequency of the first harmonic of a h.f. signal is given by

$$\omega_f = 2\pi v / T \tag{3}$$

The T value is selected such that $\omega_f > \omega_{ij}$ is satisfied.

One possible arrangement of the interference method for measuring current velocity is shown in Fig. 1. Spectra of amplified signals
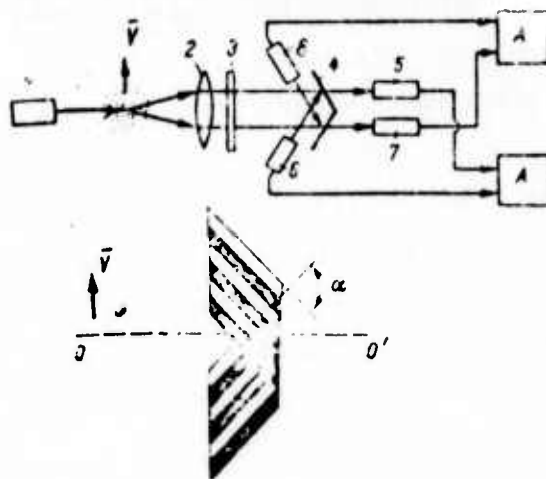
Fig. 1. Current velocity interferometer: 1- laser, 2- lens, 3- interference filter, 4- grating, 5,7- transmitted radiation sensors, 6,8- reflected radiation sensors.

-49-

from each pair of sensors are analyzed. Magnitude and direction of v vector is measured simultaneously by turning two gratings around the 00' axis to increase w to ω_{max}. Then v is normal to the bisecting plane of the gratings and its magnitude is given by

$$v - \omega_{max} \frac{T}{2\pi} \sin \frac{\alpha}{2} \qquad (4)$$

For measurement of the sea current velocity, both laser and sensor units may be located above or below the surface or the laser may be shipborne and photosensor unit below the surface. A large selection of lasers with tabulated characteristics is offered. A cw semiconductor laser is recommended to minimize dimensions of the device. A LG-106 argon gas laser emitting in the transmission range of sea water is cited as the most suitable for measuring sea current velocity. The resolution of the device with respect to v is evaluated on the assumption that the analyzer scans the spectrum from $\omega_1 < \omega_f - 1/2 \Delta\omega$ to $\omega_2 > \omega_f' + 1/2 \Delta\omega$. The maximum relative error of v determination is typically 1%.

Berezkin, G. V., and V. V. Khlopov.
Evaluating the vertical heat flow in the active
layer of the North Atlantic, from standard
observation data. IN: Trudy Arktich. i
antarktich. n.-i. in-ta, no. 312. Issledovaniya
po programme POLEKS, Leningrad, 1974, 46-52.

Vertical heat flow Q_z across the upper boundary z of the thermally active oceanic layer is evaluated. The study uses the water temperature data of deep-water hydrological stations of the R/V Professor Zubov at 60 to 70° N latitude in the North Atlantic (east of Iceland). The data were collected in 1969-1970 during the 3rd, 4th, and 5th cruises of the

vessel. The method used to evaluate Q_z was introduced by Kogutovskiy (Trudy LGMI, no. 24, 1967) and did not require a preliminary calculation of the coefficient K_z of eddy thermal diffusion.

Heat flow across z is calculated from

$$Q_z = K_z \frac{\partial T}{\partial z} = \frac{(H - z)(\overline{T}_2 - \overline{T}_1)}{t_2 - t_1} .$$ (1),

where (H-z) is the active layer thickness and $(T_2 - T_1)$ is the difference in average temperatures measured at times t_2 and t_1 in the same point of the layer H-z. It is assumed that the vertical T distribution functions converge at a point on the lower boundary H. There is heat release to the atmosphere if $Q_z < 0$ and heat influx across z, if $Q_z > 0$. In the region of observations, (H-z) was 200 m. The effect of currents was eliminated by making T_1 and T_2 curves converge at the H level. Time intervals between stations of a selected pair varied from several hours to several months.

The averaged Q_z values calculated for 15 groups of paired stations with $(t_2 - t_1) = 10-15$ h. for each pair are inaccurate, mainly as the result of the strong effect of diurnal variations of the heat balance components. The Q_z data obtained for the groups of stations with $(t_2 - t_1)$ longer than a day or a month are shown in Tables 1 and 2, respectively. Analysis of all tabulated data indicates that the absolute Q_z values in the active oceanic layer decrease as the $(t_2 - t_1)$ between the stations of each pair increases. At the same time, the data become more reliable as $(t_2 - t_1)$ is increased. It follows also from the cited data that Q_z is mostly <0 in the region of observations. It is shown that Q_z decreases rapidly at increasing depths down to 150 m; the bulk heat reserve of water is stored in the 0 to 100 m layer. Comparison of the present Q_z data with Q_z data obtained by two other methods with preliminary calculation of K_z shows that the Kogutovskiy method can be used in evaluating Q_z within relatively short

Group of Stations	Time intervals, h	Heat flow cal/cm² h	Group of Stations	Time interval, h	Heat flow, cal/cm² h
1	60	−200.0	13	78	−170.2
2	24	−60.0	14	60	26.7
3	24	25.0	15	82	17.1
4	96	−35.4	16	55	−30.3
5	24	8.4	17	97	−87.0
6	35	−80.0	18	123	8.2
7	112	−45.2	19	122	9.1
8	123	−18.8	20	36	−221.1
9	60	−150.0	21	25	−50.0
10	83	50.6	22	84	−30.9
11	98	−12.3	23	40	−120.0
12	124	−1.6			

Table 1. Vertical heat flow for stations with 24 to 120 hr. time intervals.

Group of Stations	Month	Days	Heat flow, cal/cm².day
1	December – May	146	−4.1
2	October – November	45	−106.6
3	October – December	61	−203.3

Table 2. Vertical heat flow for stations with longer than one month interval.

time intervals between consecutive hydrological stations. The conditions required to obtain reliable Q_z data are listed. It is concluded that in the region of observations heat is rel ased from the ocean to the atmosphere all year round, the rate being slower during warming than during cooling intervals.

Savchenko, V. G. Stability of internal waves near the interface of heterogeneous fluids. IN: Trudy Arktich i antarktich. n. -i. in-ta, vol. 312, 1974. Issledovaniya po programme POLEKS, 118-132.

The title problem is analyzed to establish instability criteria for internal waves propagating along a discontinuity layer between two

heterogeneous fluids. Instability of an internal wave is defined as the loss of its sinusoidal profile. An analytical solution to the stability problem is obtained for free internal gravitational waves propagating near the interface $z = 0$ of two ideal incompressible fluids of finite thickness $z = h_1$ and $z = h_2$. The Coriolis force is neglected.

By applying basic equations of fluid mechanics to each layer, the turbulence from internal wave propagation can be described by the Whittaker equation, if the Vaisala-Brunt period $N^2 = -g \, d/dz \, \log \bar{\rho}$ and the vertical gradients of average transfer velocity are assumed to be constant within each layer. The Whittaker equation is approximated by a modified Bessel differential equation of the $(1/4 - Ri)^{1/2}$ order, where Ri is the Richardson number. It follows that criteria for internal wave stability depend on whether $Ri > 1/4$ or $Ri < 1/4$ is satisfied. Instability criteria are derived for three particular cases by solving the known dynamic equation of pressure continuity at the interface and the modified Bessel equation for the upper and lower layers. The particular boundary cases are:

A) $\lambda \ll \min_j \left[2\pi \left| c - \tilde{u}_j \right| N_j^{-1} \right]$

$B_1)$ $\lambda \gg \max_j \left[2\pi \left| c - \tilde{u}_j \right| N_j^{-1} \right]$ and $Ri_j \, 1/4$, and

$B_2)$ " " " and $Ri_j < 1/4$,

where λ is the internal wave length, c is the complex propagation velocity of the internal wave, and $\tilde{u}_j$ is the current velocity in respective layer ($j = 1$ in the upper and $j = 2$ in the lower layer).

Only a very approximate analytical solution of the cited equations was obtained by introducing numerous limitations. The scope of the limitations is explained from both mathematical and physical standpoints. Physical interpretation of the B cases becomes evident from consideration of the corresponding inequalities by making $u = 0$. Then N^2 becomes the lower boundary of the internal wave periods over the entire fluid layer considered. The A case can be realized, because $N^2 = 0$, and hence the lower λ boundary at the interface is zero.

The following conclusions are made: 1) in contrast with previous findings, stable internal waves may exist at the interface of two heterogeneous fluids even at $0 < Rij < 1/4$ if their λ and hydrodynamic characteristics of the principal current are such that the derived instability criteria for the case A and B_2 are not satisfied; 2) in the B_1 case, the effects of the vertical velocity gradient of principal current and fluid heterogeneity are insignificant on wave stability at the interface, hence the instability criterion for homogeneous fluids is applicable; 3) in the A and B_2 cases generally the vertical velocity gradients may have some effect on wave stability at the interface; numerical examples show that the data obtained with allowance for the vertical current velocity gradient in the upper layer are not greatly different from the classical theory data; 4) the instability conditions corresponding to cases B_1 and B_2 are very rare in the world ocean; and 5) the derived criteria for internal wave instability are applicable only in the presence of a density discontinuity surface.

Khlopov, V. V. Methods for determining turbulent heat exchange in the ocean (review of research). IN: Trudy Arktich. i antarktich. n.-i. in-ta, vol. 312. Issledovaniya po programme POLEKS, Leningrad, 1974, 143-174.

Experimental research and calculation of turbulent heat exchange in the ocean are reviewed in relation to the general problem of the ocean-atmosphere interaction, which is the subject of the Polar Experiment (POLEKS) program. Soviet and Western open source materials are reviewed, including some 1972 Soviet publications. Two main directions of research are outlined and relationships between different parameters of turbulence are explained.

The methods for determining the vertical and horizontal coefficients of eddy thermal diffusion are treated separately. Indirect methods developed by Soviet scientists for calculating the vertical coefficient K_z are based on the heat equation (Shtokman, Pivovarov, Boguslavskiy, Zhukov, Tsikunov), energy balance equation (Laykhtman and Doronin, Kagan), or a simplified diffusion equation with the use of optical data for sea water (Voytov). Several types of deep-sea self-sustaining sensitive and quick-response turbulimeters have been designed by Kolesnikov et al. at the Marine Hydrophysical Institute (MHI). They have been used to measure turbulent exchange parameters from the Severnyy Polyus-4 and 6 drift stations and in the Antarctic regions of the Pacific and Indian Oceans. Thus far, only the Zhukov method has been successfully applied in the Arctic. It is believed that the methods based on solution of the energy balance equation could also be successful for K_z determination in the Arctic.

The horizontal eddy heat exchange in the ocean has been studied theoretically and experimentally by Ozmidov, Obukhov, Shtokman and others. Ozmidov developed theoretical requirements for instruments designed to measure statistical characteristics of turbulence field with a given error; the requirements are listed. Numerous Soviet observations of eddy statistical characteristics were conducted from 1935 to 1970 in various oceans. The dust-flow method, fluorescent and radioactive tracers, and aerial methods were used by Ozmidov and others to determine the coefficient of horizontal eddy diffusion K_ℓ in various seas and oceans. The Bussinesq and Karman equations were used by Shtokman and others to calculate K_ℓ from the sea current observation data. The simple linear dependence of K_ℓ on the scale of flow has been confirmed experimentally by a number of Soviet researchers. The dust-flow and fluorescent tracers methods are believed to be the most promising; any of the cited methods can be used in the POLEKS region.

Soviet contributions to calculation of heat flow in the ocean are detailed. Soviet scientists have calculated heat advection on account of sea currents with allowance for horizontal turbulence in the North Atlantic (Strokina), Kara and Norwegian Seas (Shuleykin), and advective-turbulent heat distribution with depth (Shtokman, Zhukov, Kagan, Kolesnikov, Smirnova). Bortkovskiy, Bogdanova, and others have determined the ratio of advection to horizontal turbulence in the eddy heat exchange process in different Atlantic currents and in the Black Sea.

Progress is also reviewed in designing quick-response and high sensitivity instruments for measuring water temperature, salinity and current velocity fluctuations in the ocean. The Marine Hydrophysical Institute has been the most successful in this respect. Most of these Soviet instruments were designed and used for the first time in the 1950-1966 period. Their sensitivity and response times are given. More recently the Doppler acoustic method has been used to measure sea current velocity. The turbulimeters already cited have been used for salinity measurements. Very recently, the fifth model (GAT-5) of a turbulimeter was designed at the MHI for turbulence studies at depths to 2,000 meters. The GAT-5 records current velocity components and temperature fluctuations with sensitivities of 0.5 mm/sec and 0.0005°, respectively.

In his conclusion, the author expresses the opinion that study of statistical characteristics in connection with hydrometeorological factors is the most promising direction for research on oceanic turbulence. Presently, this type of study is hampered by the lack of adequate instrumentation. Some practical applications of the statistical methods of forecasting oceanic current velocity fields are cited and possible future research directions are outlined. There are 110 references including 89 Soviet sources.

A spectral analysis is given of current velocity components
and temperature time series for a hydrophysical test area near the Rockall
Bank. The observations were made in June-July 1971 from three buoy
stations of the vessel Professor Vize, to separate the most energetically
significant motion dimensions out of the fluctuation spectra. The total
number of observations made, either by means of a BPV current meter or
FTG photothermograph, are tabulated separately for each station and for
depth levels from 50 to 1000 m. The period of observations varied from
one hour to several days.

The calculated frequency spectra of fluctuations of the
meridional current velocity component, u, are shown as topographic maps
(Fig. 1) and a relief map (Fig. 2). Both maps represent u fluctuation
spectra S_{ij} (f) in a (T, H) coordinate system, where T = 1/f is the period
of an elementary fluctuation and H is the depth. Analysis of the calculated
data shows relatively narrow f bands which correspond to u fluctuations
with T = 5-6 days and 12-15 h. The former may originate from self oscillations
of the ocean-atmosphere-land system, or may be due to meteorological
factors, e.g. a series of cyclones. The latter are due to semidiurnal tides
and inertial oscillations. Both f bands stretch over all levels for all
stations of the test area.
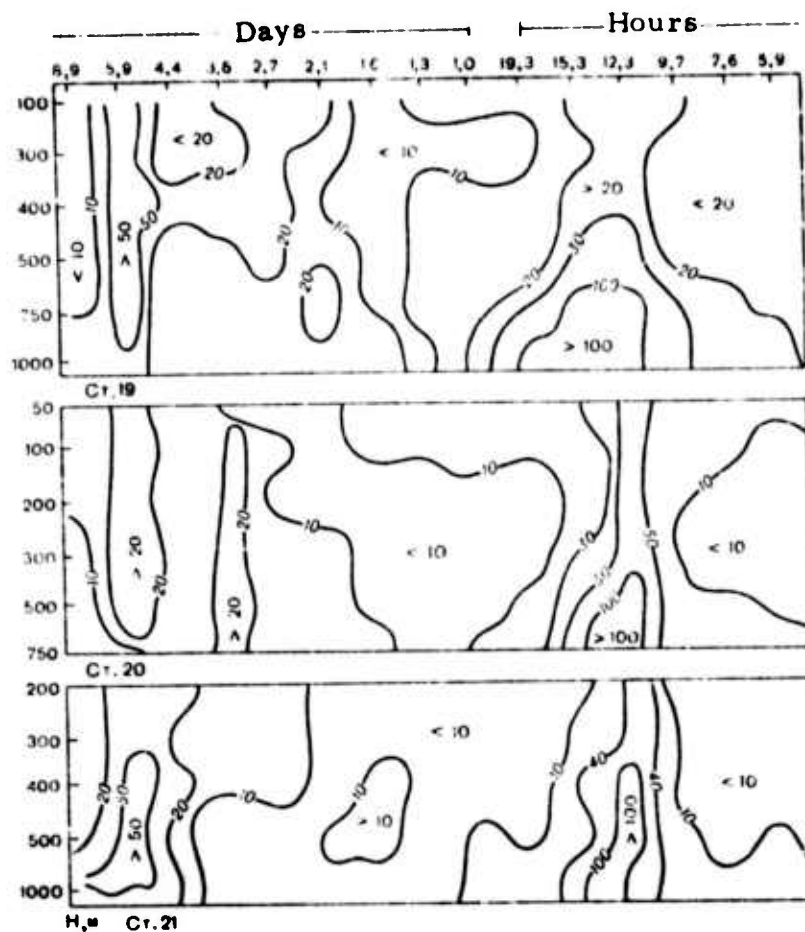
Fig. 1. Topographic map of natural time fluctuation spectrum of u current velocity component. Numerical values of fluctuations intensity are multiples of 10^2.
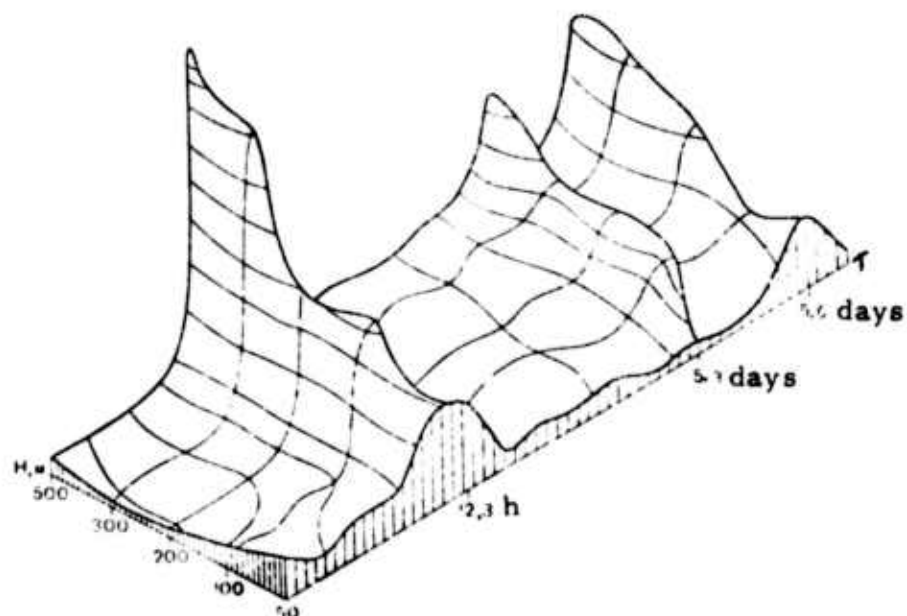
Fig. 2. Relief map (in relative units) of the spectrum of natural frequency fluctuations of u velocity component for station 20. Isolines are drawn with spacing equal to 10.

A topographic map of the combined S_{ij} (f) of u component fluctuations at the upper and each of the lower levels shows that the phase of u fluctuations with both cited T values is constant in depth and space. All the cited facts point to the significant effect of water density stratification on the vertical distribution of current velocity in tidal flow (T = 12-15 h). This effect is only weakly reflected in current velocity fluctuations with T = 5-6 days. The fragmentary data on temperature fluctuations show that the peak spectral densities correspond to fluctuations with T = 5-6 days, 1.5-2.0 days, and 12-15 hours, with predominance of the first ones. The calculated intensities of heat flow in meridional and latitudinal directions were found to be maximal for low-frequency fluctuations with T = 5-6 days. The second maximum of horizontal heat flux intensity is weakly expressed in the region of tidal frequencies.

The authors conclude that the most energetically significant ranges are the 12-15 hr. and 5-6 day fluctuations of the current velocity fields; the 5-6 day 1.5-2.0 day, and 12-15 hr. fluctuations of water temperature fields; and the 5-6 day and 12-15 hr. fluctuations of horizontal heat fluxes.

Vladimirov, O. A., I. D. Zykov, A. P. Nagurnyy, and V. G. Savchenko. Vertical structure of currents in the western portion of the Greenland Sea. IN: Trudy Arktich. i antarktich. n.-i. in-ta, no. 312, 1974, 95-102.

Statistical characteristics and the results of spectral analysis of sea currents in the western portion of the Greenland Sea are reviewed. The work is presented as a contribution to the study of extreme fringes of the North Atlantic in the framework of the POLEKS program. The cited results

are based on oceanographic data collected in 1970 from a recording buoy station during the 9th cruise of the R/V Professor Vize. The station was located at $70^{\circ}26'$ N latitude and $17^{\circ}39'$ W longitude.

A statistical treatment of a discrete set of measured meridional (u) and zonal (v) components of the current velocity vector is detailed. Statistical numerical characteristics of u and v are tabulated for 25 to 1000 m depth levels. It is shown that the empirical distribution functions of u and v at levels below 25 meters do not approach the Gaussian (normal) distribution law. This finding, which is supported by the measured temperature (T)-salinity (S) date (Table 1), is explained by a

Level, $_{\mathsf{M}}$	T, °C	S, ‰	Level, $_{\mathsf{M}}$	T, °C	S, ‰
0	2,53	33,24	200	0,01	34,92
10	2,68	33,27	250	1,08	34,96
20	2,65	33,30	300	1,01	34,96
30	2,64	34,18	400	0,73	34,96
50	—0,95	34,31	500	0,41	34,94
75	—0,52	34,43	600	0,15	34,92
100	—0,35	34,63	800	—0,36	34,88
125	0,15	34,76	1000	—0,59	34,87
150	0,77	34,81	1200	—0,74	34,92

Table 1. Temperature and salinity vertical distribution near the buoy station.

turbulence-shielding effect of the high-gradient density layer at the 30-50 m. level. The conclusion as to a sharp drop in turbulence at increasing depth is confirmed by the decreasing ratio of current velocity fluctuation intensity at each level down to tne 25 m level. Plots of the structural function of u versus time show that only at the 25 m level within the 1.5 to 4th period can the function be described reasonably well by the 2/3 power law. The linear dimensions of eddy formations above the 25 m level are 200 to 500 m and 400-1300 m for u and v, respectively.

The calculated spectral density S_* of the u and v sets of data over a period T is plotted for all depth levels within the cited range (Fig. 1). Fig. 1 shows regions of S_* maxima within the periods of tidal and inertia waves at all levels, except the 100 m level for v and 200 m level for u, where S_* is minimum. Spectral maxima are noted at the 50 to 200 m levels within short periods. It is assumed that the tidal and inertia waves in the 50 to 200 m layer lose stability and generate high-frequency eddies.

In the light of the cited results, the loss of stability of low-frequency internal waves may be caused by the proximity to the critical latitude ($73°20'$) for the semidiurnal tide. At upper levels the Vaisala-Brunt period was higher than the inertial period, hence the condition for loss of stability by inertia-gravitational waves in the upper ocean layers is fulfilled.

(Fig. 1. on next page)

-61-
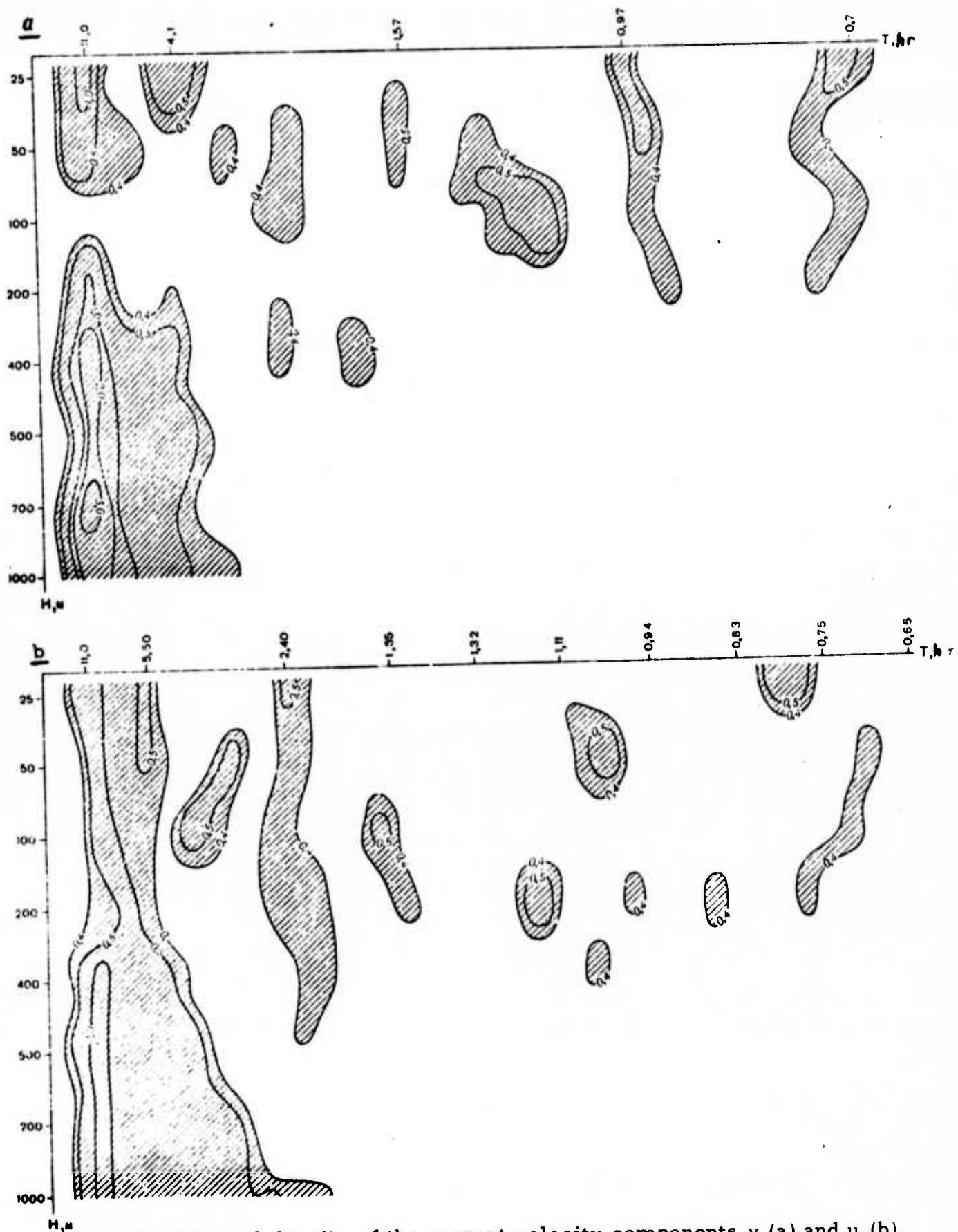
Fig. 1. Spectral density of the current velocity components v (a) and u (b). Spectral density values exceed 0.4 $(1/c)^{-1}$ within the shaded areas.

Vladimirov, O. A., A. P. Nagurnyy, Yu. V.
Nikolayev, and V. G. Savchenko. Experimental
use of a vertical profiler and water sampler for
studying high-frequency fluctuations in water
temperature near a pycnocline. IN: Trudy
Arktich i antarktich. n.-i. in-ta, no. 312,
1974, 32-41.

Experimental water temperature data recorded over a one
hour period at a fixed depth level within the 0-137.5 m. layer near a
pycnocline are analyzed. The data were recorded during the 11th cruise
of the R/V Professor Vize, using an experimental prototype of the
temperature-pressure-electric conductivity profiler and water sampler
aboard the drifting vessel. The salinity and conductivity data were not
analyzed owing to a malfunction of the device.

Temperature observations were carried out in 1971 at
$49^{\circ}46.5'$ N latitude and $18^{\circ}37'$ W longitude in a gentle wind. Maximum
error of temperature determination was ± 0.03 deg. The temperature,
salinity, and Vaisala-Brunt frequency (N) vertical profiles in the upper
ocean layer are plotted from the preliminary bathometric data. The
maximum average vertical temperature gradient in the pycnocline was
0.123 deg/m. Practically no halocline was present.

A typical recording of temperature fluctuations in the
thermocline (Fig. 1) shows significant fluctuations during relatively short
time intervals, and intensified fluctuations at the crest and trough of
temperature waves. The latter observation suggests a decay of internal
waves in extremal points, hence generation of high-frequency oscillations.
Oscillations with a period $\gamma < \gamma_0 = 6.5$ min. were considered to be turbulence
fluctuations (γ_0 is the period of free-propagating internal waves in a
stationary fluid). The difference $\theta - \tilde{\theta}$ represents high-frequency
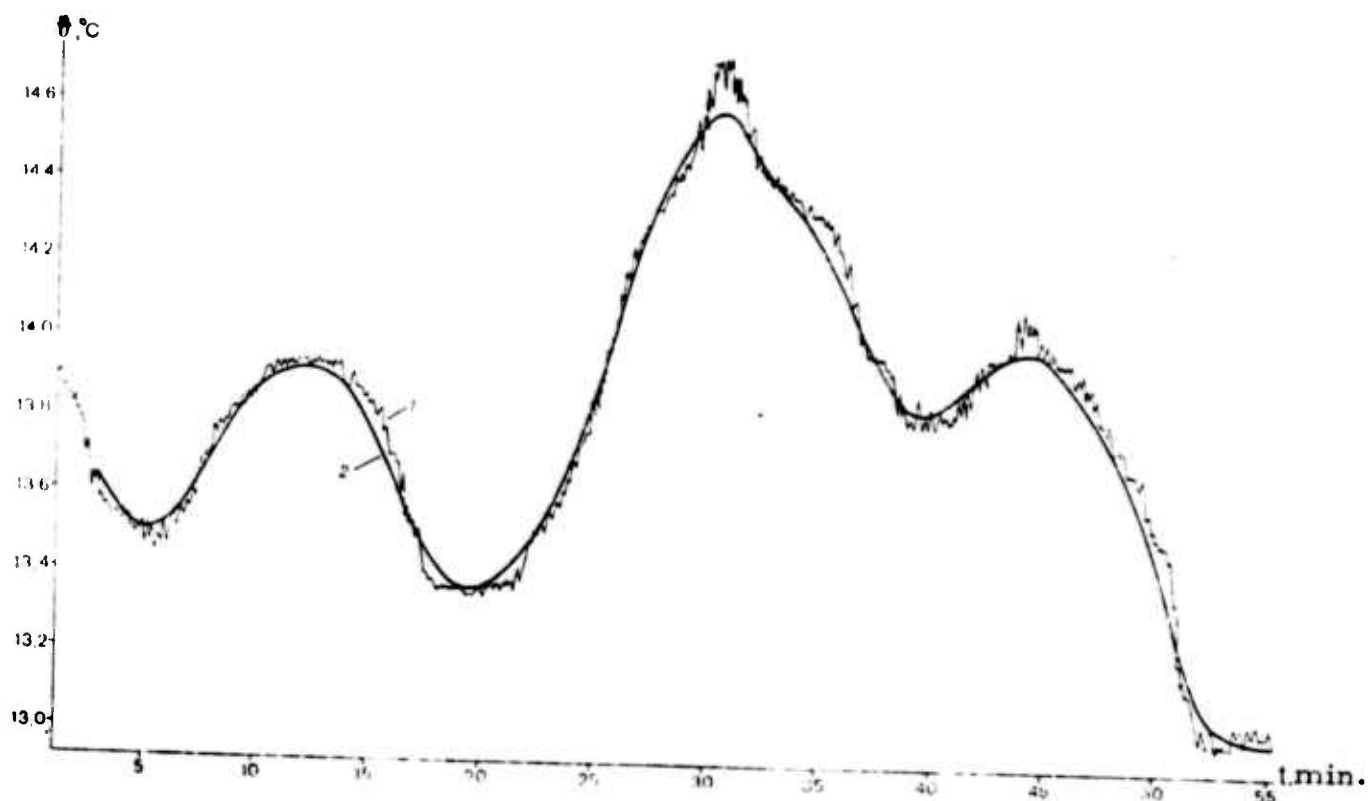
Fig. 1. Time fluctuations of water temperature (°C) at 36 meters depth: 1- measured values, 2- smoothed values. A cosinusoid filter was used with cutoff period $T_1 = 6$ min. Convergence interval $n_1 = 35$.

oscillations θ'; the range of θ' was found to be 0.22°. The frequency of internal waves was determined by harmonic analysis of the smoothed set of data. The period T, amplitude A, the initial phase, the amplitude η_j of fluid particles shift from equilibrium, and the vertical velocity component w_j (j = 1 to 5) were all calculated from $\tilde{\theta}$ curves for the first five harmonics of internal waves (Table 1). The maximum A_j and η_j values of these

Harmonic No.	T, min.	A, °C	Initial phase	η, м	w, cm/sec
1	54	0.38	258°	12.1	0.75
2	27	0.24	20	7.6	0.91
3	18	0.28	295	8.9	1.65
4	13.5	0.10	73	3.2	0.79
5	10.8	0.07	82	2.4	0.74

Table 1. Numerical characteristics of internal waves.

-64-

harmonics are calculated to be 0.77^{O} and 24.4 m, respectively.

A spectral analysis of θ' data (Fig. 2) confirms the
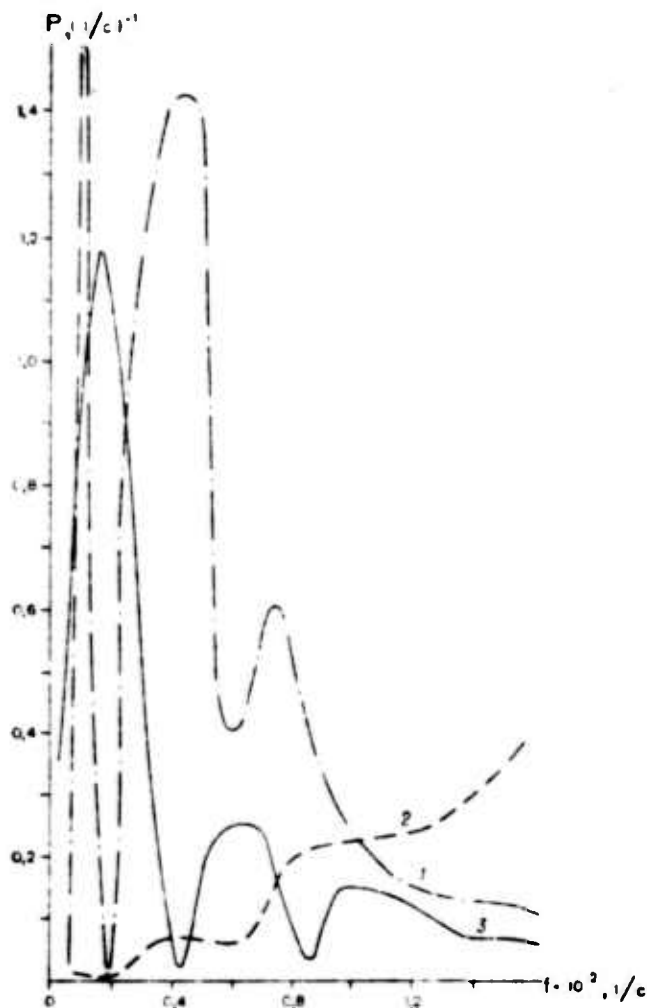
Fig. 2. Legarithmic spectra of power density P
of high-frequency temperature fluctuations θ',
calculated at different convergence intervals of θ:
$n_1 = 35$ (1), $n_2 = 9$ (2), and $n_3 = 72$ (3).

suitability of selecting γ_1 as cut-off period for the study of turbulent
θ fluctuations near the pycnocline. Some discrepancy is noted between
the $P(f)$ function in Fig. 2 and the spectra $S_*(\omega)$ of high-frequency
temperature fluctuations, as calculated from the Fourier cosine transform

of the autocorrelation function K ($\Delta \tau$). This discrepancy is explained as the result of lesser sensitivity of the S_{*} spectra calculation method to periodical disturbances. A discussion of the physical mechanism of internal wave decay in extremal points was inconclusive; however the mechanism proposed by Phillips was ruled out (O. M. Phillips, Dinamika verkhnego sloya okeana. M., Mir, 1969).

Vladimirov, O. A., I. D. Zykov, A. P. Nagurnyy, and V. G. Savchenko. On using the BPV-2R current meter for oceanographic observations. IN: Trudy Arktich i antarktich. n. -i. in-ta, no. 312, 1974, 110-117.

The ocean current velocity data measured with the BPV-2 and BPV-2R propeller-type current meters at the same depth level are treated statistically, and the statistical data are compared to determine the difference between the readings of the two meters. The comparison data were obtained in June-September 1972 during the 15th cruise of the R/V Professor Vize. The two meters were placed in pairs at different levels, and were spaced about 1.5 m apart. The tabulated statistical characteristics of the zonal (u) and meridional (v) velocity components at the 100 and 300 m depth levels are significantly different for the two meters. This is particularly true for the components' mean values u and v and variance S^2 which are 1.5 to 3.3 times and 2.2 to 4.2 times higher for BPV-2R data than for BPV-2 data. These differences are caused by differences in recording of the velocity modulus of water transport by the two meters. The latter difference in turn results from different design characteristics of the nonreversing velocity sensor in the BPV-2R meter. To determine whether the discrepancy between u, V, and S^2 values is significant or not the hypothesis was tested of equality

of the two sample mean values X_1 and X_2 of each component u or v
and the equality of the sample values S_1^2 and S_2^2 of variance, where the indices
1 and 2 in subscript refer to the BPV-2 and BPV-2R meters. Both tests
were made on assumptions of the normal or different from normal distribu-
tions of the sample universe. Student's t with significance levels 0.010
or 3 was used as criterion of divergence of X_1 and X_2 on the assumption
of normal or different from normal distribution, respectively, and also
with significance level 3 as a criterion of the divergence of S_1^2 and S_2^2,
assuming different from normal distribution. Fisher's F with significance
level $\alpha = 0.005$ was used for the test of S_1^2 and S_2^2 divergence on the assumption
of a normal distribution. Results of both tests are tabulated (Tables 1 and 2).

Level μ	velocity component	$\lvert \bar{x}_1 - \bar{v}_1 \rvert$	$t_{(obs.)}$	$P(t \geq t_{(obs.)})$
100	u	3.8	5.4	0.000
	v	3.8	5.3	0.000
300	u	3.6	8.0	0.000
	v	1.4	2.7	0.006

Table 1. Data from testing the equality hypothesis of mean velocity component
values calculated from measurement data of BPV-2 and BPV-2R
meters. $P(t \geq t_{obs})$ is the probability that a random t value
will be not less than the calculated t_{obs}.

Level μ	velocity component	$F_{(obs.)}$	P	t_s
100	u	3.9	1.0	19.4
	v	4.2	1.0	20.3
300	u	2.2	1.0	11.9
	v	2.3	1.0	12.2

Table 2. Data from testing the equality of variance of velocity components,
calculated from measurement data of BPV-2 and BPV-2R meters.

The tabulated data show that the alternative to the equality hypothesis holds, i.e., that divergencies $(X_1 - X_2)$ and $(S_1^2 - S_2^2)$ are significant to the point that the data of the two instruments must be considered as samples of two different universes. The random error variance $\bar{\beta}^2$ and the mean absolute error η of the measurement method are evaluated by extrapolating the structural functions of u and v components to zero on the assumption of normal distribution. The table of $\bar{\beta}^2$ and η values shows that the η value for the BPV-2R instrument is twice the η value for the BPV-2 instrument at both the 100 and 300 m levels. It follows that the empirical distribution curves of u and v components (Fig. 1) are significantly
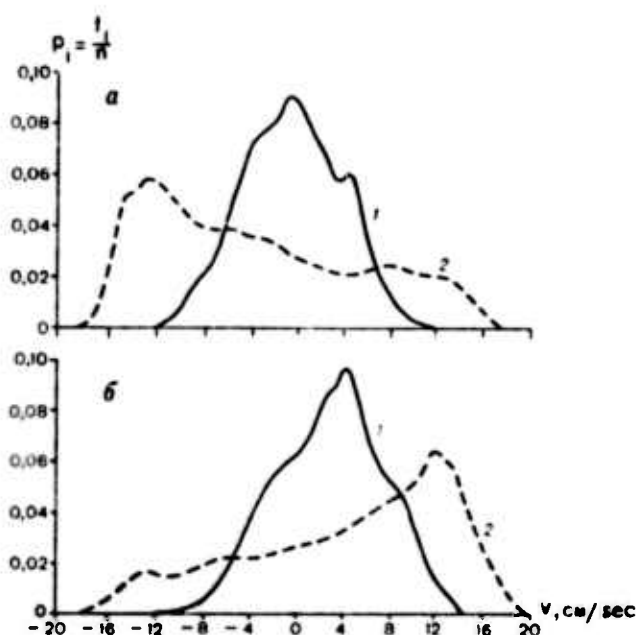
Fig. 1. Empirical distribution curves of u (Fig. 1a) and v (Fig. 1b) velocity components at the 100 m level: 1- BPV-2 data, 2- BPV-2R data (p_i = fi/n is statistical frequency of the i-th interval of velocity component fluctuations).

different for the two meters. An addition to the horizontal velocity component value recorded by the BPV-2R meter results from its greater sensitivity to vertical displacement in the open ocean due to surface wave effects. It is concluded that the use of the BPV-2R meter is not suitable for oceanographic observations in the open ocean.

Kopyl, Ye. A. **Effective coefficient of sound reflection from the ocean surface.** FAiO, no. 12, 1973, 1327-1330.

Results are given of an experimental study of sound reflecting characteristics of the open ocean surface, under more varied meteorological conditions and in a narrower range of grazing angles than in a previous Soviet study by Yu. Zhitkovskiy (DAN SSSR, v. 188, no. 2, 1969). The present study was carried out in 1970-71 in the Atlantic aboard the R/V Petr Lebedev. The sound emitter produced 10 msec pulses at 1 to 8 kHz frequencies in main-lobe directional patterns within 8 to 60° angles. A nondirectional hydrophone was used as the sound pickup. The grazing angle of the central beam with the surface varied from 15 to 30°. From 100 to 600 backscattered signals were recorded at each of the 20 grazing angles within the cited range for 0-11 m/sec wind speeds. The maximum angular spread of the effective scattering function was estimated to be 12°. This estimate was interpreted as an indication that the effective reflection coefficient

$$V_{ef} = (R_{refl}/R_f) \sqrt{\overline{P^2_{refl}}/\overline{P^2_f}},$$

(1)

is a characteristic of the ocean surface reflectivity. P_{refl} and P_f in (1) are the pressure amplitudes of the reflected and direct signals, R_{refl} and R_f are the averaged emitter-to-receiver distances travelled by the respective signals. All V_{ef} data calculated from (1) were divided in four groups according to wind speed, since V_{ef} was found to be independent of grazing angle. The frequency dependence of V_{ef} (Fig. 1) shows that V_{ef} tends to decrease at f = 8 kHz, particularly in high winds. This fact is explained as the result of increased ocean surface roughness and the development of air bubbles in the surface layer at higher wind speeds and the increased relative effect of small-scale roughnesses and bubbles on hf sound scattering. An
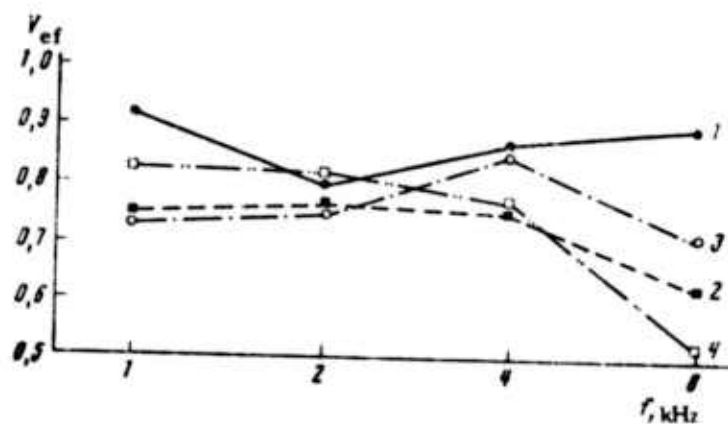
Fig. 1. Effective reflection coefficient versus frequency at 0-2 (1), 4-7 (2), 7-9 (3), and 9-11 (4) m/sec wind speeds.

additional confirmation of the validity of the interpretation of sound backscattering from the ocean surface in terms of the effectiveness scattering function and V_{ef} was seen in the finding that the angular width of the emitter directivity pattern decreased by half, when f was doubled. The experimental plots of the variation factor

$$\eta = \sqrt{(\overline{P^2_{refl}} - \overline{P}^2_{refl})/\overline{P}^2_{refl}} \qquad (2)$$

of backscattered signal amplitude indicated a significant incoherence of scattering field, probably due to saturation of backscatter fluctuations at high Rayleigh numbers. In this case, the effective scattering area is estimated to be small in relation to the sea roughness correlation distance. Comparison of the experimental integral distributions of the backscattered signal amplitudes at 1 and 8 kHz with the theoretical distribution functions indicated a satisfactory agreement between the experimental points and the Rayleigh-Rice (?) distribution function with the parameter q = 1.2.

Gavrikov, V. K., and A. V. Kats. Vynuzhdennoye
rasseyaniye zvuka na granitse dvukh sred. (Induced
sound scattering at the boundary of two media).
Khar'kov, 1973, 53 p. (RZhF, 11/79, no. 11Zh631)

A theory is developed for induced sound scattering in surface
waves, generated at the boundary of two media during oblique incidence of a
sound wave on it. Two types of equations are jointly solved: 1) wave
equations for sound under conditions of continuity in pressure and normal
velocity component at the boundary, and 2) equations for LF oscillations of
the boundary, obtained by transformation of Green's formula, as
approximations of small and mildly sloping boundary irregularities.
Conditions of spatial synchronism are recorded only for tangential components
of wave vectors. The amplitude of scattered waves and dispersion equations
for gravitational-capillary waves with acoustic field are determined approximately
by means of three reflected (Stokes, anti-Stokes, mirror) and three refracted
waves.

Nonlinear conditions at the boundary create the possibility of
induced sound scattering in surface waves, i.e. instability occurs above a
definite threshold of sound intensity; this leads to an increase of surface
wave amplitude and consequently to the increase of sound scattering which in
turn further increases the surface wave amplitude, etc., leading to a
cumulative sound scattering effect. In the megahertz range, the threshold
intensity at the boundary of air-water equals 3 watts/cm^2. Effects of finite
time and space intervals during interaction of sound and surface waves
are analyzed. The threshold of induced sound scattering in surface waves
is significantly lowered under surface resonance conditions, when one of
the scattered waves slips along the boundary. In this case it is necessary
to take into account dissipative losses according to Konstantinov. Effects
are also discussed of the finite width of the sonic beam. Conditions of
using the developed theory are analyzed in detail.

Zel'dis, V. I., I. A. Leykin, A. D.
Rozenberg, and V. G. Ruskevich. Study
of the phase characteristics of acoustic
signals scattered by a wavy water surface.
Akusticheskiy zhurnal, no. 2, 1974, 235-241.

Experimental phase fluctuations (frequency shift) spectrum
S_ψ and the spectrum central frequency fluctuations $\Delta F_0/F_0$ of hydroacoustic
signals backscattered from a wavy water surface are analyzed in the frame-
work of the theory of resonance scattering. Simultaneous measurements
were made of S_ψ and water surface characteristics mostly in a wave basin,
as well as some in the sea. The frequency f of the hydroacoustic signal and the
glancing angle ψ were varied in the 15 to 60 kHz and 10 to 50 degs. ranges
respectively. The experimental apparatus and test procedure have been
described elsewhere by the authors (Akust. zh., no. 2, 1973, 170). The
experimental data are presented in graphical form. The data in Fig. 1,
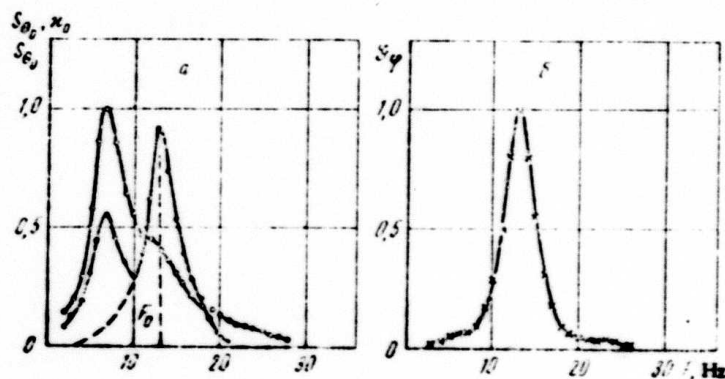
Fig. 1, a- Three-dimensional $S_+ \theta_0, \varkappa_0$ (F) and two-
dimensional $S_+ \theta_0$ (F) wave spectra; 1b- frequency
shift spectrum S_ψ at surface wave number $\varkappa_0$ = 2.5 cm^{-1},
signal f = 35 kHz, ψ = 30 deg; θ_0 = const. is the angle
of incidence in the horizontal plane.

-72-

which were obtained in a basin at 4 m/sec wind flows, confirm the resonance characteristic of scattering. It is shown that the F_0 value in Fig. 1a coincides with that calculated from the dispersion equation for surface gravity waves in a smooth sea. Thus the cited equation can be used to calculate F_0 instead of going to complicated measurements of $S_{\pm \theta_0}, \varkappa_0(F)$ spectra.

Other experimental $\mathcal{Y}_q$ data obtained at different orientations of the transceiving antenna versus wind direction ($\theta_0 = 0$ to 90 deg.) show an equally good agreement between experimental F_0 values and F_0 values calculated from the dispersion equation. The presence of wind deflection affects F_0 depending on θ_0. Another factor determining F_0 value is the existence, under natural conditions, of a standing wave which results from interference between surface waves of the same $\varkappa$. In that case, it is necessary to determine $S_{\pm \theta_0, \varkappa_0}(F)$, then $\mathcal{Y}_q \sim \sum S_{\pm \theta_0, \varkappa_0}(F)$. It follows that the spectrum $\mathcal{Y}_q$ must exhibit two peaks shifted by $\pm F_0$ from the emitted signal frequency. This was confirmed by an experiment in which waves were propagated simultaneously in the direction $(-\theta_0)$ of the incident acoustic signal and in direction θ_0 opposite to it. Tests in a wave basin at 2 to 7 m/sec winds show that $\mathcal{Y}_q$ spectra broaden and $\Delta F_0 / F_0$ increases linearly from 0.1-0.2 to >1 as winds increase. Broadening of the spectrum is attributed mainly to an additional frequency modulation of the ripples by high waves. The same observation was made in the experiments at sea. A typical $\mathcal{Y}_q$ spectrum obtained (Fig. 2a) shows that a high $\Delta F_0 / F_0$ value = 1.5 is characteristic of the spectra. The approximate width of the $\mathcal{Y}_q$ spectrum can be determined from $\Delta F_0 = V_{orb} \varkappa_0 / \pi$, where $V_{orb} = \Omega H / 2$ is the orbital velocity of the high wave and Ω is the modulation frequency. Frequency modulation of the scattered signal is shown in Fig. 2b.
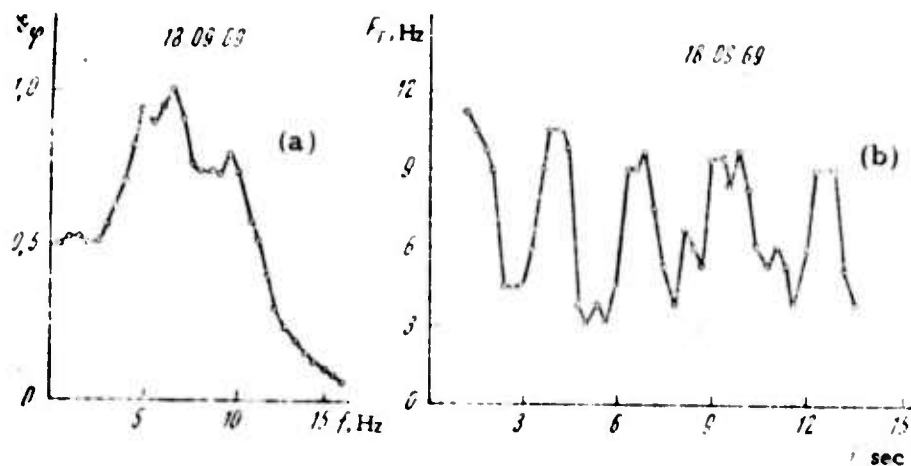
Fig. 2.   Frequency shift spectrum   (a) and instantaneous frequency F_T (b) of a signal scattered from the sea: smooth sea, wave height H = 0.3 m, wave period T = 3 sec, incident frequency f = 15 kHz, ψ = 30 deg.

Morozov, Ye. G.   **Experimental study of the breaking of internal waves.**   Okeanologiya, no. 1, 1974, 25-29.

Time variation of temperature fluctuations in a seasonal thermocline was experimentally investigated during the 40th expedition of R/V Vityaz' in the Arabian Ocean. Hydrological measurements were taken approximately once a day.   Bathometric measurements were taken such that the intervals between bathometers in the seasonal thermocline were 10 m. Water temperatures were recorded by means of photothermographs at 15 minute intervals simultaneously from five floating platforms, located at different levels in the thermocline.   Temperatures thus obtained were subjected to spectral analysis.   Energy fluctuation was found to change significantly with time.   Variations in temperature fluctuations were studied

during the period from February 22 to March 12. During this time the
r.m.s. deviation of the temperature fluctuations, calculated after high
frequency filtration, increased from 0.04 to 0.12°, and subsequently again
decreased to 0.05°. Fig. 1 shows the spectral density of temperature
fluctuation, offset in time, for the 125 m level, as well as the
coherence function between temperature fluctuations at the 125 m and 150 m
levels. It is seen from the figure that the spectral density at first increases
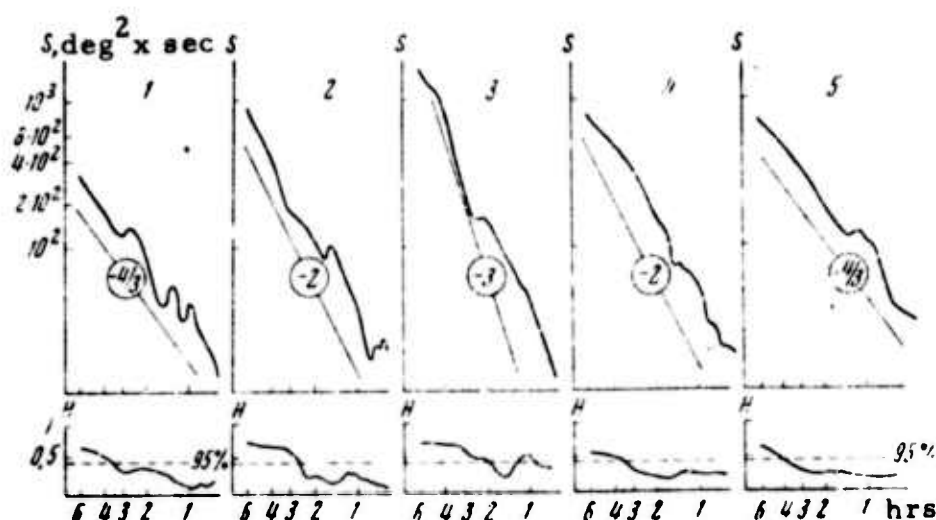
Fig. 1. Spectral density of temperature fluctuation
at 125 m, and coherence between fluctuations at 125 m
and 150 m. 1, Feb. 22; 2, Feb. 26; 3, March 1;
4, March 5; 5, March 9. (test interval = 3 days,
sampling interval = 15 min).

(spectrum slope and coherence value increase) and then decreases, followed
by a decrease in spectrum slope and lowering of the coherence. The increase
in spectral density is connected with the growth of internal wave amplitude.
The subsequent drop in density and increase of potential energy of the water
column are explained by the breaking of an internal wave pocket, leading to
vertical intermixing.

Marchuk, G. I., and B. A. Kagan. Internal gravity waves in a real stratified ocean. IN: Vnutrenniye volny v okeane, SOAN SSSR, Novosibirsk, 1972, 89. (Author's abstract)

Investigation of internal gravity waves in the ocean has been treated widely in the literature. In most of these works, different gravity models were assumed in writing the vertical structure of density fields, thus more or less describing the real density distribution in the ocean. The problem of arbitrary density distribution was first solved by Fjeldstad. However, his solution, as shown by Grun, is applicable only in the case of very long waves, so that up to the present time the different parts of internal gravity wave spectra in the ocean seem to have been studied in an unbalanced fashion.

In the present work characteristic curves are drawn and natural solutions are found, which correspond to internal gravity waves in a real stratified ocean.

(This paper was published in FAiO, no. 4, 1970).

Vladimirov, O. A., and Yu. V. Nikolayev. Water temperature anomalies in the North Atlantic and their correlation with various hydrometeorological phenomena. IN: Trudy Arktich. i antarktich. n-i. in-ta, no. 312, 1974, 175-191.

Previous studies have shown that the basic cause of anomalies in surface water temperatures is the change of hydrometeorological regimes in the North Atlantic and adjacent regions. Amot (Meteorol. Annaler, Bd. 4, no. 1, 1955) showed that based on thermal regimes of these waters, the heat

content of the upper ocean layer can be well estimated, and consequently the quantity of heat flowing into the Artic basin from southern latitudes can be estimated. According to Amot, the difference between water temperatures measured at the surface and at 10 meters depth in most cases does not exceed 0.1°, and the value of this difference is not subject to annual variation.

The present work undertakes verification of the above conclusions, and attempts to establish correlations between some hydrometeorological phenomena and distribution of water temperature anomalies. The problem is analyzed based on the results of series of observations (Table 1). During analysis of the problem, mean annual air

Table. 1. Periods of different observations

Observations	Observation Period	Observation Not Conducted
Water temp. off sourthern Iceland	1889 - 1960	1940 - 1944
Air temp. in the North Atlantic	1901 - 1960	-
Air pressure in the North Atlantic	1900 - 1964	1944 - 1945
Position of ice edge in Barents Sea during May and August	1900 - 1962	-
Air pressure in the Arctic	1900 - 1961	-

temperature anomalies, atmospheric anomalies and data on ice edge locations are also taken into account along with the mean annual water temperature anomalies. The authors' conclusions are:

1.   The first natural orthogonal component of water temperature anomaly fields, located south of Iceland, indicates epochal changes of the thermal state in this region of the ocean.

2.   Epochal changes in water temperature anomalies at the indicated region have the largest values in the Iceland region.

3.   Variability of the water temperature anomaly fields, taking into account epochal changes, can be represented by six classes, distributed irregularly over the considered period.

4.   For the case in which epochal changes are not considered, the water temperature anomaly fields are characterized by the presence of seven more or less evenly distributed classes.

5.   Each of these classes corresponds to the particular anomaly fields of air temperature atmospheric pressure, height of sea level and ice edge location. It can be shown that the most important role in the said phenomena is played by the variability of pressure fields, which clearly explains the rearrangement of fields of the remaining characteristics, including formation of classes of water temperature anomalies.

6.   The overall variability in fields of a hydrometeorological system, which consists of anomalies in water temperature, air temperature and pressure in the considered region, can be represented by seven classes. If the pressure is considered to be the determing factor, then a logical connection exists between separate schemes, expressing distribution of the said anomalies inside each class.

7.   The presence of quasiperiodicity with an average value of 3 years has been noted in the recurrence period of classes of hydrometeorological systems.

Byshev, V. I., and Yu. A. Ivanov. A model of
the nonstationary thermohaline structure of the upper
ocean layer. Okeanologiya, no. 2, 1974, 235-241.

The temperature field, salinity and flow velocity of the ocean
are each considered as a sum of two components: a) stationary, depending
upon spatial coordinates and b) transient, being a function of these
coordinates and time. Dimensionless equations are developed for transient
components, and a model is suggested for the formation of nonstationary
thermohaline structures at the upper ocean layer. Diffusion and convection
processes are taken into account. The condition for introducing a convection
mechanism in the model is seen to be the occurrence of unstable stratification
in the diffusion process. Formation of structures with changing boundary
conditions is studied on annual and synoptic period scales.

Types of vertical structures of temperature and salinity
obtained during experiments are qualitatively in good agreement with
the measured data. The main features of vertical temperature and salinity
distributions (of uniform thermo- and halocline layers, intermediate
extremums and microstructures) obtained by calculations are also close to
observational data. Examples of the latter are given.

The authors note that it is very important to account for the
process of convection, not only for investigating thermohaline structures,
but also for studying processes of interaction between the ocean and
atmosphere.

Kremzer, U., and V. Matteus. Average
coefficient of vertical turbulent heat exchange
in the Baltic Sea. Okeanologiya, no. 5, 1973,
768-775.

Coefficients of vertical turbulent thermal conductivity K^*
and turbulent heat exchange K were calculated at two stations in the central
part of the Baltic Sea - the Gotland Depression ($57^\circ 20'$ N. lat. and $19^\circ 59'$
E. long. - stations F81 and BY15A) and Landsort Depression ($58^\circ 35'$ N. lat.
and $18^\circ 14'$ E. long. - stations F78 and BY31A). Calculations were made
for mean values of K^* and K as functions of depth for a whole year, and
were based on measurements made from 1902 to 1970. A series of annual
temperature variations were analyzed at 10 meter intervals to a depth of
100 m. Curves were drawn based on Fourier series, which permitted
calculation of the daily mean temperature for selected levels. Equations
are obtained for calculating K^* by Fjeldstad's equation and Pivovarov's equations.
Values of K^*, calculated according to the above two formulas for the Gotland
and Landsort   Depressions as functions of depth for annual and semiannual
components of temperature fluctuations are shown in Table 1.   Curves

Table 1

Coefficients of turbulent thermal conductivity K^*.
(a) Fjeldstad method; (b) Pivovarov method.

DEPTH, м	GOTLAND		LANDSORT		DEPTH, М	GOTLAND		LANDSORT	
	K^*, cm² cek⁻¹					K^*, cm² cek⁻¹			
	k=1	k=2	k=1	k=2		k=1	k=2	k=1	k=2
	Метод (a)					Метод (б)*			
0	37.7	16.7	59.7	10.1	0—10	50.2	17.5	43.4	21.8
10	2.3	2.0	1.5	1.8	10—20	1.6	0.2	1.2	0.3
20	0.6	23.6	0.7	7.6	20—30	0.4	—	0.6	—
30	0.8	4.1	0.9	1.0	30—40	1.4	—	1.1	—
40	0.8	1.9	0.5	—	40—50	0.7	1.4	0.3	0.6
50	1.2	1.5	0.3	2.7	50—60	5.9	8.9	0.4	—
60	0.7	2.1	0.2	1.1	60—70	6.4	2.5	0.2	2.5
70	1.1	0.7	0.1	1.7	70—80	0.2	0.3	0.02	1.6
80	0.1	0.4	0.03	2.6					

drawn for these values of K^* (Fig. 1) show that results of the two methods
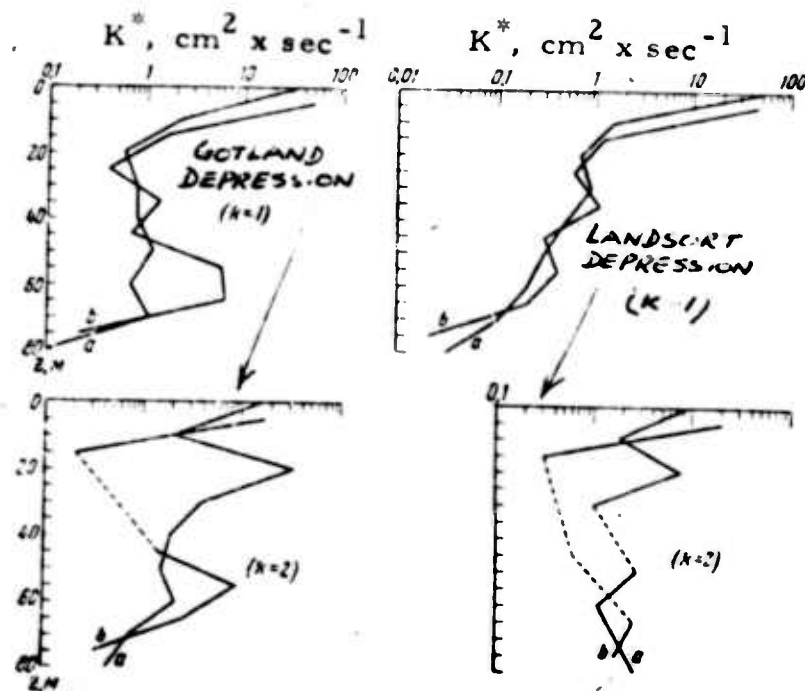
Fig. 1. Coefficients of turbulent thermal
conductivity K calculated in the central
part of the Baltic Sea by (a) Fjeldstad and
(b) Pivovarov methods for annual (k = 1)
and semiannual (k = 2) components of
temperature fluctuations.

are in good agreement for the annual component (k = 1). These results are
also seen to agree well with those of the data given in Lundberg's work
(Tr. Gos. Okeanogr. in-ta, no. 81, 1964).

A brief description is outlined on the Shtokman method of
determining coefficient K^* as a function of time. Improved methods of
calculating vertical turbulent coefficient of heat exchange K are proposed.
Equations are obtained for the heat exchange coefficient K_p and temperature
gradient at any layer P. It is seen that the annual variations of the above
coefficients correspond to hydrometeorological conditions of the sea region
in question.

Krupin, V. D. Properties of internal waves
and numerical solution of the Fjeldstad equation.
IN: Vnutrenniye volny v okeane, SO AN SSSR,
Novosibirsk, 1972, 135-151.

This article investigates the frequency dependence of wave
number, phase and group velocity of internal gravity waves in a vertically-
inhomogeneous ocean.   Certain characteristics are outlined, which are
true for arbitrary variations of the Vaisallaa frequency $N(z) = (g/\rho \; d\rho/dz)^{1/2}$,
where ρ = density of medium, depending on the vertical coordinate, z;
g = acceleration of gravity.   The problem is treated analytically, based on
the Fjeldstad theory of internal waves.

Fjeldstad considered natural internal oscillations in a
vertically-inhomogeneous infinite ocean of constant depth, and showed that
a system of linearized hydrodynamic equations for wave processes, harmonic
in time ($\sim e^{i\omega t}$, ω = frequency), can be reduced to a spectral boundary
problem.   It is shown in the present work that the wave number of the
internal mode continuously increases with increase of ω, while phase
velocity decreases and tends to zero; the group velocity reaches a maximum
value within the interval $\Omega < \omega < N_m$ where Ω = inertial frequency of the
earth's rotation and $N_m = \sup_{0 \leq z \leq H} N(Z)$.   These characteristics of internal
waves are true for any type of Vaisallaa frequency variations in the ocean.

Along with analytical solutions, a numerical method is
suggested for solving spectral boundary problems for Fjeldstad differential
equations; this enables one to investigate characteristics of internal waves
by computer.

Polyanskaya, V. A. Effect of high-frequency
internal waves on the sound field of a point
source in the ocean. Akusticheskiy zhurnal,
no. 1, 1974, 95-102. (Author's abstract)

Results are described of calculations based on a radial
approximation of the sound field of a point source deep in the ocean, in
the presence of internal waves with a plane front in a discontinuity layer.
It is shown that if the first mode of internal waves with sufficiently high
amplitude and short wavelength propagates in the discontinuity layer, a
system of caustic surfaces is formed at the nearest illuminated zone,
connected with wave crests. Lines of return of surfaces and isosurfaces,
equal to relative amplitudes, are located approximately parallel to the
internal wave front. The depth of their location can be taken as a measure
of distortions of an undisturbed sound field. The possibilities are discussed
of the formation of a secondary illumination zone, or the reduction of
shadow zone dimensions, owing to refraction at the crest of high amplitude
internal waves in the transmitter region.

Fedorov, K. N. Internal waves and the vertical
thermohaline microstructure of the ocean. IN:
Vnutrenniye volny v okeane, SO AN SSSR.
Novosibirsk, 1972, 90-118.

Thermohaline microstructures observed in the ocean consist
of inhomogeneities of varying size, developed on a background of averaged
hydrostatically stable vertical distribution of temperature and salinity (Fig. 1).
Observations show that the relation between horizontal and vertical dimensions of
different microstructure elements is a known constant. Table 1 shows the
results of studies conducted by different authors.

Fig. 1. Typical thermohaline structure in the
tropical Atlantic. (a) Temperature variations
with depth. (b) Vertical salinity distribution.
1- Small temp. inversions; 2- Uniform layer of
10 m. thickness.

Close interrelationships are found to exist between
thermohaline microstructures and internal waves. The present work
considers these interrelationships under the following sections:

1. <u>Action of internal waves on thermohaline microstructure formation.</u>

Thin elements of thermohaline microstructures occur due to
vertical rearrangements of the initial structure or at the background of
large scale deformations in layers, where conditions exist for such
rearrangements. The energy required for these vertical rearrangements of

Table 1. Relation of vertical and horizontal dimensions
of microstructure forms.

AUTHORS	STRUCTU-RAL ELE-MENTS	THICK-NESS l	TRANSVER-SE SEC LENGTH	RELATION h
STOMMEL & FEDOROV (1)	LAMINA			
Cox, C. et al.(2)				
NASMYTH (3)	LAMINA			
FEDOROV (4)	INVERSION			
			AVERAGE	

(1) Stommel, H., and K. N. Fedorov (Tellus,
   v. 19, no. 2, 1967, 306-325).
(2) Cox, C., Y. Nagata, and T. H. Osborn.
   (Bull. Japan. Soc. Fish. Oceanogr., special
   no., 1969, 67-71).
(3) Nasmyth, P. V. (Ph. D. Thesis. University
   of British Columbia, Vancouver, 1970).
(4) Fedorov, K. N. (FAiO, no. 2, 1972).

a stable thermohaline structure is obtained as a result of internal wave
destructions. It is pointed out that vertical thermohaline microstructures
may be the result of complex interaction of diffusion-convective and dynamic
mechanisms, the most important of which is the energy dissipation of
internal waves.

2. <u>Internal waves in the presence of complex thermohaline and dense
microstructures.</u>

The dynamics of internal waves in the ocean is connected
with the Vaisalla-Brunt frequency N_o $(\cong (g/\rho \, \partial \rho/\partial z)^{1/2}$, where g - acceleration

of gravity, ρ - water density, z - axis, positive downwards), the upper limit of which is the internal wave frequency itself. In the presence of fine thermohaline structures, the vertical profile of N_o seems to be abrupt or sectioned as compared to the case of smoothly varying density. It can therefore be assumed that in a real stratified thermocline, several wave channels may exist, each having its own set of internal waves propagating in it. The author notes that short internal waves can occur in all thermoclines, and not only near the surface. This helps in the faster energy dissipation of internal waves at still lower frequencies.

3. Distortions in measuring vertical profile of temperature and salinity due to internal waves.

Oscillations of water layers, resulting from internal waves, are readily observed from fluctuations in temperature and salinity as measured by sensors at fixed levels. These fluctuations are connected with the vertical intermixing of separate portions of,or all,thermocline structures; such intermixings have a periodic as well as random character. Graphs drawn for water temperature variations at different levels show that the actual distribution of temperature variation limits with depth is irregular, and that this distribution depends on the vertical profile of temperature gradient. A detailed discussion is given here on errors in measuring parameters, due to the limiting inertia of sensor elements during their descent into the water. Effects of internal waves on the response of a smoothly-lowered measuring device of temperature and salinity are discussed. It is emphasized that it is very necessary to select carefully the lowering speed of the sounding device, depending on the variability character of measured parameters (which depend on internal waves) and the technical characteristics of the device.

4. Thermohaline microstructures and generation of periodic and random fluctuations in temperature and salinity at a fixed depth.

During harmonic displacement of a temperature profile vertically up or down relative to a fixed level z_0, temperature fluctuations at this level have harmonic oscillations with a frequency ω equal to that of internal waves. If this temperature distribution along the vertical is itself a harmonic function of the vertical coordinate, then the temperature at the fixed level z_0 becomes a complex function of time, in which additional frequencies higher than ω are generated. These harmonic fluctuations of temperature or salinity at fixed levels may be due to the result of advective effects, which are connected with harmonically changing horizontal currents (e.g. tidal or inertial).

Byshev, V. I., and K. A. Chekotillo.
Statistical analysis of some measurements
of current speed in the North Atlantic.
FAiO, no. 3, 1974, 266-275.

The time range of predominant long-period fluctuations in ocean currents is evaluated and a vertical distribution of some characteristics of wide-range oceanic motion is obtained. This was done by harmonic analysis of a series of current velocity components, measured during 1970 in the central part of the North Atlantic. The measurements were made at buoy stations arranged in the form of a symmetric cross with the center located at $16°30'$ N latitude and $33°30'$ W longitude, each arm of the cross being 105 km long. Only data from the buoy station located 5.2' east of the cross center were analyzed. The data were collected over the period from February to September at 10 depth levels from 25 to 1,500 m.

The tabulated periods T_d of predominant fluctuations at each level were evaluated from the peaks of kinetic energy distribution E(T) (Fig. 1).
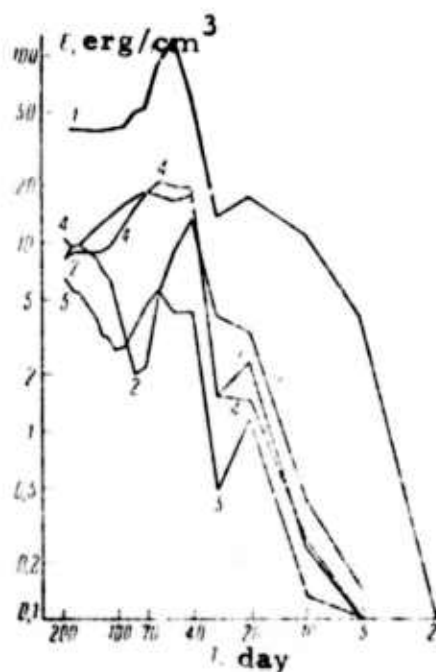
Fig. 1.   Kinetic energy E (per unit volume) of horizontal fluctuations vs. period T.   The figures 1, 2, 3, 4, and 5 at the curves correspond to 25, 100, 300, 500, and 1,000 m levels, respectively.

It appears from the tabulated T_d values that fluctuations with $T_d = 40$ to 70 days predominate in the hydrophysical polygon explored.   The modulus $\overline{V}(\tau)$ of the rms velocity vector and the dispersion $D_v(\tau) = (\overline{u}'^2(\tau) + \overline{v}'^2(\tau))/2$ of the velocity vector, where u', v' are fluctuations of the velocity components, were calculated using a series of daily means of u and v.   It was found that at small τ, the $\overline{V}(\tau)$ and $D_v(\tau)$ functions fluctuate strongly, but at $\tau > 115-120$ and >150-170 days, respectively, remain nearly constant.   The $D_v(\tau)$ function fluctuations have the same period as the cited predominant fluctuations of current.

At a sufficiently high τ (> 170 days), the estimated $\bar{V}(\tau)$ and $D_v(\tau)$ differ little from their true values, $\bar{V}$ and D_v. The fundamental characteristics of current motion (Table 1) were obtained by averaging data over a period $\tau = 198$ days. The plots of these characteristics versus

Table 1

Depth, m	$\bar{V}$, cm/sec	E_m, erg/cm³	E_f, erg/cm³	E_d, erg/cm³	E_d/E_f, %	$E_m + E_f$, erg/cm³	E_f/E_m
25	6.6	21.5	291.1	119.4	41.1	312.6	13.5
50	5.3	14.2	183.6	76.2	41.5	197.8	12.9
100	0.8	0.4	47.7	14.0	29.4	48.1	133.6
200	0.8	0.3	35.6	15.0	42.0	36.0	113.4
300	2.0	2.1	51.0	18.5	36.2	53.1	24.5
500	3.6	6.4	51.9	21.2	40.9	58.3	8.1
1000	2.9	4.3	3.8	5.7	41.3	18.1	3.2
1500	2.1	2.3	3.3	1.8	54.9	5.6	1.4

depth show their evident correlation with the typical depth distribution of the Vaisalaa-Brunt period N. Specifically the distribution pattern of the ratio E_d/E_f of kinetic energy of fluctuations with T_d period to that of total fluctuations exhibits a minimum approximately at the same depth as the N maximum. The E_d/E_f figures indicate a very significant contribution of fluctuations with period T_d to the total E_f. The E_f/E_m ratios, where $E_m = \rho V^2/2$ is the kinetic energy of averaged motion, indicate a surprisingly high excess of E_f over E_m at the 100 and 200 m levels, where N is maximum. The data in Table 1 and the tabulated correlation coefficients of u and v at different levels led to the conclusion that there is an evident correlation between large-scale motion within the 0 to 1500 m oceanic layer and the vertical density profile. Kinetic energy of horizontal motion within the cited layer is almost entirely determined by E_f. The E_d energy with $T_d = 40$ to 70 days comprises about 40% of E_f. The averaged values of the velocity components within the layer are tabulated (Table 2).

Table 2

Averaged current velocity components over a 108 day period

Depth, m	u, cm/sec	v, cm/sec
25	—1.1	6.5
50	3.0	4.4
100	—0.8	0.2
200	—0.8	0.1
300	—1.2	—1.5
500	—3.6	0.5
1000	—1.2	—2.7
1500	—1.5	—1.7

On the assumption that predominant fluctuations of current fields originate from shifting eddies, the latter are believed to be the consequence of baroclinic instability of motion. The hodograph in Fig. 2, which is plotted on the basis of data in Table 2, shows the mechanism of
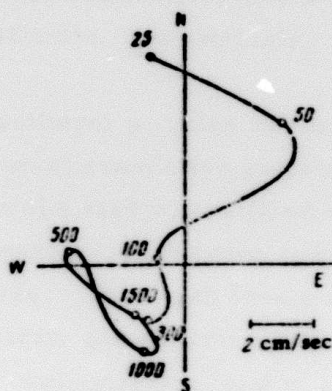

Fig. 2. Hodograph of vertical distribution of average current velocity. Figures are depths in meters.

baroclinic instability, i.e., transfer of warmer surface water to the north and that of colder deep water to the south. Unstable baroclinic wavelength,

and hence eddy size, is evaluated approximately using a two-layer model of the ocean. This evaluation is in agreement with earlier data on eddy dimensions.

Navrotskiy, V. V. <u>Structural analysis of velocity and temperature fluctuations in the upper layer of the ocean.</u> FAiO, no. 3, 1974, 276-288.

Spatial and temporal structures of the temperature and velocity mesoscale fluctuations in the 0 to 200 m oceanic layer are analyzed. The study used BPV-2 integrator and photothermograph data obtained at buoy stations (b/s), and vertical isotherm profiles obtained from towed thermistor chains. The observations were made in 1968 through 1970 during the 3rd, 5th, and 8th cruises of the R/V Akademik Kurchatov in the eastern, western, and mid-tropical regions of the Atlantic, respectively.

Typical isotherm profiles reveal stable internal waves within the entire layer; a horizontal convective instability layer generated by internal waves which propagate in the stable stratified layers above and below the convective layer; and dynamic instabilities (eddies) owing to well developed small-scale internal waves. The depth levels of the maximum modulus h_i of current horizontal velocity are determined from observations at five buoy stations. Velocity components u_i and v_i are calculated using the observed h_i values and the smoothed phase. Phase distribution density typical for a stable current shows the usefulness of smoothing. Typical temporal structural functions of h, u, v, and t fluctuations as well as the spatial function of t fluctuations (Fig. 1) illustrate the following conclusions.
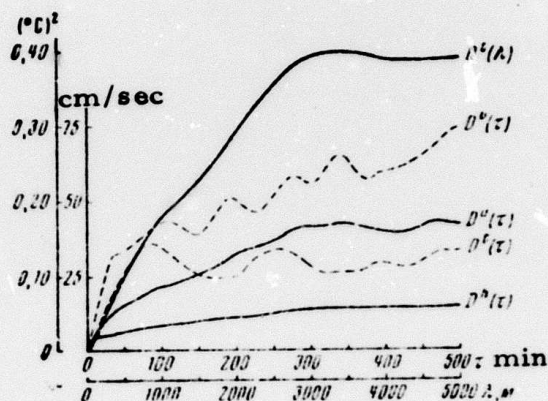
Fig. 1. Temporal structural functions of h(D^h),
latitudinal (D^u) and meridional (D^v) velocity components,
and temperature (D^t) fluctuations at 50 m depth, and
spatial structural function D^t (λ) of t fluctuations at
54 m depth from observations during the 3rd cruise.

Fluctuations of h are significantly less energetic than those
of u and v. Periodic fluctuations of t may occur during observations at b/s,
but periodic fluctuations of h are not observed. The energy of t fluctuations
in a vertical isotherm profile is significantly greater than energy determined
from measurements of the time dependence of fluctuations in one point (b/s)
This latter conclusion signifies that, at the same process scale, steady state
is possible in the absence of spatial homogeneity. Generally, the relative
velocity of spatial fluctuations is greater than the velocity of temporal
fluctuations. Initially, the relation

$$D(\lambda) = D(\tau = \lambda/c), \tag{1}$$

where C = const is the transfer velocity, is assumed to hold true. The
value of C = 17 cm/sec determined from Fig. 1 at τ = 75 min and λ = 500 m
coincides with the C value determined for the 50 m level at a neighboring b/s.
The constant C within a certain scale range can be used to distingish horizontal
turbulence from internal waves. The C values determined from congruence
of the velocity data at a b/s and temperature data from the profile, or
temperature data at a b/s and from the profile, are tabulated for different
depths and fluctuations scales. The tabulated C data show that some inhomo-
geneities are transferred at a nearly average speed of current, and the
phase velocity of others is very different from average speed.

-92-

The fine structure of velocity and temperature fluctuations is shown in three vertical cross-sections of corresponding structural functions, as determined from data during the 3rd cruise. They indicate that generation of internal waves is possible on account of a vertical shift of average velocity. Periodic fluctuations of temperature and velocity are observed for fairly large scale (3-5 km) and long period (5-10 h) fluctuations within the 50 to 100 m layer. The periodicity of $D^t(\lambda)$ is expressed much more strongly for small scale fluctuations, e.g., 600-800 m at $H > 80$ m, as shown by the $D^t(\lambda)$ plots at different H, obtained during the 8th cruise. The observed inhomogeneous vertical structure of the layer below 50 m is interpreted in terms of destruction of the short internal waves generated at the upper boundary of a stratified layer. This process leads to formation of the thermocline step structure. It follows that the Vaisalaa criterion is not always a reliable indicator of internal waves.

Statistical tests for deviations from steady state revealed the existence of large-scale waves, stepwise fluctuations, and a general variation in the mean velocity and temperature values. The nonstationarity of dispersion indicates a great intermittence of the processes and the trend toward formation of large-amplitude internal wave packets, widely spaced. Thus variability of the structure requires smoothing of dispersions or accounting for intermittence effect to obtain reliable conclusions.

Kozlyaninov, M. V. Using optical methods for observing internal waves in a highly stratified ocean. FAiO, no. 3, 1974, 312-314.

Location of water layers having high vertical gradients in density and transparency were determined with the help of optical methods, in experiments conducted for 17 hrs at an oceanographic station.

Transparency tests were done at $\lambda = 520\ \mu$; no other details of the test method are given. It was noted that a fast increase in density led to a sharp reduction in transparency. Fig. 1 shows the change in time of the
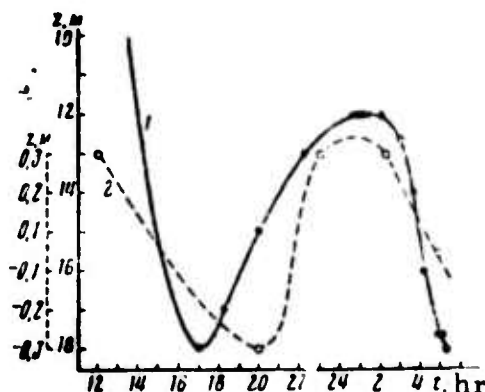
Fig. 1. Time change of depth of layer with max. transparency gradient (1) and sea level oscillation (2).

depth of the underlying water layer having a maximum vertical transparency gradient (solid line). The curve gives a graphic representation of the optically observed surface oscillations of the section between water masses, highly differing in density, i.e. internal waves. This has a smooth shape with a distinct semidiurnal period.

The dotted curve shows oscillations of the sea level during transparency measurement. The similarity of these two curves suggests that the cause of internal wave generation may be the tide-generating force. The amplitude of internal waves in this case was 6-7 m, while that of sea level oscillations was 50 cm. It is pointed out that this difference in amplitude may be explained by the significantly low difference of densities in water compared to that at the water-air boundary. Fig. 2 shows the curve for a fixed internal wave with semidiurnal period, generated on the surface of a section between water masses having a sharp difference in salinity. In

Fig. 2.   Interna' wave with semidiurnal period
(same as curve (1) in Fig. 1).

this case, the tidal effect is weak, and the cause of internal waves may
be seiche oscillations with a semidiurnal period, occurring in the
observation region.

Miropol'skiy, Yu. Z., and B. Ch. Filyushkin.
Statistical characteristics of isotherm variations
in the ocean in the presence of internal waves.
IN: Vnutrenniye volny v okeane, SO AN SSSR,
Novosibirsk, 1972, 119-134.

Temperature variations with periods from 2 to 40 min were
observed in a developed seasonal thermocline in presence of internal
waves.   The test program used a system of vertically located sensors in
the Black Sea, and was conducted by the Institute of Oceanology, AN SSSR.
Results of the observations, conducted in the open sea using eight sensors
placed vertically in a seasonal thermocline at 2-4 m spacing, were subjected
to statistical analysis.   Effects of the ship motion and vertical displacements
were neglected.   Horizontal drift equalled 0. 2 m/sec.   The total set of
recordings from all 8 sensors was taken during a period of 1 min.

Distribution of average characteristics with depth are shown
graphically.   A distinct thermocline was found to exist in the depth range
from 15 to 33 m, with a temperature drop of 10° C.   Two layers of water,
having a temperature gradient of 1° c/m, resulted in a complex stratification
of water in the thermocline.   The Vaisallaa frequency profile N had two

maxima spaced 6 m apart. All these characteristics indicate the fine structure of the studied thermocline.

Curves drawn for r.m.s. deviations of the average temperature and temperature gradient show that low-frequency oscillations exist only in the upper part of two thermocline layers. It is noted that the use of a filter allows exclusion of LF oscillations with periods over one hour. Curves are also drawn for the spectral function of temperature fluctuations, and it is seen from these that the fluctuations in temperature are due to the presence of internal waves.

A study was also conducted on the variation of temperature fluctuation energy with depth. Most of the energies were found to concentrate within the range of 15-27 m, i.e. in the zone of the maximum value of frequency N. Characteristic energy fluctuations in the presence of two maxima of N are explained theoretically with the help of a resonance mechanism of internal wave energy transfer from one layer to another.

Gavrilin, B. L., and A. P. Mirabel'. A numerical model of the energy spectrum, generated by the interaction of internal waves. IN: Vnutrinniye volny v okeane. SO AN SSSR, Novosibirsk, 1972, 152-167.

A mathematical model of a three-dimensional viscous incompressible fluid is discussed. Dynamic equations are obtained for a stratified form of the fluid. Exciting motions are assumed to be caused by the vertical velocity, given in the form of stationary waves, which are harmonically distributed in a horizontal direction and have a vertical profile corresponding to the internal wave profile. Emphasis is laid on large scale oceanic

processes, which are horizontal in nature and play an important role in forming vertical structures of hydrophysical elements. This role has been well illustrated by a simple thermocline model in a paper by G. I. Marchuk (Sbornik. Nekotoryye voprosy matematiki i mekhaniki, 1970). In the present work mathematical modelling of these horizontal motions is further analyzed, taking into account the energy distribution and vertical structures caused by oceanic processes.

2. Surface Effects

Zagorodnikov, A. A., and K. B. Chelyshev.
The application of optical processing to remote
measurements of waves. IN: Trudy Gos.
okeanograf. inst., no. 117, 1973, 25-34.

Automatic electrooptical processing of the vertical aerial
photographs and radar images of a sea surface is discussed. The
schematic diagram shown in Figure 1 of the image processing illustrates
the mathematical treatment. The transparency (x, y) in P_1 is illuminated
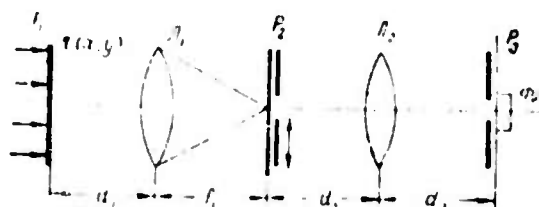
Fig. 1. Schematic electrooptical processing
of a sea surface image.

P_1 - object plane, L_1, L_2 - lenses, P_2 - frequency
plane, P_3 - photocathode plane.

with a coherent parallel light beam. Sea brightness B distribution over
the charted area, e. g., 10 x 10 km is correlated with sea surface contour.
In vertical aerial photography, there is a nonlinear correlation between
optical density D of the negative image and B; but there is a linear
correlation between D of the positive transparency and the back-scattered
light flux Q proportional to B, if only the positive contrast $Y_p = 1$.

It is shown that a two-dimensional wave spectrum $S_z(k, \theta)$,
where k is the wave number and θ is the polar angle, can be obtained by a
two-step processing of the positive transparency in P_1 and P_2 with $Y = 2$.
Also a negative transparency can be processed in P_1 and P_2, if the increment
of $Q, \Delta Q, < Q$. In any case, it is advisable to use a low-contrast film or plate
with maximum dynamic range.

A radar image of the sea surface in a P_1 transparency
can be obtained most advantageously using a side-looking radar, e.g.,
the Toros type, and converting the signal $Q(x, y)$ into D of the film. The
possibility is shown of obtaining in a single-step a positive transparency
with a linear $Q(x, y)$ dependence of the radar signal. The transparency
with a characteristic γ_θ such, that $\gamma_\theta \gamma_n = 2$, is obtained by
illuminating the film with contrast γ_n at incident intensity proportional to
that of an auxiliary amplifier, then proceeding to obtain two-dimensional
complex $S'_Q (U, V)$ and energy $S_Q (U, V)$ spectra of the radar image in a
U, V coordinate system. The $S_{QA}(k, \theta)$ and $S_{Q\,rd}(U, V)$ spectra of the
aerial photographs and radar images of the sea surface are correlated
with the corresponding two-dimensional wave spectra $S_z(k, \theta)$ and $S_z(U, V)$
and are used to determine other statistical characteristics of sea surface
waves. Thus, one-dimensional frequency and angular wave spectra $S_z(k)$
and $S_z(\theta)$ can be obtained by processing aerial photographs and radar images
of the sea surface. A simplified formula for $S_z(k)$ as a function of $S_{Qrd}(k)$
is derived for the case of an isotropic radar filter. A comparison of a sea
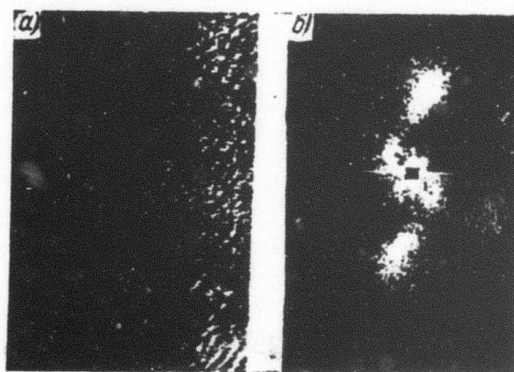surface photograph with its energy spectrum is shown in Fig. 2.

Fig. 2. Aerial photo of wavy surface (a) and its
two-dimensional energy spectrum (b).

Zagorodnikov, A. A. Wave parameter
measurements as a function of the speed of
the measuring equipment platform. IN:
Trudy. Gos. okeanograf. inst., no. 117,
1973, 35-45.

The author discusses remote measurement of wave parameters
to obtain desired information on sea profile and other wave characteristics.
The effects of motion of the measuring equipment carrier on the results of
wave parameter measurements have been dealt in a series of previous works.
However, these works do not give concrete relationships which could be used
for estimating errors and selecting conditions of minimum error during such
measurements. The author asserts that, at high speeds of the equipment
carrier, e.g. an aircraft, which may exceed by several times the phase
velocity of wave spectral components, it may be necessary to correct for
the difference between the apparent spatial spectrum and the time-fixed
spectrum of wave profiles. The problem is treated analytically, based on
equations for elementary plane waves. It is shown that if the information on
the cross-section of a surface wave profile in the direction of radiation is
obtained by hydroacoustic or e-m waves, then motion distortions in these
case are so negligible that the wave profile can be considered fixed. In case
of a moving equipment platform, the level of distortions is also minimal,
if platform movement is along the wave crest line. In summary, the
conclusions are:

1. In obtaining information on spatial wave characteristics
by remote methods, motion distortions occur in the recorded spectrum as
compared to the spectrum of a fixed profile.

2. Distortions due to finite velocity of e-m and hydroacoustic
wave propagations can be neglected.

3. In obtaining a spatial cross-section of the profile by displacement of the measuring equipment platform at a finite velocity, the degree of distortion depends on the relation between average phase wave velocity and the carrier velocity. Minimum distortion occurs during motion of the carrier along a crest line.

4. At $\bar{c}/V_n = 0.1$ (where $\bar{c}$ - phase velocity, and V_n = carrier velocity), maximum variations in average wavelength as measured by the remote method amount to 6-7% relative to the wavelength in a fixed profile.

5. During measurements of the time characteristics of waves with a drifting carrier, compression and expansion of the frequency-time spectrum take place depending on the relation between the carrier velocity projection in the main direction and the average wave phase velocity.

Zhilko, Ye. O., A. A. Zagorodnikov, I. V. Kireyev, V. I. Korniyenko, B. A. Maksimov, and A. V. Svechnikov. The results of comparative measurements aboard the weather R/V Passat of wind wave parameters using radar techniques and a wave gage. IN: Trudy. Gos. okeanograf. inst., no. 117, 1973, 5-16.

Tests are described in which wind-wave parameters were measured with radar and a high-sea wave gage. The experiments were conducted during the 6th cruise of the weather R/V Passat from 4 May to 2 August 1971. The major part of experiments was conducted in the ship's

main operating area (37° N, 70° W) by means of comparative wave measurements using shipboard radar and a GM-62 high-sea wave gage. Measurements were made with the Don navigational radar (nonstabilized antenna) and a Meteorit meteorological radar (stabilized antenna. The experiment procedures are described in detail. Relationships of the reflected signal intensity as a function of antenna azimuth, obtained at different times and under different hydrometeorological conditions, are shown in Fig. 1. Main direction of the wave motion is determined by
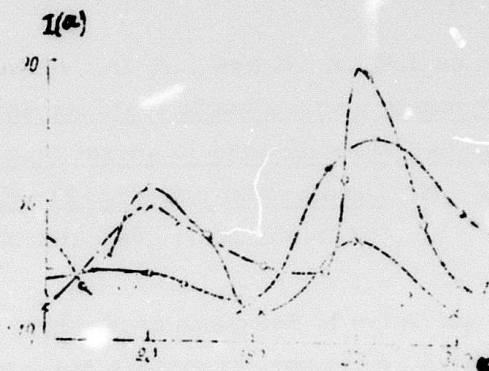
Fig. 1. Relationship of reflected signal intensity to antenna azimuth, under different wave conditions.

angles 90° (curve 1), 270° (curve 2) and 90° (curve 3). Curve 3 was plotted for wind and swell in the same direction, and curves 1 and 2, for different directions. Error in wave height measurements was determined by comparing the readings of the Don's wave-height measurement attachment with wave heights measured by the GM-62 gage. It is concluded that:

1) Heights of the sea waves can be measured with conventional navigational radars equipped with devices which separate the necessary information from the radar signals;

2) To determine the main direction of wave motion with an accuracy of several degrees, it is necessary to equip the navigational radar with an additional manual drive for antenna rotation and rotation angle indicator;

-102-

3) Maximum error in wave height measurement can be kept within the 10-15% range;

4) It is advisable to install an automatic gain control in the IF amplifier circuit for extending the optimum range and thus improving the unit's operation.

Buznikov, A. A., and N. A. Polyakova.
On the problem of automating measurement and processing of experimental results aboard the IL-18 airborne laboratory. IN: Trudy GGO, no. 295, 1973, 124-133.

The problem is analyzed of selecting an automatic data recording and conversion system to convert an existing airborne analog data recording system into a digital system. This conversion is necessary to process the great flow of data from numerous current scientific experiments, such as the complex experiment with atmospheric energy (KENEKS) conducted aboard the IL-18 aircraft of the GGO, or the synchronous study of optical characteristics of the atmosphere-underlying surface system during flights of the Soyuz manned spacecrafts and the Salyut space station.

Selection of a suitable airborne recording system is made on the basis of the minimum query interval Δt of instantaneous signal values, necessary to prevent loss of significant information. A simple method is given to calculate Δt_{min}, namely

$$\Delta t = \frac{2(v_{\text{макс}} - v_{\text{мин}})}{100 \, v_{\text{макс}}} \cdot \frac{\Delta x}{v_{\text{макс}}},$$

(1),

where $(x_{max} - x_{min})$ is the minimum increment of the variable x, ϵ is the admissible error of measurement for a given system, and Δx is the output resolution. Calculation of Δt for the instrument systems aboard the IL-18 airborne laboratory led to the conclusion that a system having t = 4-5 times/sec and 50 information channels is required.

The existing K60-42 airborne magnetic storage is described as satisfying the cited requirement. It was designed to convert sensor analog signals in the 0-5 GHz frequency range to a 9-unit binary parallel code, with magnetic tape recording and storage of coded signals. In addition to the airborne magnetic storage (Fig. 1) the K60-42 data system includes
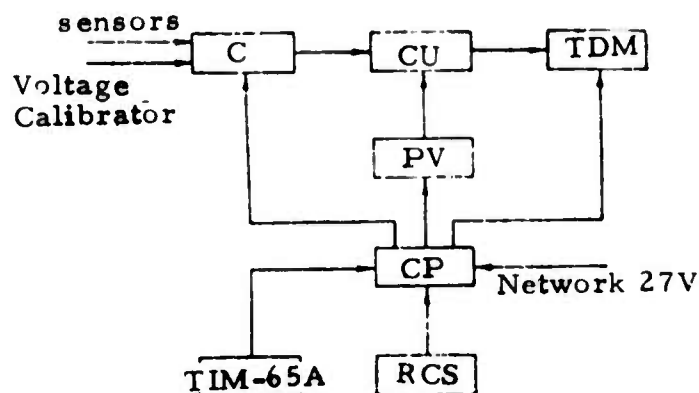

Fig. 1. Airborne apparatus of the K60-42 data system: C - commutator, CU - converter unit, TDM - tape-drive mechanism, PU - power unit, CP - control panel, RCS - remote control station, TIM-65A-time interval meter.

a ground digiverter for fast information retrieval and input hardware for the M-220 and Dnepr-21 computers.

Performance characteristics of the K60-42 data system are given. Comparison of these characteristics with the requirements of the data system aboard the IL-18 laboratory showed the suitability of the K60-42 system for given purpose. A similarity in automation fundamentals and engineering solutions is noted between the K60-42 system and the U.S.-developed ARIS-II hybrid data system for atmospheric research, although the latter system is considered the more flexible.

The authors conclude that the K60-42 data system in conjunction with digital computers would solve the problem of automating the measurement and processing of experimental data aboard the IL-18 laboratory, and would increase its overall efficiency.

Marchenko, Yu. I., N. N. Lazarenko, and B. M. Andreyev. Airborne radar wave gage. IN: Trudy Gos. okeanograf inst., no. 117, 1973, 57-67.

Theoretical aspects of wave height measurement are discussed, an operational model of airborne radar wave meter is described, and some results from in-flight tests are given. The meter's operation is based on the Huygens-Kirchhoff theory of reflected waves. In the framework of this theory, formulas are derived for calculation of radii of the mirror reflection and diffuse reflection areas and the flight line l as functions of flight altitude R and the transmitted pulse length τ_t. The radii and l data necessary for averaging wave heights h over a sea area are tabulated for a 10 m radar wavelength, $\tau_t = 1 \mu sec$, and R = 2000-10,000 m. It is shown that for airborne measurements, the ratio P_c/P_n of the coherent to noncoherent power components of the reflected signal is a more practical measure of h than P_c and P_n, because of mutual compensation of destabilizing factors in P_c/P_n measurements. Thus, h can be determined more accurately than

by measuring P_c and P_n separately. Actually, the σ_F/m ratio of the root mean square value of target envelope fluctuations to the mean value of the target envelope is measured, then the σ_h/λ ratio of the root mean square value of surface roughness to the radar wavelength is determined from the formulas for σ_F/m as a function of P_c/P_n, and P_c/P_n as a function of σ_h/λ. The mean $\bar{h}$ is given by

$$h \mid 2 \pi \sigma_h \tag{1}$$

and the wave height with a given permissible value in Rayleigh distribution

$$h_F - \bar{h} \sqrt{-\frac{4}{\pi} \ln F} \tag{2}.$$

It is shown that h up to 3.5 m can be measured at $\lambda = 10$ m. The radar wave meter model is composed of an antenna with a wide radiation pattern, a receiver, a peak detector, a synchronizer, a filter unit measuring σ_F/m, a dial indicator of σ_F/m, which is calibrated in $h_{3\%}$, a microammeter, and a EMO-2 control oscilloscope. The peak detector and its output stage (filter unit) are described in detail. The wave meter weighs about 25 kg. The flight tests were carried out aboard an LI-2 aircraft at 900-3000 m altitudes over the Caspian Sea. The maximum wave height $h_{3\%}$ was 3 m in 15 m/sec winds. Simultaneous comparative measurements were made using a wire-type wave gage. Two sets of $\bar{h}$ data are shown in Table 1.

Table 1

Average wave period, sec	Mean wave height from:	
	wave recordings	radar wave meter data
5.1	1.05	1.10
5.2	1.17	
5.2	1.07	1.08
5.2	1.09	
4.8	1.18	1.08
4.9	1.10	
4.8	1.07	1.05
4.8	1.04	
5.2	1.17	1.00
5.1	0.95	

The two sets of tabulated data differ by a maximum of 10%. The spectral density functions $S(\omega)$ were calculated from three recordings of the wire-type wave gage and from the output-signal records of the radar wave meter. An unexplained discrepancy, particularly at low frequencies ω, is shown between the $S(\omega)$ plots calculated from two sets of data. It is concluded that the airborne radar wave meter can be used to determine h of the sea waves measuring sea states 1-5.

Vinogradov, V. V., and N. N. Lazarenko.
Airborne stereophotogrammetric survey of
storm waves. IN: Trudy Gos. okeanograf.
inst., no. 117, 1973, 46-56.

Surveying equipment and methods, including data processing methods, are presented which have been used in two-aircraft stereophoto-grammetric surveys of storm waves, up to 11-12 m high, in the Baltic, White, and Barents Seas, in connection with coastal engineering constructions. In addition to the measuring instruments and two AFA aerial photo cameras, the airborne equipment included an automatic radio synchronizer designed in 1966 at the Leningrad Branch of the State Oceanographic Institute, in collaboration with the Leningrad Electrotechnical Institute. The radio synchronizer (Fig. 1) consists of two electronic units aboard the lead and trailing aircraft, which control the AFA-1 shutter-opening delay relative to AFA-2 shutter opening. This control can be either automatic (using a comparison circuit) or manual (by turning the control knobs until the pulse oscilloscope traces coincide). The maximum error of automatic and manual synchronization of the two AFA cameras is 3 and 1-2 msec, respectively. In actual surveys from two aircraft, the minimum scale was 1:8500 and the base (distance between the aircraft) was selected according to a given side lap of the stereograms. The requirement is stressed for a maximum possible overlap allowing for accurate measurement of wave height at different
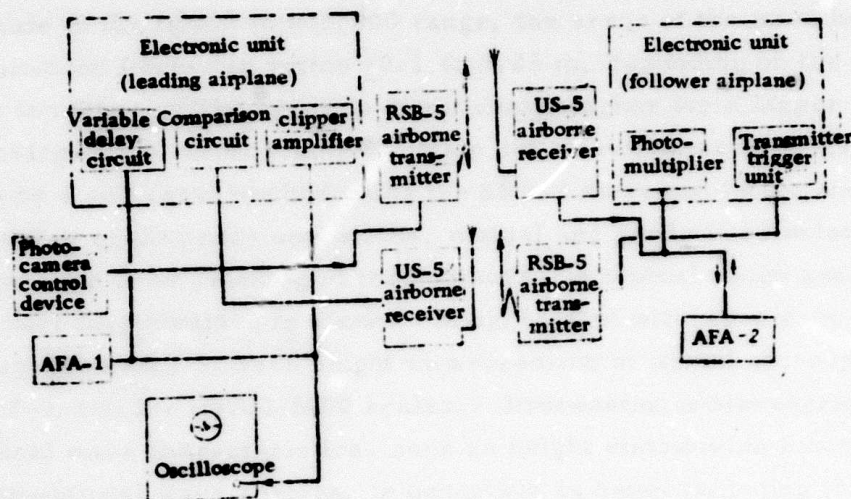
Fig. 1.   Automatic radio synchronizer.

scales.   At equal scale and flight altitude, the surveyed area on the
stereogram increases by 23%, when the overlap is increased from 65 to
80% (Table 1).

Table 1

Scale	Altitude, m	Overlap		Overlap	
		Base, m	Area, m	Base, m	Area, m
1:2000	140	108	252×360	72	288×360
1:5000	350	270	630×900	180	720×900
1:10 000	700	540	1250×1800	360	1440×1800
1:20 000	1400	1080	2520×3600	720	2880×3600

At a scale in the 1:2000 to 1:15,000 range, the error of the wave height determination fluctuates within +0.1 to 0.25 m, depending on the increase in side lap (base). The error is significantly higher for a larger scale. Processing of the stereograms to obtain sea wave characteristics was done mainly by a universal method using the SPR-2 stereoprojector, and consisted of preliminary operations, mutual and geodetic orientation, contour mapping, and point pricking of the contours. A typical rough seas plane-table chart thus obtained is shown. In agreement with wave gage data, the mean square error of wave height measurement by aerial stereophotogrammetry was 0.2-0.3 m for 1:3000-5000 scales. Processing of stereograms for statistical wave characteristics, such as height distribution functions and two-dimensional wave spectra, is described in detail including the use of computers.

Ivanov, A. P., and I. I. Kalinin. Determining the optical characteristics of ocean water by laser sounding. IN: Morskoye gidrofiz. issledovaniye, no. 1, 1973, 189-199.

First experiments on the practical possibility measuring light absorption coefficient k and attenuation factor $\mathcal{E}$ ($\mathcal{E} = k + \sigma$, where σ is dispersion coefficient) in water are described by A. P. Ivanov et al. (ZhPS, v. 17, no. 2, 1972). The present work describes results of further studies conducted during the 26th expedition of the R/V Mikhail Lomonosov.

The light source used was a neodynium glass laser with Q-switching and frequency doubling. Power output at 530 nm was 100 kw and pulse duration was 25 nsec. Angular beam divergence of the source was variable within 9 to 15'. Light dispersion from the medium was recorded on an Sl-ll oscillograph. For checking this laser sounding method, an

independent determination of ε was made by means of a basic transparency meter, designed at the Institute of Physics, AN BSSR. It was found from oscillographic data that the pulsed sounding method can be used with sufficient accuracy in regulating sea water transparency up to a value $\varepsilon \cong 0.2 \ m^{-1}$; however at higher ε the error introduced by scattering becomes intolerable.

Measurements were similarly conducted of the coefficient of absorption k. A detailed description is given of the experimental as well as theoretical procedures. Results of the measurements of k, determined by laser sounding of the water surface, are given in Table 1. Other optical

Table 1

Values of optical characteristics of water at surface layer.

Date	$\kappa, \ m^{-1}$	$\varepsilon, \ m^{-1}$	Λ
1.4.72	0,02	0,22	0,91
2.4.72	0,13	0,40	0,68
19.4.72	0,05	0,35	0,86
21.4.72	0,05	0,47	0,89
23.4.72	0,07	0,20	0,65
26.4.72	0,01	0,08	0,87
28.4.72	0,02	not determined	
21.5.72	0,03	0,18	0,83
22.5.72	0,03	0,10	0,70
23.5.72	0,03	0,30	0,90
29.5.72	0,02	0,10	0,80
30.5.72	0,03	0,20	0,85

characteristics are also indicated in the table (attenuation factor ε was measured here by basic transparency meter). It is seen from the table that in spite of different water transparencies there is a high probability of photon existence Λ on the upper water surface in most cases. Specific

correlations between $\mathcal{E}$ and Λ were not evident in the cited experiments ($\Lambda = \mathcal{E}/\mathcal{E} + k$, probability of photon existence).

A brief abstract of this article was given earlier. (<u>Soviet Material on Internal Wave Effects</u>, 30 April 1974, p. 25)

Lyapin, K. K., V. A. Polyanskiy, and I. F. Shishkin. <u>Target selection from sea surface clutter</u>. Radiotekhnika, no. 2, 1974, 76-77.

An improved experimental radar for selecting targets from sea surface clutter was tested; the arrangement is shown in Fig. 1. In the receive-transmit mode, polarization was rotated at a rate of 0.5 rev/sec using motor M. The sweep indicator I rotates synchronously in angle, and its deviation from the center of the CRT corresponds to the signal received.
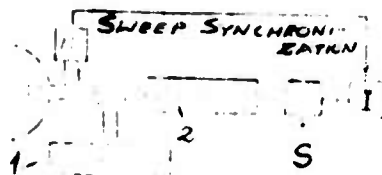
Fig. 1. Experimental Scheme
1- Transmitter; 2- Receiver; M- Motor;
S(C)- Gating pulse; I- Sweep indicator.

Range gating of the sea surface sectors and targets was accomplished by using matching stage S. Figures 2 and 3 show typical photographs of the display (I) obtained for a 3-second exposure while irradiating a 15 x 60 m area of the sea surface and a tugboat. The grazing angle of the beam was 1°, and sea state was 2. The engineering development of this method is much simpler,

Fig. 2.

Sea surface return.

Fig. 3.

Return from surface vessel.

as compared to the automatic adjustment of a radar antenna unit to an optimum polarization during radiation and receiving modes. A limitation to the method's use lies in the fact that the spatial scanning rate decreases due to accumulation during the polarization sweep.

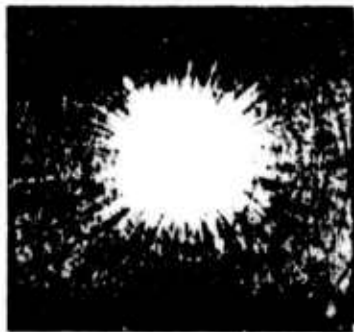Chudakov, V. I., and A. M. Shalygin. Some results of the radar investigation of a cover glacier. IN: Trudy. Sovetskaya antarkticheskaya ekspeditsiya, no. 59, 1973, 147-152.

Results are described of radar sounding of glaciers in order to measure their thickness by estimating electromagnetic signal absorption in ice, together with a study of the depolarization of e-m waves in the glacier. Simultaneous measurements of glacier thickness by radar and of the modulus of total magnetic field intensity vector by a proton magnetometer were conducted for the first time during the 15th Soviet Antarctic expedition in the region of Molodezhnaya Station - 125 km deep in the continent along a meridian. The radar was operated at 60 MHz, at a pulse power P_{imp} = 20 kw. Fig. 1 shows
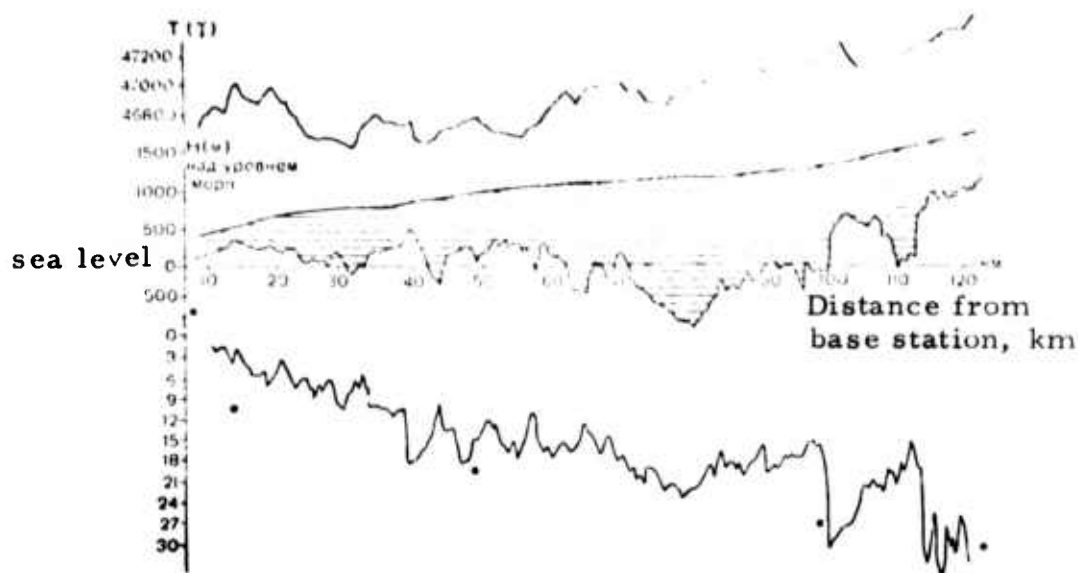
Fig. 1. Glacier cross-section, temperature
absorption by glacier (mean annual) and modulus
of the total magnetic field intensity vector (T)
along the expedition route.

the cross-section of glacier, temperature absorption by glacier, and
change in modulus of the total magnetic field intensity vector. Glacier
thickness was calculated assuming a propagation velocity of e-m waves
C = 167 m/ sec. Results obtained were found to be in good agreement with
those of the 14 th Soviet Antarctic expedition.

The study of the depolarization of e-m waves reflected from
the glacier was conducted at a frequency of 440 MHz. Dipole antennas with
reflectors were used in these experiments, and polarization diagrams were
drawn for various positions of the transmitting and receiving dipoles.

Measurements of glacier thickness were also conducted at
Waterloo Island in the Bellingshausen Sea region. The radar was operated at
f = 440 MHz, with P_{imp} = 10 watt. Temperature absorption by the glacier
was not determined in this case, because of the difficulties in calculating loss
of e-m energy due to surface thawing of glaciers.

Kapitanov, V. A., Yu. V. Mel'nichuk, and
A. A. Chernikov. Spectra of centimeter-band
radar returns from forests. RiE, no. 9, 1973,
1816-1825.

Effects of the motion characteristics of scatterers on the
shape of spectra of radar returns are studied. Experimental results are
described of investigations of reflection spectra from a forest at the 3.2 cm
wavelength up to spectral density levels of (-) 36 to (-) 40 db relative to
the maximum. It was seen that at small grazing angles, the spectral density
to (-)10 to (-) 15 db levels for values of the parameter $4\pi\sigma_1/\lambda \gg 1$ (where
σ_1 is the rms tree crown and trunk top sway; λ is the wavelength) may be
approximated by a Gaussian curve; further decrease of the spectral density
is described by power law with an exponent of about -4. For $4\pi\sigma_1/ \ll 1$,
the spectral density for levels lower than (-) 15 to (-) 20 db follows the
above power law.

Along with above measurements, horizontal motion of tree
limbs and trunk were investigated simultaneously. A model is suggested for
shaping spectra of radar signals from forests. Comparision of the measured
parameters of radar signal spectra with those of calculations showed that
the suggested model is quite satisfactory. Spectrum measurements of
orthogonally polarized components of return signals for waves of different
polarization are also found to be in good agreement with the model.

The authors point out that the results of the present work apply
mostly to mixed forest conditions and small grazing angles. For extending
these results to different conditions, additional experimental investigations
probably are necessary. It is suggested that along with radar and meteorological
measurements, it would be advantageous to conduct more thorough investigations
on the dynamics of the basic elements of multiple targets, so that both the phase
and amplitude characteristics of elementary signals could be obtained
simultaneously.

Kondrat'yev, K. Ya., Ye. M. Shul'gina, O. M.
Pokrovskiy, and Yu. M. Timofeyev. Possibility
of remote sensing of soils in the centimeter
band. IN: Trudy GGO, no. 295, 1973, 86-97.

A numerical solution to the inverse problem of the soil
temperature profile $T(z)$, as reconstructed from radio-frequency remote
sensing data on soil brightness temperature T_b (λ), is analyzed for
accuracy. Also, the amount of information in the T_b (λ) measurement
data is discussed.

The numerical solution reduces to that of a Fredholm integral
equation of the first kind on the assumption that vertical profiles of soil
absorption coefficient and its moisture content, w, are constant and w is
given. Two methods of stationary solution of the Fredholm equation, i.e.
with and without use of empirical statistical data, are described briefly.
The methods make it possible to analyze the amount of information in the
measurements. A graphical comparison of the kernels of the cited integral
equation, which were calculated in the process of reconstruction of the soil
$T(z)$ and the atmospheric $T(p)$, indicates limits to applicability of the indirect
determination of soil $T(z)$. As to the amount of information in T_b (λ)
measurements, the analysis of calculated kernels showed than an experimental
apparatus with two to three sensing channels, e.g., for 3 and 60 cm wavelengths,
is sufficient to measure one or two independent parameters of T_b (λ) with
$0.5\text{-}1^o$ K accuracy. The program of numerical calculations consisted of
solving first the direct problem, then the inverse problem by introducing
random errors and using w values of 3, 6, 9, and 12%.

The tabulated and plotted data of the numerical experiment led
to the conclusions that: 1) reconstruction of $T(z)$ with $1\text{-}3^o$ K accuracy is
feasible, if T_b (λ) is measured with 0.5^o K accuracy; 2) accuracy of
reconstruction by a statistical method depends significantly on the adequacy
of the statistics used, and 3) independent determinations of w accurate to 1%

are necessary, for an accurate $T(z)$ reconstruction. It follows from the conclusion under 2) that the use of the reconstruction methods, based on general <u>a priori</u> assumptions of the unknown solution, is advisable since statistics are very scarce in the literature.

Kondrat'yev, K. Ya., and O. I. Smoktiy.
<u>Determining spectral transfer functions for</u>
<u>brightness and contrast of natural formations,</u>
<u>from space spectrophotometry of the atmosphere-</u>
<u>underlying surface system.</u> IN: Trudy GGO, no. 295, 1973, 24-50.

A theoretical solution is presented to the problem of reducing to the surface level the spectrophotometric data from space on brightnesses I_{ob} and I_B of a surface object and background, and their contrast k. The problem arises in geological and geographic surveys of the Earth and planets, aerial photography, geodesy, etc, due to the presence of an atmospheric light-scattering layer between a manned spacecraft or unmanned interplanetary station and the planet surface. The solution is obtained by introducing spectral transfer functions Π_{ob}, Π_B and P_{ob}, P_B for I and k, respectively. The Π_{ob} and Π_B are defined as the functions of I_{ob}^0/I_{oB} and I_B^0/I_B, where I_{ob}^0 and I_B^0 are the unknown values of I at the surface level. Using the plane-parallel layer model of the atmosphere and the above definition of Π, the function P_{ob}, in the case of $I_{ob} > I_B$, is defined as the ratio k_0/k, where k_0 is given by

$$k_0 = I_{ob}^0 - I_B/I_{oh}^0 \gg O \qquad (1).$$

The function P_B is defined similarly for the case $I_B > I_{ob}$. Fundamental

functions of the light scattering theory are used to calculate Π, its component I_0, and P in the classical case of a surface uniformly extended to infinity with albedo A, and in some particular cases. The classical-case formulas of Π and I_0 are applicable with some modifications to the cases of a uniform infinitely extended surface formed by two uniform half-planes with albedo A_i (i = 1, 2). The modification consists of substituting A_i for A in the and I_0 formulas for the boundary value problem far from the interface of two half-planes. In two other boundary value problems analyzed (near the interface and at some intermediate distance from it), A_i is approximated by the arithmetic mean A = 1.2 ($A_1 + A_2$) and by the parameters α_i, β_i intermediate between A_i, min and A_i, max, respectively. The $P_i = P_i = k_{0,i}/k_i$ values of the contrast between two surfaces are calculated using

$$k_i = \frac{|I_1 - I_2|}{I_i} \ge 0; \quad k_{0,i} = \frac{|I_{0,1} - I_{0,2}|}{I_{0,i}} \ge 0, \tag{2}$$

in the problems far from and near the interface and an approximate formula for I_i in the third problem. Corresponding simplified formulas are derived for Π, Π_i, $\bar{\Pi}_i$, P_i, and $\bar{P}_i$ in the case of pointing in a direction close to the nadir ($\eta \sim 1$), small zenith distances to the Sun ($\bar{\zeta} \sim 1$), and A > 0.5. These formulas are applicable in the visible and IR spectral ranges. In the particular case of a small terrestrial object and an extensive background with varying albedo A_{ob} and A_B, approximate formulas for I_{ob}^0, I_B^0, Π_{ob}, Π_B, P_{ob}, and P_B are derived, under certain assumptions. Also, simplified Π_{ob}, Π_B, P_{ob}, and P_B formulas are given for the case of $\eta \sim 1$, $\zeta \sim 1$, A_{ob} and A_B > 0.5. In the classical case, the tabulated results of numerical calculations Π_λ, P_λ, $I_{0,\lambda}$, and their components show that identification of geological and geographic formations from space is most efficient in the near IR spectral range with the Sun in a high position, pointing to nadir, and in the absence of aerosols. The $\bar{\Pi}_i$, $\bar{P}_i$, and their component data calculated for sandclouds and sand-sea interfaces are tabulated for comparison purposes.

Volosyuk, V. K., S. Yu. Oleynikov, and
V. G. Yakovlev. Estimating effectiveness
of selecting moving targets in sea background.
IN: Sb. Radioelektronika letalel'n. apparatov.
Khar'kov, no. 5, 1973, 87-94. (RZhF, 11/73,
no. 11Zh123). (Translation)

Values are calculated of the coefficient of below-noise visibility and the effectiveness of a per-period subtraction device is estimated, for target detection in a wavy sea background at [transmitted] wavelengths of 1-30 cm.

3. SOURCE ABBREVIATIONS

AiT	-	Avtomatika i telemekhanika
APP	-	Acta physica polonica
DAN ArmSSR	-	Akademiya nauk Armyanskoy SSR. Doklady
DAN AzSSR	-	Akademiya nauk Azerbaydzhanskoy SSR. Doklady
DAN BSSR	-	Akademiya nauk Belorusskoy SSR. Doklady
DAN SSSR	-	Akademiya nauk SSSR. Doklady
DAN TadSSR	-	Akademiya nauk Tadzhikskoy SSR. Doklady
DAN UkrSSR	-	Akademiya nauk Ukrainskoy SSR. Dopovidi
DAN UzbSSR	-	Akademiya nauk Uzbekskoy SSR. Doklady
DBAN	-	Bulgarska akademiya na naukite. Doklady
EOM	-	Elektronnaya obrabotka materialov
FAiO	-	Akademiya nauk SSSR. Izvestiya. Fizika atmosfery i okeana
FGiV	-	Fizika goreniya i vzryva
FiKhOM	-	Fizika i khimiya obrabotka materialov
F-KhMM	-	Fiziko-khimicheskaya mekhanika materialov
FMiM	-	Fizika metallov i metallovedeniye
FTP	-	Fizika i tekhnika poluprovodnikov
FTT	-	Fizika tverdogo tela
FZh	-	Fiziologicheskiy zhurnal
GiA	-	Geomagnetizm i aeronomiya
GiK	-	Geodeziya i kartografiya
IAN Arm	-	Akademiya nauk Armyanskoy SSR. Izvestiya. Fizika
IAN Az	-	Akademiya nauk Azerbaydzhanskoy SSR. Izvestiya. Seriya fiziko-tekhnicheskikh i matematicheskikh nauk

IAN B	-	Akademiya nauk Belorusskoy SSR. Izvestiya. Seriya fiziko-matematicheskikh nauk
IAN Biol	-	Akademiya nauk SSSR. Izvestiya. Seriya biologicheskaya
IAN Energ	-	Akademiya nauk SSSR. Izvestiya. Energetika i transport
IAN Est	--	Akademiya nauk Estonskoy SSR. Izvestiya. Fizika matematika
IAN Fiz	-	Akademiya nauk SSSR. Izvestiya. Seriya fizicheskaya
IAN Fizika zemli	-	Akademiya nauk SSSR. Izvestiya. Fizika zemli
IAN Kh	-	Akademiya nauk SSSR. Izvestiya. Seriya khimicheskaya
IAN Lat	-	Akademiya nauk Latviyskoy SSR. Izvestiya
IAN Met	-	Akademiya nauk SSSR. Izvestiya. Metally
IAN Mold	-	Akademiya nauk Moldavskoy SSR. Izvestiya. Seriya fiziko-tekhnicheskikh i matematicheskikh nauk
IAN SO SSSR	-	Akademiya nauk SSSR. Sibirskoye otdeleniye. Izvestiya
IAN Tadzh	-	Akademiya nauk Tadzhiksoy SSR. Izvestiya. Otdeleniye fiziko-matematicheskikh i geologo-khimicheskikh nauk
IAN TK	-	Akademiya nauk SSSR. Izvestiya. Tekhnicheskaya kibernetika
IAN Turk	-	Akademiya nauk Turkmenskoy SSR. Izvestiya. Seriya fiziko-tekhnicheskikh, khimicheskikh, i geologicheskikh nauk
IAN Uzb	-	Akademiya nauk Uzbekskoy SSR. Izvestiya. Seriya fiziko-matematicheskikh nauk
IBAN	-	Bulgarska akademiya na naukite. Fizicheski institut. Izvestiya na fizicheskaya institut s ANEB
I-FZh	-	Inzhenerno-fizicheskiy zhurnal

IiR	-	Izobretatel' i ratsionalizator
ILEI	-	Leningradskiy elektrotekhnicheskiy institut. Izvestiya
IT	-	Izmeritel'naya tekhnika
IVUZ Avia	-	Izvestiya vysshikh uchebnykh zavedeniy. Aviatsionnaya tekhnika
IVUZ Cher	-	Izvestiya vysshikh uchebnykh zavedeniy. Chernaya metallurgiya
IVUZ Energ	-	Izvestiya vysshikh uchebnykh zavedeniy. Energetika
IVUZ Fiz	-	Izvestiya vysshikh uchebnykh zavedeniy. Fizika
IVUZ Geod	-	Izvestiya vysshikh uchebnykh zavedeniy. Geodeziya i aerofotos"yemka
IVUZ Geol	-	Izvestiya vysshikh uchebnykh zavedeniy. Geologiya i razvedka
IVUZ Gorn	-	Izvestiya vysshikh uchebnykh zavedeniy. Gornyy zhurnal
IVUZ Mash	-	Izvestiya vysshikh uchebnykh zavedeniy. Mashinostroyeniye
IVUZ Priboro	-	Izvestiya vysshikh uchebnykh zavedeniy. Priborostroyeniye
IVUZ Radioelektr	-	Izvestiya vysshikh uchebnykh zavedeniy. Radioelektronika
IVUZ Radiofiz	-	Izvestiya vysshikh uchebnykh zavedeniy. Radiofizika
IVUZ Stroi	-	Izvestiya vysshikh uchebnykh zavedeniy. Stroitel'stvo i arkhitektura
KhVE	-	Khimiya vysokikh energiy
KiK	-	Kinetika i kataliz
KL	-	Knizhnaya letopis'
Kristall	-	Kristallografiya
KSpF	-	Kratkiye soobshcheniya po fizike

LZhS	-	Letopis' zhurnal'nykh statey
MiTOM	-	Metallovedeniye i termicheskaya obrabotka materialov
MP	-	Mekhanika polimerov
MTT	-	Akademiya nauk SSSR. Izvestiya. Mekhanika tverdogo tela
MZhiG	-	Akademiya nauk SSSR. Izvestiya. Mekhanika zhidkosti i gaza
NK	-	Novyye knigi
NM	-	Akademiya nauk SSSR. Izvestiya. Neorganicheskiye materialy
NTO SSSR	-	Nauchno-tekhnicheskiye obshchestva SSSR
OiS	-	Optika i spektroskopiya
OMP	-	Optiko-mekhanicheskaya promyshlennost'
Otkr izobr	-	Otkrytiya, izobreteniya, promyshlennyye obraztsy, tovarnyye znaki
PF	-	Postepy fizyki
Phys abs	-	Physics abstracts
PM	-	Prikladnaya mekhanika
PMM	-	Prikladnaya matematika i mekhanika
PSS	-	Physica status solidi
PSU	-	Pribory i sistemy upravleniya
PTE	-	Pribory i tekhnika eksperimenta
Radiotekh	-	Radiotekhnika
RiE	-	Radiotekhnika i elektronika
RZhAvtom	-	Referativnyy zhurnal. Avtomatika, tele-mekhanika i vychislitel'naya tekhnika
RZhElektr	-	Referativnyy zhurnal. Elektronika i yeye primeneniye

RZhF	-	Referativnyy zhurnal. Fizika
RZhFoto	-	Referativnyy zhurnal. Fotokinotekhnika
RZhGeod	-	Referativnyy zhurnal. Geodeziya i aeros"-yemka
RZhGeofiz	-	Referativnyy zhurnal. Geofizika
RZhInf	-	Referativnyy zhurnal. Informatics
RZhKh	-	Referativnyy zhurnal. Khimiya
RZhMekh	-	Referativnyy zhurnal. Mekhanika
RZhMetrolog	-	Referativnyy zhurnal. Metrologiya i izmer-itel'naya tekhnika
RZhRadiot	-	Referativnyy zhurnal. Radiotekhnika
SovSciRev	-	Soviet science review
TiEKh	-	Teoreticheskaya i eksperimental'naya khimiya
TKiT	-	Tekhnika kino i televideniya
TMF	-	Teoreticheskaya i matematicheskaya fizika
TVT	-	Teplofizika vysokikh temperatur
UFN	-	Uspekhi fizicheskikh nauk
UFZh	-	Ukrainskiy fizicheskiy zhurnal
UMS	-	Ustalost' metallov i splavov
UNF	-	Uspekhi nauchnoy fotografii
VAN	-	Akademiya nauk SSSR. Vestnik
VAN BSSR	-	Akademiya nauk Belorusskoy SSR. Vestnik
VAN KazSSR	-	Akademiya nauk Kazakhskoy SSR. Vestnik
VBU	-	Belorusskiy universitet. Vestnik
VNDKh SSSR	-	VNDKh SSSR. Informatsionnyy byulleten'
VLU	-	Leningradskiy universitet. Vestnik. Fizika, khimiya
VMU	-	Moskovskiy universitet. Vestnik. Seriya fizika, astronomiya

ZhETF	-	Zhurnal eksperimental'noy i teoreticheskoy fiziki
ZhETF P	-	Pis'ma v Zhurnal eksperimental'noy i teoreticheskoy fiziki
ZhFKh	-	Zhurnal fizicheskoy khimii
ZhNiPFiK	-	Zhurnal nauchnoy i prikladnoy fotografii i kinematografii
ZhNKh	-	Zhurnal neorganicheskoy khimii
ZhPK	-	Zhurnal prikladnoy khimii
ZhPMTF	-	Zhurnal prikladnoy mekhaniki i tekhnicheskoy fiziki
ZhPS	-	Zhurnal prikladnoy spektroskopii
ZhTF	-	Zhurnal tekhnicheskoy fiziki
ZhVMMF	-	Zhurnal vychislitel'noy matematiki i matematicheskoy fiziki
ZL	-	Zavodskaya laboratoriya

4. AUTHOR INDEX